POLITECNICO
MILANO 1863

SCUOLA DI INGEGNERIA INDUSTRIALE
E DELL'INFORMAZIONE

Numerical Evaluation of Thermo-Mechanical Residual Stress Induced During Cold Spray Additive Manufacturing

TESI DI LAUREA MAGISTRALE IN
MECHANICAL ENGINEERING
INGEGNERIA MECCANICA

Author: **Mahdi Asadpour Kakelar**

Student ID: 10703642
Advisor: Dr. Sara Bagherifard
Co-advisor: Amir Ardeshiri Lordejani
Academic Year: 2020-22

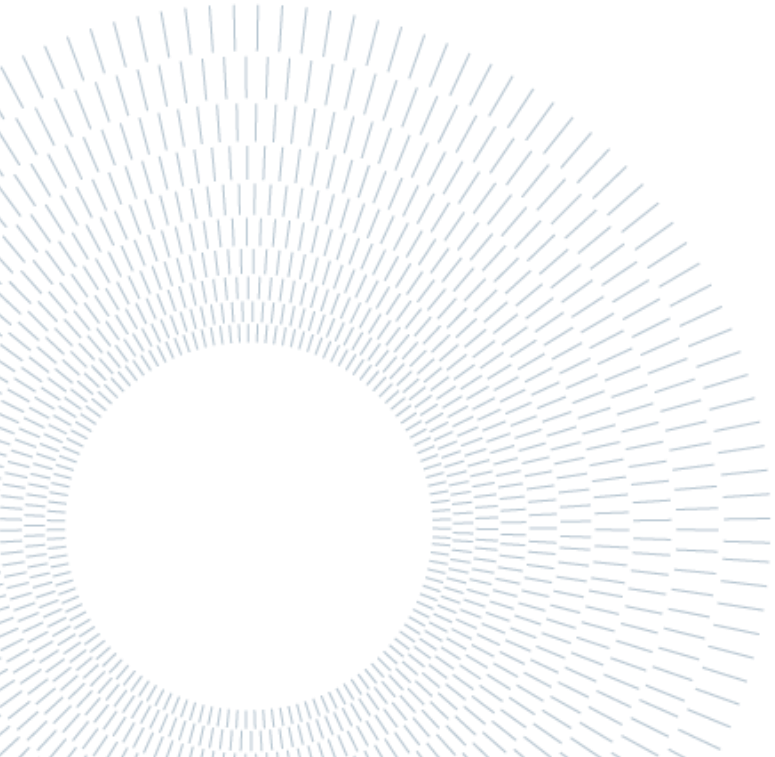

Abstract

This Master of Science thesis is intended to provide an insight on the trend of the induced residual stress during layer deposition with the help of cold gas dynamic spraying technology.

The cold gas dynamic spraying (CGDS) process is referred as cold spray. In this process, particles with specific temperature and initial velocity higher than critical velocity are propelled towards the substrate by a carrier gas. Particles by acquiring high kinetic energies while keeping temperatures much below their melting temperatures impact the substrate. The subsequent deformation of the particles will be followed by bonding to the substrate. Due to insignificant heating of impacting particles, avoidance from some disadvantages is possible, however, the presence of residual stress due to the nature of the referred technology is inevitable.

As the purpose of this work as prediction of the induced residual stress during cold spraying process, a model based on previous numerical models for prediction of stress during high velocity impact techniques was developed with significant modifications. Initially an explicit axisymmetric displacement-thermal analysis of single particle impact has been modeled. The extracted stress profiles in radial and axial directions from the axis of the model, through the application of axial pressures in the top partitioned segment of the substrate, and predefined initial radial stresses in the top sectioned segment of substrate and added layer is induced using an iterative corrective approach. By acquisition of loads responsible for induction of the read stress from single particle impact analysis, and repetitively applying the loads, peening stress during the cold spray additive manufacturing is obtained.

Thermal stress distribution due quenching and post cooling is obtained by an uncoupled thermal- mechanical analysis. Initially the temporal thermal field with the presence of convection and radiation, and conduction through the added layer and substrate is obtained. Then the obtained thermal temporal field is used in an implicit model to obtain the residual stress due quenching and post cooling. Stress measurement techniques can measure in plane stress, and the model has proved to be effective in the radial trend acquisition. As a matter of fact, the modeling process with

the previous well regarded papers' process parameters, concluded in close and complaint results.

The experimental part consists of deposition of grade 316 stainless steel on substrate made of grade 316 stainless steel: 1st test, with deposition of 1 layer, 2nd test with deposition of 2 layer with bidirectional scanning strategy, the 3rd test, with deposition of 2 layers with cross-hatching scanning strategy, 4th test, with deposition of 10 layers with cross-hatching scanning strategy, and 5th test with deposition of 10 layers with bidirectional scanning strategy. The deposition has been carried out at the university of Politecnico di Milano with Impact Innovations spray systems 5/8, and head guidance by KUKA KR 16 3 robot.

Residual stress measurements were performed using AST X-Stress 3000 portable X-ray diffractometer. In depth measurements were performed via layer-by-layer electropolishing to avoid introducing residual tensions in the surface of the samples. The stress relaxation effect due to layer removal after electropolishing is corrected based on Moore Evan's Theory

The previously mentioned FE modeling technique is used to acquire the thermal and peening stresses based on the experimental parameters and good compliance of the stress trend to the measured results is witnessed.

Key words: cold gas dynamic spraying, residual stress, peening stress, thermal stress, corrective iterative approach, x-ray diffraction

Contents

1 State of Art Cold Spray Technology

In the first chapter, after an introductive explanation on the cold spray technology, origin of cold spray, cold spray equipment, as the purpose of the thesis project, different factors that have influence in the profile of induced residual stress during cold spray coating were described.

1.1. Introduction to cold spray technology

The cold gas dynamic spraying (CGDS) process, is referred as cold spray[1]. In this process, preheated particles with specific temperature and initial velocity are propelled towards the substrate by a carrier gas. The accelerated particles in the form of powders of materials ranging in size from 1 to 50 microns, acquire high kinetic energies(with velocities in the range of 300 and 1000 m/s), while keeping temperatures much below their melting temperatures.[1] Upon exit from the nozzle, the deformation of the particles, will be followed by bonding to substrate. The succession of the deformations of the particles on the substrate and previously deposited particles, lead to formation of a coating on the substrate. In other processes belonging to the family of Thermal spray processes like, flame, arc, and plasma spraying, it is of high importance to completely melt sprayed material. In contrast in high velocity oxygen fuel (HVOF) spray process, for guaranteeing high quality coating partial melting of the particles are sufficient, the reason for lather mentioned issue, lies in higher particle velocities. So deformation of particles even in the solid state would be possible.[2]. In cold spraying process, development of higher particle velocities has been continued by simultaneous decrease of heat input.[2] Due to insignificant time of heating of impacting particles, by post-impact microstructure observations, no significant signs of melting were observed.[3] The process is being called cold spray due to its relatively low temperature with respect to other thermal coating processes. Comparison of approximate process gas temperature and velocity ranges for several common thermal spray processes and cold spray is presented in Figure 1.

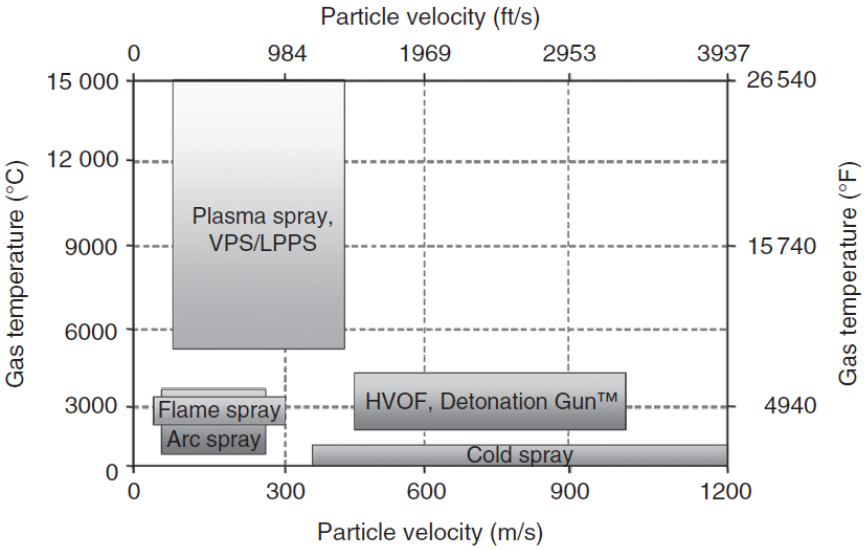

Figure 1_ Comparison of approximate process gas temperature and velocity ranges for several common thermal spray processes and cold spray [4]

Thanks to the low temperature of the process, spraying onto substrates containing temperature-sensitive materials is possible. In addition, avoidance from high-temperature oxidation, phase change, evaporation, melting, crystallization, significantly high residual stresses, debonding, gas release, strict substrate surface preparation and other accompanying difficulties related to traditional thermal spraying methods are achieved.[5]

The possibility to achieve high particle velocities in cold spray process is fulfilled by implementation of converging-diverging nozzle known as De Laval nozzle, due to expansion of process gas. In this way, the acquired supersonic velocity of the gas, accelerates particles towards the substrate surface, leading to the creation of the coating layer by consecutive splat formations on the substrate.[5] The mentioned velocity in order to result in attachment of particles to the substrate, should be above a critical impact velocity that depends on the pair of deposited material and substrate.[3]

1.2. A Brief history of origin of cold spray technology

The cold spray process originally was developed in 1980s at the Institute of Theoretical and Applied Mechanics of the Siberian Branch of the Russian Academy of Science in Novosibirsk by Dr. Anatolii Papyrin and several others: V. Kosarev, K.V. Klinkov, A. Alkhimov, V. M. Fomin, M. M. Shushpanov, A. I. Kashirin, O. F. Kljuev, and T. V. Buzdygar while studying two phase flow around solid particles in supersonic wind tunnel. [6][5][7]

The cold spray process was discovered by accident, [6] while concentrating on understanding flow parameters near different bodies, by alteration of gas flow, in the presence of the particles.[7]

It was observed that during the impact of particles of various sizes, impact angles, and velocities on various materials, the solid particles was deposited onto the surface when the velocity of impact was higher than certain critical value. Since then, efforts have been devoted for the development of this process into a practical industrial technology and the number of related patents and research publications has grown exponentially.[8]

1.3. Cold spray equipment

Cold spray systems, can operate either with robotic arm or manually operating, being possible to be portable or fixed in the position. The schematics of cold spray additive manufacturing system is represented in Figure 2. The main components of the cold spray system are:[9]

1- Powder feeder
2- Compressed gas source
3- Gas heater
4- Supersonic nozzle
5- Spraying chamber
6- Control system for monitoring spraying parameters

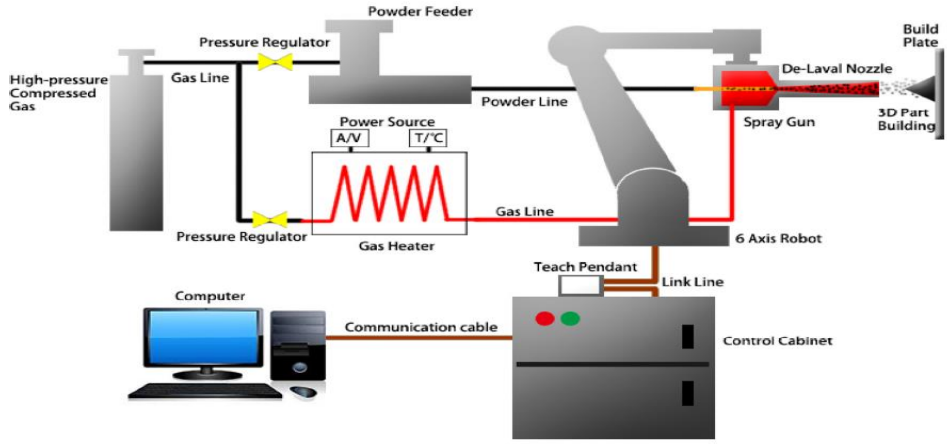

Figure 2_ schematics of CSAM system [10]

Depending on the operational Pressure and injection point of powder into nozzle, two types of systems are developed: Low-Pressure Cold Spray (LPCS) and High-Pressure Cold Spray (HPCS).

1.3.1. Low pressure cold spray (LPCS)

In the case of low-pressure cold spray, usually air or nitrogen as process gas at relatively low pressures (5-10 bar) and heated up to 550 degrees of centigrade, is forced through the supersonic nozzle, while the powders are drawn radially to the

downstream of the throat of the nozzle by Venturi effect, by keeping the static pressure within the nozzle below the atmospheric pressure.

In this type, as the need to high pressure delivery is not needed, the operational cost would be lower, as well due to the injection position of the powder into the nozzle, just the supersonic part of the nozzle experiences wear, which ensures longer service life, however, the deposition efficiency in the system is not higher than 50 %.[8][10] The operating principle of low- pressure cold spray is presented in Figure 3.

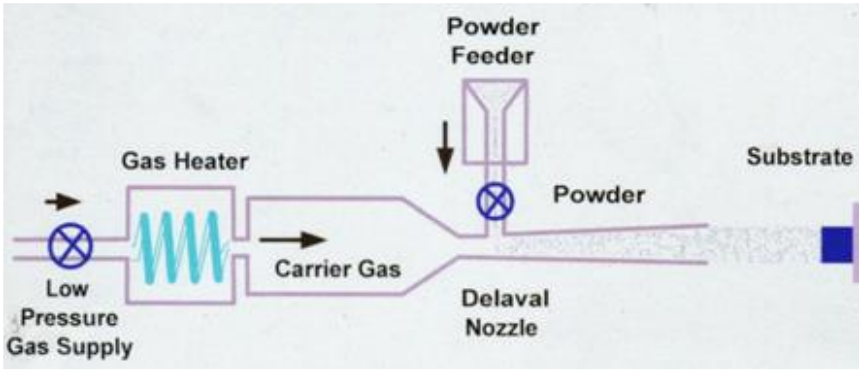

Figure 3_ Operating principle of low-pressure cold spray [11]

1.3.2. High pressure cold spray (HPCS)

In the case of high-pressure cold spray, usually air or nitrogen as process gas at relatively low pressures (25-30 bar) and heated up to 1000 degrees of centigrade, is forced through the supersonic nozzle. The solid powder feedstock particles mix with the propellant gas in the pre-chamber zone and then axially are fed into the gas stream, upstream of the converging section of the nozzle at a higher pressure than the accelerating gas to prevent backflow of the carrier gas to the powder feeder. The spray efficiency in this HPSC system is very high, reaching up to 90%.[8][11]

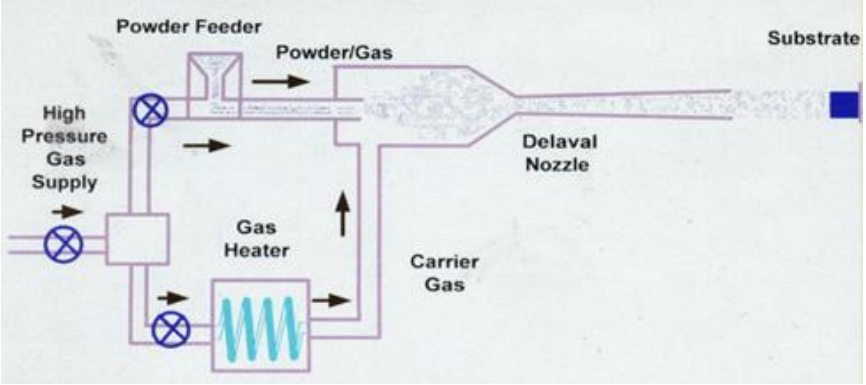

Figure 4_ Operating principle of high-pressure cold spray[11]

1.4. Particle's critical velocity

Critical velocity is the minimum speed a particle must have in order to get attached to the substrate/previously deposited material which is affected on the type of material of the powder and substrate, as well the size of accelerated particles.[12] Particle critical velocity measurement and approximations versus particle diameter for copper and steel 316L are presented in Figure 5.

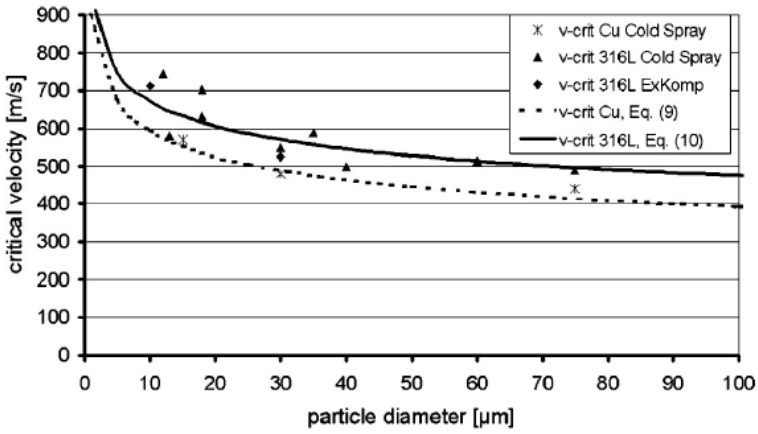

Figure 5_ Particle critical velocity measurement and approximations versus particle diameter for copper and steel 316L [12]

It must be noted with particle speeds lower than critical velocity, with particles bouncing back of the surface of the substrate, erosion in the substrate takes place. As well with too high particle speed, high erosion in the substrate can be witnessed.[12]

Based on Figure 6, it is possible to identify particles' size range that enables deposition since particle speed at the substrate results in higher velocity than critical velocity.

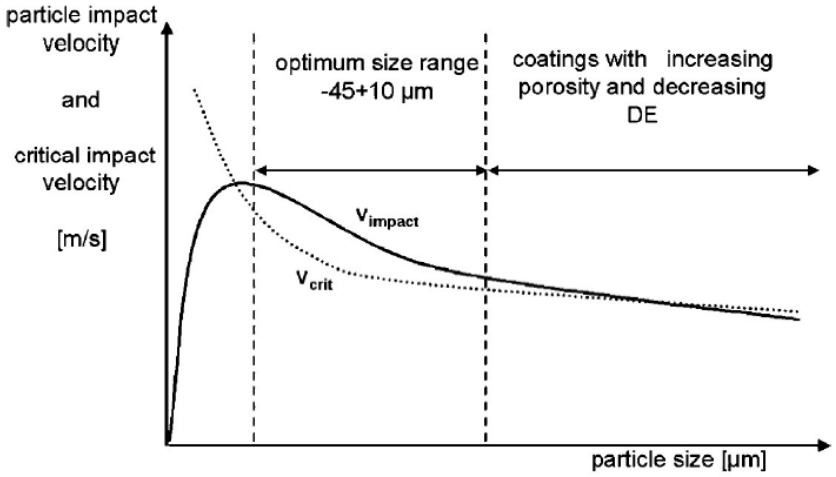

Figure 6_The region where the impact velocity is higher than the critical one corresponds to the so-called 'deposition window' where high deposition efficiencies can be reached.[12]

1.5. Induced residual stress during cold spray process and influential parameters in the induced residual stress

The process is being called cold Spray due to its relatively low temperature with respect to other thermal coating Processes, which would bring about notable advantages, however the presence of residual stress due to the nature of referred mechanism is inevitable.

The peculiarity of the cold spray coating process is the presence of two contradictory factors affecting the residual stress state by induction of compressive stress due to high impacting velocity and the simultaneous opposing annealing due high temperature with the compression reliving effect. [13]

1.5.1. Influential mechanisms in induction of residual stress

A number of mechanisms influencing the added up residual stress in cold spray coating are quenching the sprayed material due to high cooling rate, temperature gradient in multi-pass deposition processes, peening effect due to the plastic

deformation of particles impacting the substrate, and thermal mismatch between the coating and substrate materials. [13]

The induced residual stresses by cold spray process are classified by the 3 aforementioned mechanisms, namely high thermal gradient and quenching dominant, peening dominant, and mismatch dominant, present different residual stress pattern evaluated by researchers.

In the case of peening dominant, the peening stresses originating from the plastic deformation caused by constant bombarding of the high-velocity spraying particles are dominant over thermally induced stresses. The submissive nature of thermal stresses is a result of reduced thermal input in the peening dominant cold spray process due to the use of lower deposition temperature and pressure, also the negligible difference in the coefficients of thermal expansion between the deposited and substrate materials. [14][15]

The examples of peeing dominant mechanism and the pattern of induced residual stress are presented in Figure 7 with details described in Table 1.

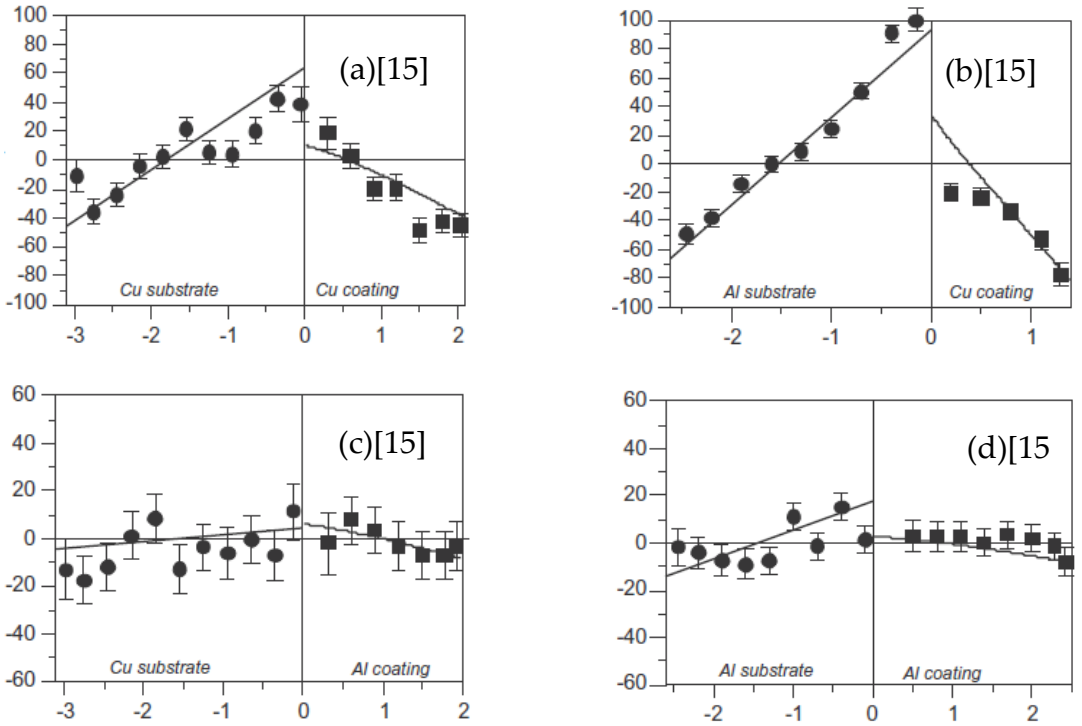

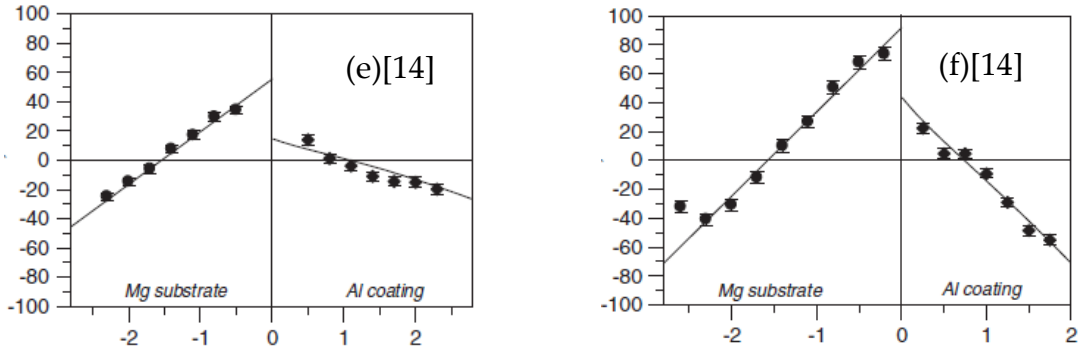

Figure 7_ Stress Profile description with the horizontal axis as through thickness distance in mm and the vertical axis as Stress in MPA. (a)(b) in order Cu/Cu and Cu/Al with process gas of He (pressure 0.62 MPa and temperature 140°C), (c)(d) I order Al/Al and Al/Cu with process gas of He (pressure 0.62MPa and temperature 200°C), (e)(f) in order Al6061/Mg and Al7075/Mg with process gas of N2(pressure 3.9MPa and temperature 400°C) [14][15]

Table 1_ Description of Material pair and Controlling parameters resulting in peening dominant mechanism

Residual stress profile[4]	Deposit/Substrate	Process gas, Pressure and Temperature
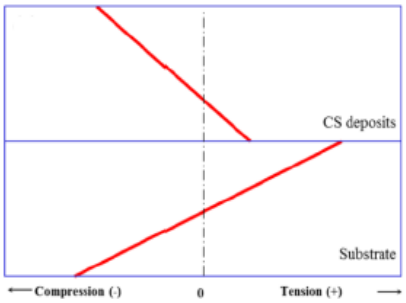	Cu/Cu Cu/Al [5]	He at 0.62 MPa/140°C [5]
	Al/Al Al/Cu [5]	He at 0.62MPa/200°C [5]
	Al/Mg [14]	He at 0.62 MPa/77-132°C [14] N2 at 0.76 MPa/217°C
	Al6061/Mg [14] Al7075/Mg	N2 at 3.9MPa/400°C [14]

As presented by Figure 7, peeing dominant mechanism in general stresses are compressive both at the top side of deposited layer deposits and towards the bottom of the substrate, and tensile at the interface, a trend that can be seen in the Table 1.

In the case of the thermal mismatch dominant cold spray processes, higher deposition temperature and pressure are used. Here, the thermal stresses are dominant, owing to different thermal contraction of the substrate and the deposited material, which is significant if there is a considerable difference in the coefficients of thermal expansion between the substrate and CS deposited material. [14] Moreover materials with similar thermal expansion coefficeints, may behave diversely depending on the spraying

condition. As an example, Al/Mg assembly when sprayed at a temperature range of 77-132°C using He as process gas and 217°C using N2 as process gas is found to behave like peening dominant, however the thermal mismatch dominant mechanism would be seen when sprayed at temperature of 550 °C using N2 as the process gas.[15] The trend of stress in mismatch dominant mechanism is presented in Figure 8.

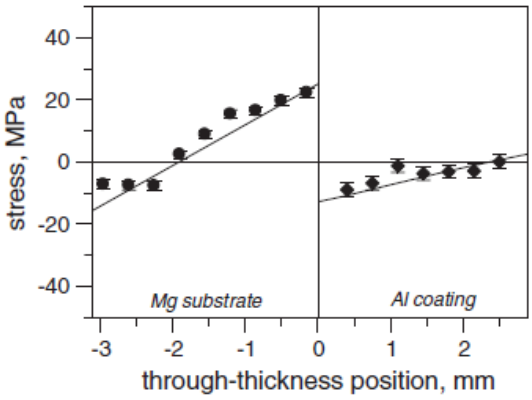

Figure 8_ Al/Mg assembly representing mismatch dominant mechanism when spraying process gas of N2 at 550°C, unlike the behavior shown when using lower process temperature for the same combination of material [14]

Residual stresses in thermal mismatch dominant category are tensile near the free surface of the cold spray deposits and in the substrate side of the interface. Compressive residual stress is towards the bottom of the substrate and in the deposits just above the interface.[14][15] Examples of thermal mismatch dominant mechanism's stress pattern are presented in Figure 8 and Table 2.

Table 2_ Description of Material pair and Controlling parameters resulting in Thermal mismatch dominant mechanism[14]

Residual stress profile	Deposit/substrate assembly	Process gas, pressure, and temperature
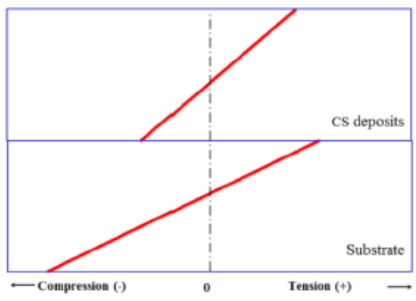	Ti/Cu	He at 0.62MPa/ 400°C
	Ti/Fe	Not referred
	Al/Mg [14]	N2 at 3.85MPa/550°C [14]

The temperature and the pressure threshold above which the transition from the peeing dominant to thermal mismatch dominant is not known. c

In the last category, as high thermal gradient and quenching dominant mechanism, it was found that stresses are highly tensile near the free surface of the CS deposits and towards the bottom of the substrate, and highly compressive near the interface. [14] An example of high thermal gradient and quenching dominant mechanism is Ti-64/Ti-64 assembly at very high temperature and pressure(1100 °C, 5 MPa) [14]. The induced residual stress profile of the high thermal gradient and quenching dominant mechanism can be seen in Figure 9, where there is the comparison of the predicted longitudinal residual stress, neutron diffraction, and contour method by D. Boruah et al. [14]

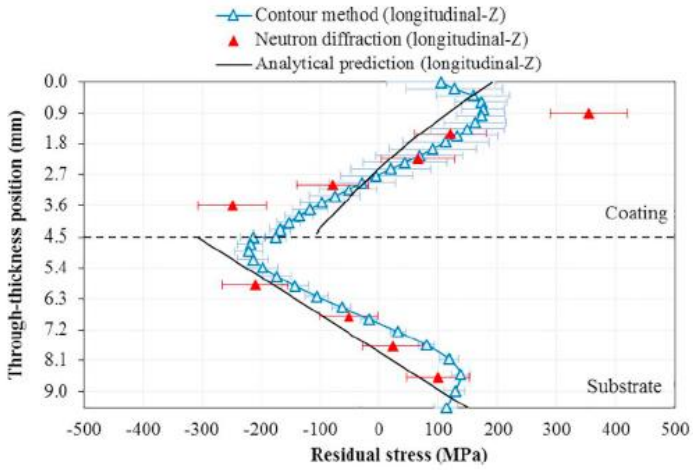

Figure 9_ Representation of stress distribution in high thermal gradient and quenching dominant mechanism including among neutron diffraction, contour method, and analytical prediction of longitudinal stress for Ti-64/Ti-64 at pressure of 5 MPa and temperature [14]

1.5.2. Influential factors in the residual stress induction

Influential factors in the induction of residual stress include the temperature of the deposited particles, impact velocity of the particle, particle diameter, impacting particle flow rate, the shape of particles, the initial temperature of the substrate, the friction coefficient between the particles and the substrate, the incident angle of the impacting particles, the number of deposited layers on the initial substrate, the deposited layer's thickness, the substrate's thickness, the size distribution of the impacting particles, the scanning pattern, the scanning speed, and the initial geometry of the substrate. In addition the external load applied for securing the substrate in position during the cold spray deposition may influence resultant residual stress pattern in the substrate and the deposited layers. [14] As well the high temperature

dependency of the material properties, since large variations in the specimen temperature may occur due to the motion between specimen and spray head leads to variations in the heat flux arriving at a given point and the consequent variation of residual stresses may arise.[16] The effect of mentioned factors would be explained hereafter:

1.5.2.1. Flow rate of impacting particle

With the higher mass flow rate with the same particles size distribution and material, the particles would be directed towards the substrate with speed higher than the critical velocity. Due to the multitude of impacts over a given zone on the substrate, and localized peening effect, higher resultant induced residual stress would be observed.[1]

1.5.2.2. The effect of diameter of the particle

By keeping constant other parameters, it can be justified that by increasing the diameter of the particle impacting the substrate, the higher kinetic, and thermal energy of the particle would lead to higher residual stresses.[17] The substrate depth affected by compressive stress considerably increases with higher particle mass.[18] In the Figure 10, the influence of diameter size of the particle in range of 20 to 60 micron on the induced residual stress can be seen for AL 1100-O particles over substrate made of Mg.[17]

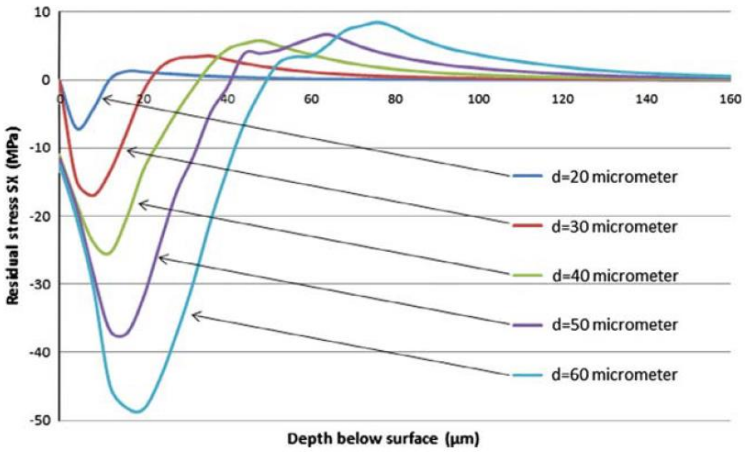

Figure 10_ Representation of effect of particle diameter size on the induced residual stress when impacting Al particles on Mg substrate [17]

1.5.2.3. Particle velocity effect

The maximum tensile and compressive residual stresses in the substrate and the deposited layer would be increased by the increase in the particle velocity. The increase in the velocity causes the increase in the kinetic energy leading to larger plastic region and larger residuals stress in the workpiece. [17] The effect of particle velocity in range of 400 to 900 m/s can be seen in Figure 11, for AL 1100-O particles impacting rectangular substrate made of Mg.[17]

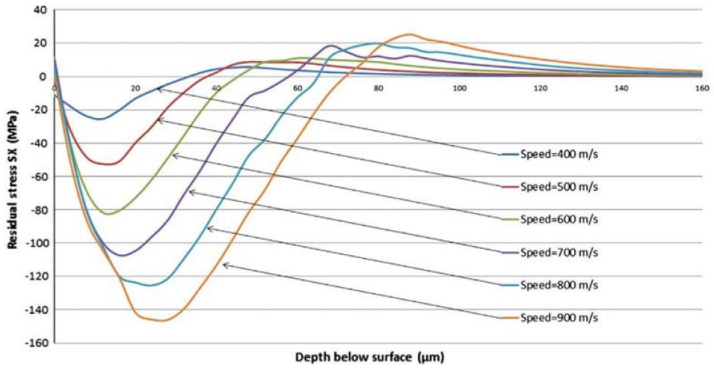

Figure 11_ Representation of effect of particle velocity on the induced residual stress [17]

As well the same result on the effect of impacting velocity of particle can be seen in Figure 12, for velocity range of 400 to 800 m/s and the temperature of 1600 K for deposit/substrate made of ss316 in radial and axial direction on a cylindrical substrate.[18]

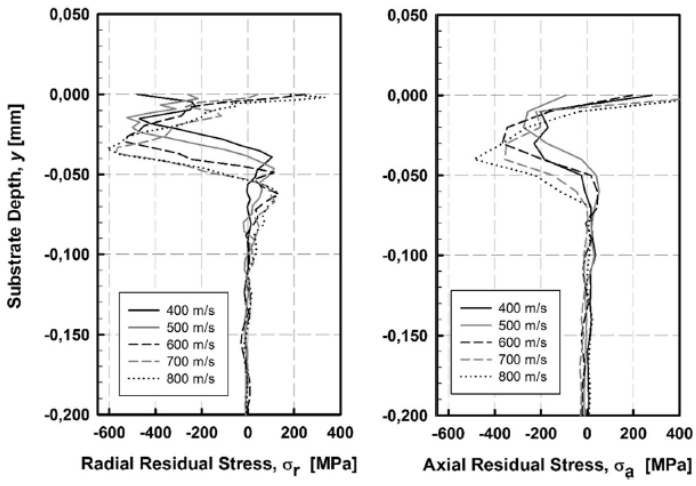

Figure 12_ Representation of effect of particle velocity on the induced residual stress in radial and axial direction with deposit/substrate pair of SS316 (the process temperature is 1600 K) [18]

In addition, based on Figure 11 and Figure 12, the position of max compressive and tensile stress gets deeper with respect to interface of deposit/substrate by increase of particle velocity.

1.5.2.4. Particle temperature

The residual stress profile for several impacts of particles with initially different particle temperatures, shows the maximum induced compressive stress is decreased by increasing the temperature level of particle. Nevertheless, the plastically deformed zone after impact is not significantly affected by different particle temperature. Furthermore, during the impact process, it is observed that the final shape of the splat depends heavily on particle temperature.[18]

The described effect of temperature on the residual stress in shown in figure 7 in temperature range of 800 to 1600 K and the particle velocity of 500 m/s with deposit/substrate pair of SS316 and initial substrate temperature of 298 K.[18]

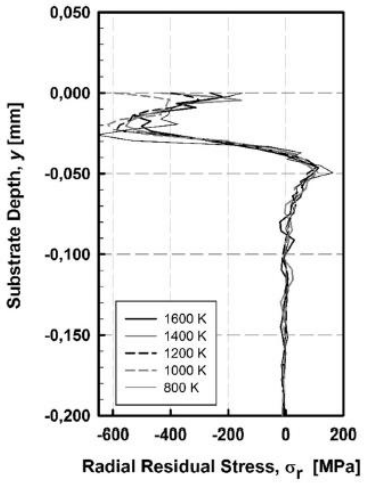

Figure 13_ Representation of effect of process temperature on induced residual stress in the substrate [18]

1.5.2.5. Shape of the particle

For considering the effect of shape of the particle, there are studies in which once particle was treated as an ellipse with different ratios of minor to major axis or, the effect of particle morphology was analyzed considering the moment of inertia with respect to the vertical axis of a rhomboidal particle. The kinetic and thermal energy was maintained constant in each case by employing particles of the same mass, velocity, and temperature.

Particles with lower area moment of inertia tend to penetrate deeper into the substrate and increase the maximum compressive stress right underneath the impact zone. The plastic deformation zone after the impact of this type was observed to be deep and narrow.[17][18]

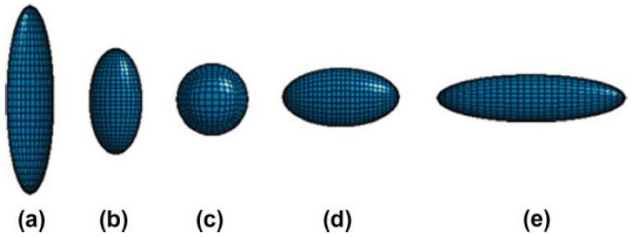

Figure 14_ Shapes of particles with different aspect ratio: (a) a/b = 0.25, (b) a/b = 0.5, (c) a/b = 1, (d) a/b = 2 and (e) a/b = 4 [17]

In the first study the aspect ratios shown in Figure 14 are implemented, and obtained the results presented in Figure 15.

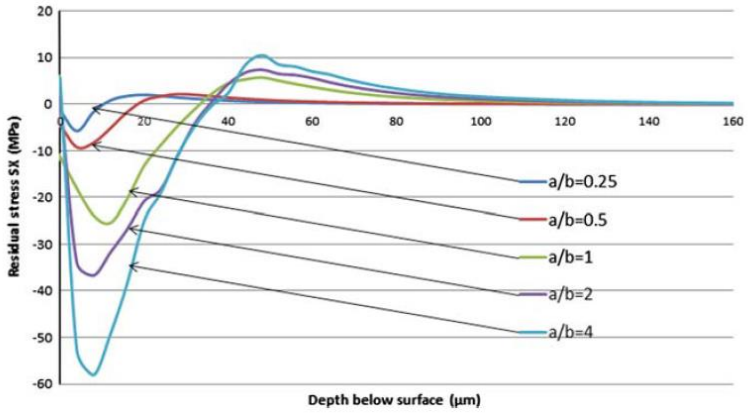

Figure 15_ Representation of effect of shape of particle on residual stress profile when impacted at 400 m/s by Al 1100-O particle with different shapes (aspect ratio) and same mass. [17]

In the second study by Oviedo et al [18] on the effect of particle shape on the induced residual stress is shown in Figure 16, where the diversifying parameter between the particles is the moment of inertia with respect to the vertical axis of the rhomboidal particle.

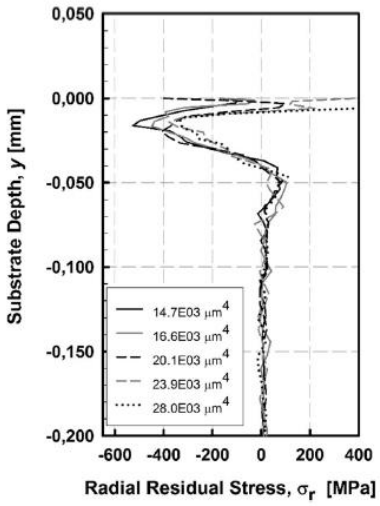

Figure 16_ Representation of effect of different area moments of inertia with respect to the particle's vertical axis on residual stress in the radial direction in a cylindrical substrate [18]

1.5.2.6. Substrate initial temperature level

The maximum compressive stress is achieved for lower substrate temperatures. This behavior is consistent with JC constitutive model, according to which, plastic deformation at lower temperatures occurs at higher flow stresses(in the substrate).[18]

1.5.2.7. The incident angle of impacting particles on the substrate

Oblique collision of particles when the cold spray gun is at the right angle with respect to the substrate may be due to two major reasons:

- Angular exit of the particles from the nozzle
- Roughness of the workpiece surface

An increase in the impact angle from 15 degrees to 90 degrees results in higher maximum tensile and residual stresses.

When the particle impacts the substrate surface with an angle less than 90 degrees, due to better slide of the particle on the surface on the target region, the friction increases, which in turn causes the increase in the temperature of particle. Therefore, less energy is transferred to the workpiece. Consequently, more tensile force is applied on the surface that decreases the surface compressive residual stress.[17]

The mentioned effect of the incident angle on the induced residual stress can be seen in Figure 17.

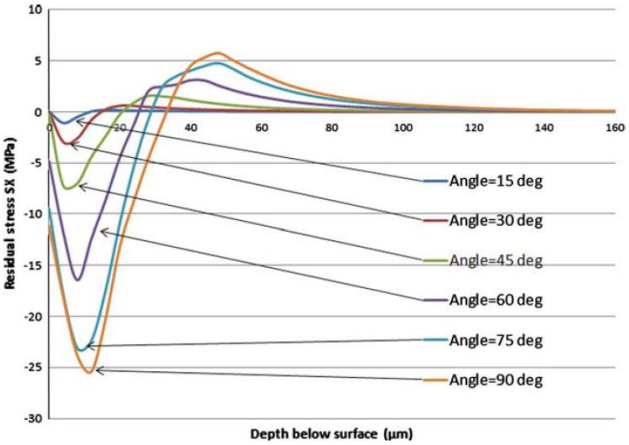

Figure 17_ Representation of effect of the incident angle on the resultant stress with particles of Al with diameter of 40 micrometers impacting on rectangular substrate made of Mg [17]

1.5.2.8. The friction coefficient

The friction coefficient depending on the matching components has shown to be influential when changing in the range of 0.1 to 0.3, however changes on the residual stress after 0.3 are negligible.[17] The effect of friction coefficient on the induced residual stress is presented in Figure 18.

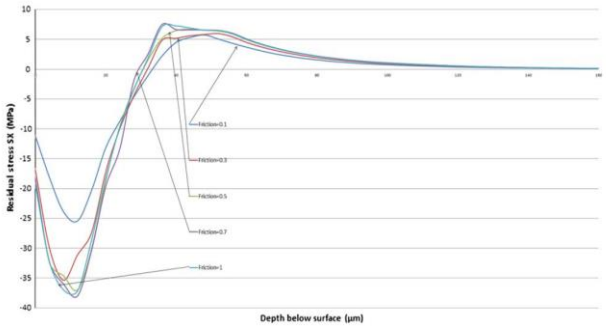

Figure 18_ Representation of effect of coefficient of friction on the residual stress [17]

1.5.2.9. The thickness of the deposited layer on the substrate

It was found that the maximum tensile and compressive residual stresses in the substrate- deposited layer gets higher by increase in the thickness of the deposited layer on the substrate, but the trend of residual stress distribution is the same.[14]

The effect of thickness of the deposited layer on the induced residual stress is represented in Figure 19. Based on the presented results in the horizontal track pattern

(CS2 and CS4), by increase of the deposited layer on the substrate, the induced residual stress experiences increase.

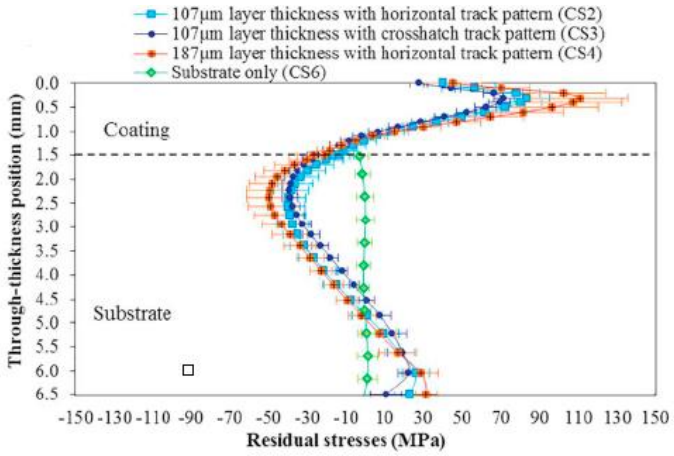

Figure 19_ Representation of effect of deposited layer on the induced residual stress pattern [14]

1.5.2.10. The thickness of the substrate

The higher the thickness of the substrate, the lower would be the resulting maximum tensile and compressive stress in the substrate- deposited layer. [14] In Figure 20, the effect of the thickness of the substrate on the induced residual stress for two different thickness of substrate (5 and 10 mm) can be seen.

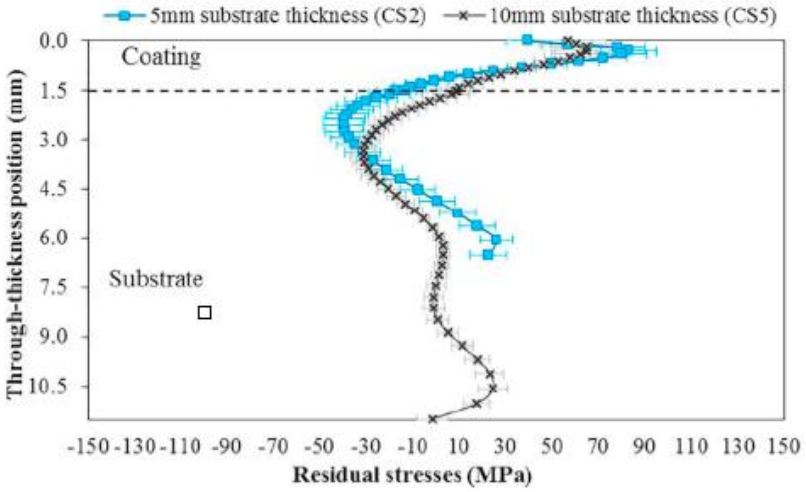

Figure 20_ Representation of effect of thickness of the substrate on the residual stress induced in deposit/substrate assembly [14]

1.5.2.11. The scanning speed of the spray head

By decrease in the scanning speed of the spray head directing the high velocity particle on the surface of the substrate, due to the multitude of the concentration of impacting particle at a localized region on the substrate, the resultant residual stress would be higher.[14], However the simultaneous effect of increase of exposure to heated gas may contract the referred effect. So, it is required considering the simultaneous effect of increased number of impacting particles and the heat flux introduced by the nozzle head.

1.5.2.12. The scanning pattern of the spray head

The influence of the spray path on the residual stress development is being systematically analyzed.[19] and has been proven to have an influential factor that would decrease the resultant residual stress especially in the case of usage of the cold spray for additive manufacturing, demanding high number of layers deposited on the substrate. Based on the work presented by Enqiang Lin, et al [19], where the second layer of copper coating is deposited on the steel substrate with two strategies:

1- Repeating deposition strategy: In this strategy nozzle moves back to the original starting point after the first layer is finished. The deposition of the second layer starts from the original starting point in the first deposited layer. 2- Reversed deposition strategy: In this strategy, the nozzle immediately starts depositing material as it traces its path backward toward the original starting point.[19] slightly lower residual stresses was witnessed through the use of repeating deposition strategy in comparison with reversed deposition strategy.[19]

The schematics of the two mentioned deposition strategy is presented in Figure 21 (A). In this figure, black lines show the deposition pattern of first layer, and 2 red arrays show the start point of second layer, following the pattern lines of first layer with 2 explained strategies. As well through thickness residual stress induced by two deposition strategies is represented in Figure 21 (B).

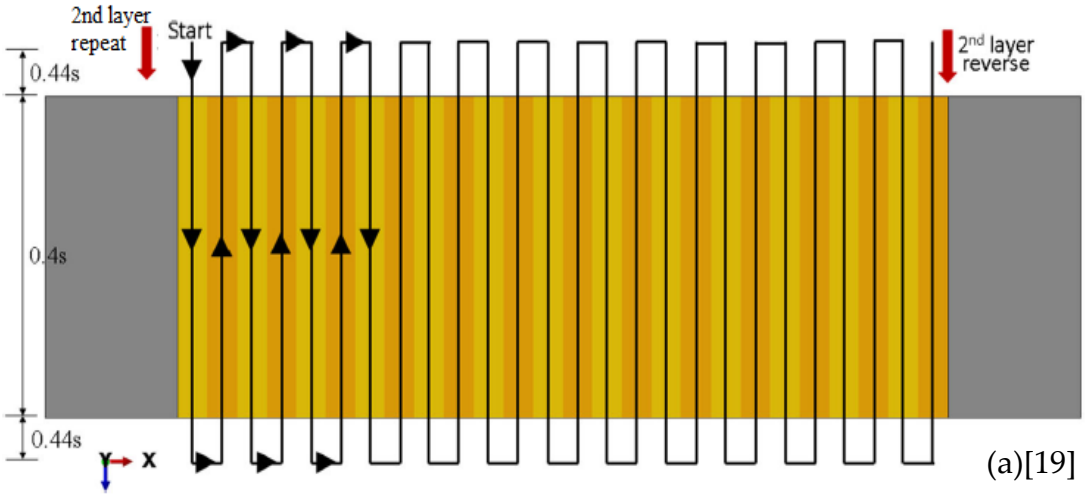

(a)[19]

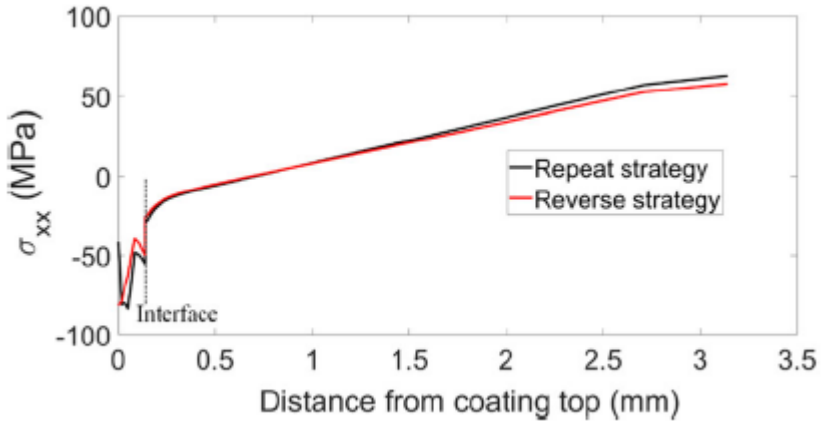

(b)[19]

Figure 21_ (a): Representation of repeating and reversed deposition strategy [19], (b): Representation of through thickness residual stress induced by repeating and reversed deposition strategies [19]

Also in work of D. Boruah, et al[14], with focus on the residual stress induced by cold spraying of Ti-6Al-4V on Ti-6Al-4V substrates, deposition with crosshatch track pattern had lower tensile residual stress in the deposited layer, and lower compressive stress just below the interface of deposited layer and substrate compared with the horizontal track pattern.[14]

The schematics of crosshatch and horizontal track patterns are presented in Figure 22 (A), and the comparison between the effect of crosshatch and horizontal track pattern on the induced stress through the thickness of deposit/substrate is presented in Figure 22 (B).

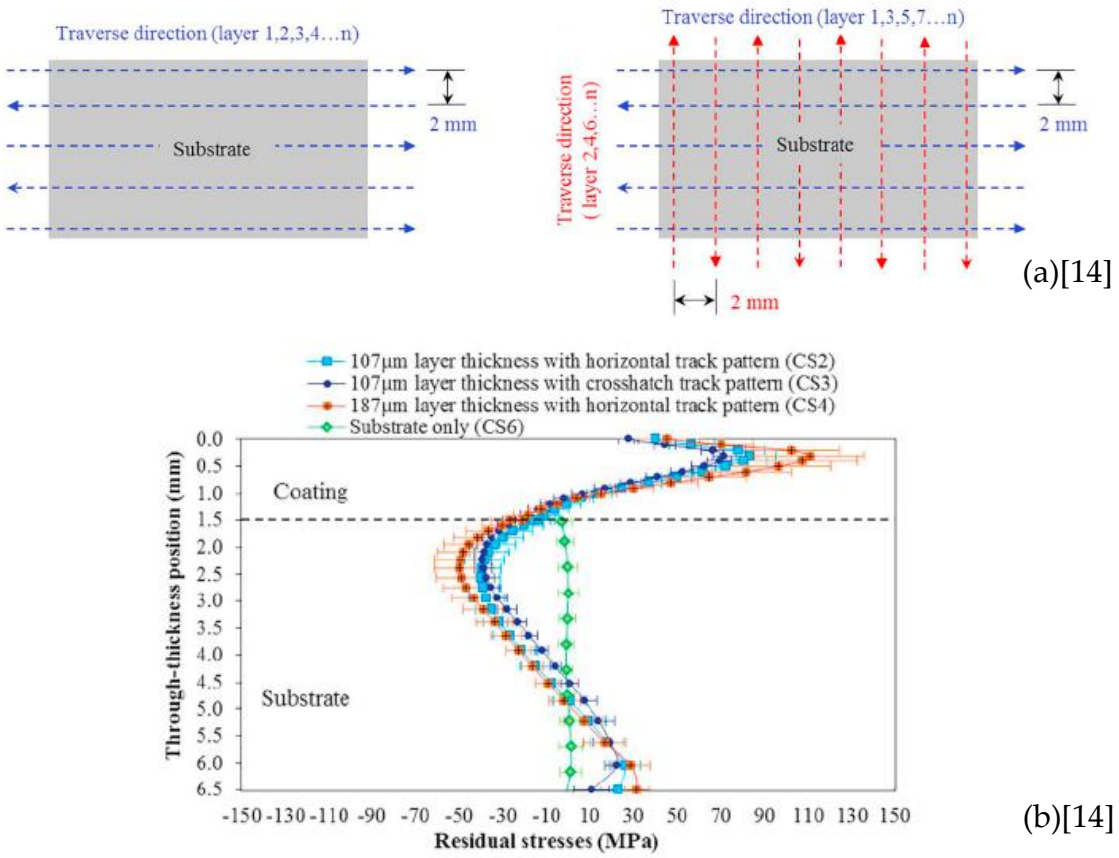

Figure 22_ (a): Representation of crosshatch and horizontal track patterns used for deposition of coating [14], (b): Comparison between induced residual stress by horizontal and crosshatch track patterns deposition (CS2 and CS3) [14]

1.5.2.13. The initial geometry of the substrate

In addition to the process parameters, the geometry of the substrate plays a vital role in defining the overall residual stresses in the cold spray deposit-substrate assembly. This conclusion was derived by D. Boruah, et al[14] based on the different results between the work of R. Singh, et al [8] and D. Boruah, et al[14], where different substrate geometries have been used. as cylindrical specimens were investigated in the research by R. Singh et al [8], whereas rectangular specimens were used in the research study by D. Boruah et al [14].

1.5.2.14. Surface preparation of substrate

The magnitudes of the residual stresses were mainly dependent on the substrate-coating material combination, but the surface preparation was also found to influence the final stress stage of the coating.

2 Developing Numerical method to predict residual stress in 2D

In this chapter, initially the previous numerical or analytical approaches that are presented for residual stress profile prediction during additive processes are explained, then a part of this chapter would be dedicated to presenting a couple of ways to predict the residual stress during cold spray additive manufacturing based on the work of Bansal et al[20] and Oviedo et al[18]. It is worth mentioning that even though it will not be possible to use the exact method presented by the referred authors, the iterative corrective approach used in their papers was worthy of implementation in the current project.

2.1. Previous attempts for prediction of residual stress profile in the assembly of substrate- added layers in additive processes

1- In the work of Y.C. Tsui et, al [16], an analytical model for prediction of residual stress in progressively deposited coatings, such as those produced by thermal spraying is introduced. This model is based on the concept of a misfit strain, caused by either the deposition stress due to quenching of splats in thermal spraying or by differential thermal contraction between substrate and coating during cooling. The deposition stress is introduced as the coating is formed layer-by-layer, with a specified layer thickness, such that the misfit strain is accommodated after each layer addition. The model is straightforward. It can be implemented with a simple customized computer program or by using a standard spreadsheet. [16]

2- In the work of Oviedo et al [18] and Bansal et al [20], a numerical model was developed for predicting thermal and peening effect in high velocity spraying techniques. To model the complex deposition process, a parametric explicit-implicit FE methodology using the commercial Abaqus 6.9 has been implemented. Initially an explicit axisymmetric single particle impact has been modeled. The stresses field is extracted in the axis of axisymmetric geometry, and through a corrective iterative process, by application of pressures on the edges of the 2d axisymmetric geometry, an implicit model where, the extracted axial and radial stresses are induced in the substrate. By knowing the pressures resulting in the desired stress extracted from axisymmetric single particle model results, and by repetition of application of aforementioned pressures, the effect of addition of layers, can be seen, which results in acquisition of peening stress during the process. Thermal stress distribution due quenching and post cooling can be obtained by an uncoupled thermal- mechanical analysis. Initially the thermal field with the presence of convection and radiation, and conduction through the added layer and substrate is obtained. Then the obtained thermal temporal field would be used in an implicit model to obtain the stresses due quenching and post cooling. Finally, the simultaneous effect of both events would result in acquisition of total induced residual stress in the assembly of

substrate-deposited layers. It should be mentioned that in the iterative corrective part, a defined error threshold in every iteration between the desired stress profile obtained by Single particle impact and the induced stress in the substrate after addition of first layer is checked. As already mentioned, the obtained loads providing the possibility of inducing stress field in the first layer would be used for acquisition of stress field after addition of higher number of layers.[18][20]

3- In the first part of work of Lan Li et al[21], for prediction of stress field during Selective Laser Melting (SLM), a sequentially coupled thermo-mechanical field analysis in commercial software ANSYS was developed for accurately predicting thermal history, distortion, and residual stress. For the sequentially coupled thermo-mechanical analysis, the calculations were done in two steps. First, the transient thermal analysis was calculated. Then the computed temperature results were used for the mechanical calculations as the thermal load to calculate the thermal stress and deformation. The model consisted of one layer of 304L stainless steel powder with dimensions of 4×3.4×0.05 cubic millimeter on a solid 304L substrate with dimensions of 4×3.4×2 cubic millimeter. For the sake of reduction of computational time, the elements interacting with the laser were finely meshed, while a coarser mesh for the surrounding loose powder and substate was used. During the SLM process, the laser energy on the powder bed can be regarded as a volumetric energy density, which obeys the Gaussian heat source distribution. As mentioned by the authors, Due to the small dimension of the simulated part, extra stress would be caused by local yielding with local thermal gradients in a small, simulated part. So, the residual stress of the large part is necessary to analyze.[21] The authors underline that, as the time needed for modeling the process in big dimensions is significant, they suggest another method to decrease the computational cost. They suggested an equivalent body heat flux proposed from the single layer scan model can be imported to as thermal load to the layer-by-layer model. The proposed method has the capability for fast temperature prediction in the SLM process, while sacrificing modeling details for time-saving purposes. As in the previously published paper by authors, the coupled thermo-mechanical multiscale method has been used to calculate the thermal stress and deformation. The hatched layer is heated up layer by layer using a body heat flux to build up the largescale part rather than simulating every

single laser pulse. The element birth or death function is used to activate or deactivate an element. Through the use of current method, authors reported significant decrease of computational time.[22] The same exact strategy used by Lan li et al[12], has been used by Abhilash Kiran et al for obtaining the thermal field during directed energy deposition additive manufacturing process.[23] Similarly, Frederic E. Bock et al [24], used the same method to obtain stress field during wire-based laser metal deposition of Al-Mg alloys.[24]

4- In the work of R.Ghelichi et al [13], a numerical model has been developed for studying the peening effect of the particles in cold spray coating. A 3D model is developed using commercial finite element code Abaqus/ Explicit 6.12-1 which is utilized to investigate multiple impact effects. The target is modelled as a rectangular body, sufficiently large to avoid the effects of boundary conditions on the residual state in the impact area. The ability of the numerical approach in order to correctly estimate the final residual stresses induced during cold spray was verified by XRD experimental measurements. The authors reported satisfactory agreement between the calculated and experimental data, except for stresses on the substrate surface. [13]

5- In the work of M.P.Mughal et al, [23] a numerical model has been developed for studying deformation and induced stress during welding process, through the use of a sequentially coupled thermo-mechanical process, which has shown promising results in comparison with the experimental data.

6- Based on the work of Baran Yildirim et al[13], Single particle impact models, are not capable of predicting the final structure of the cold spray coatings properly, as they do not include the interactions between large numbers of impacting particles and changing surface properties. So, to study these effects, impact of multiple particles was investigated by finite element method in 3D. To this end, two different configurations involving 3 and 100 particles were developed. Effects of particle positioning and process parameters on the coating properties were studied. In this work, Lagrangian formulation with material erosion was employed to cope with excessive element distortions and maintain a high-quality solution. For the parameters used during modeling process as well as the materials used in their work, the model predicted the presence of tensile residual stress in the depth of the substrate, and compressive stress near

the top surface of the substrate. Although the stresses in the particle are compressive, the amplitude of compressive stress in the particles are less than compressive stress in the substrate.[13]

2.2. A brief overview of the fundamental concepts of numerical approach in the thesis project

2.2.1. Lagrangian

The nodes of the Lagrangian mesh move together with the material. Conservation of mass is satisfied, material boundaries are clearly defined, and the interface between two parts is precisely distinguishable. This approach is ideal for following the material motion and deformation in regions of relatively low distortion, and possibly large displacements. This method is more appropriate for representing the solids like structures with the advantages of computational efficiency and ease of incorporation in complex material models. The shortcoming of this approach is that the extremely severe distortions in the deformed region, which could be led to significant effects on the accuracy and convergence. The mentioned issues can be overcome to a certain extent by applying numerical technique such as rezoning.[3][26][27][28][29]

2.2.2. Arbitrary Lagrangian Eulerian

The Arbitrary Lagrangian Eulerian (ALE) numerical approach combines the features of pure Lagrangian analysis and pure Eulerian analysis. This tool makes it possible to maintain high quality mesh during the analysis even when large deformation or loss of material occurs, with providing the possibility of motion for the mesh independent of the material. The mentioned tool does not alter the topology of the mesh. Through the use of this tool effectively a continuous rezoning is possible which is desirable for problems with large amount of non-recoverable deformation like metal forming processes such as forging, extrusion, and rolling with large amounts of nonrecoverable deformation. The loss of accuracy, a reduction in the size of the stable time increment, or even termination of the problem are the consequences of drastic change of product geometry. In other words, a previously suitable mesh experiences severe element distortion and entanglement. With respect to Lagrangian approach, an additional computational step of rezoning is employed, thus the computation cost rises. As well,

the simulation results are largely dependent on the choice of parameters, such as remeshing region, frequency, remeshing sweeps per increment.[3][26][28][27][30]

2.2.3. Coupled Eulerian Lagrangian

As already mentioned in Lagrangian analysis elements deform as the material deforms, in other words the nodes are fixed within the material. Lagrangian elements are always 100 percent full of a single material. By contrast, in a Eulerian analysis the nodes are fixed in space, and material flows through elements that do not deform. Consequently, Eulerian elements may not always be 100 % full of material. The Eulerian material boundary must be computed during each time increment an element boundary. Eulerian material can interact with Lagrangian elements through Eulerian-Lagrangian contact. Simulations that include this type of contact are often referred to as coupled Eulerian Lagrangian (CEL) analysis. In this analysis, material is tracked as it flows through the mesh by computing its Eulerian Volume Fraction (EVF) within each element. The CEL numerical approach allows complex fluid-structure interaction problems including large displacements and deformations of the structure, to be solved in a single numerical simulation.[31][32][33]

2.3. Residual stress prediction based on parameters obtained from the work of Oviedo et al [18]

2.3.1. Process

In order to predict the induced residual stress in a deposited layer and substrate assembly, a successive process is performed. Based on papers published by Bansal et al [20] , and Oviedo et al[18], the methodology is summarized in ‘‘Explicit Particle Impact Analysis’’ and ‘‘Implicit Layer Deposition Analysis’’ steps.

In the first step an axisymmetric single particle impact model, with defined geometry of the substrate, particle size, velocity and temperature of the substrate and particle, has been considered.

Based on the explicit particle impact analysis, the radial and axial stress right below the point of impact of particle would be extracted to be used as the stress field after the deposition of each layer which their thicknesses would be defined by the initial explicit single particle impact analysis.

With an iterative corrective approach, the peening stress would be induced in the assembly of one layer and substrate. The same method would be used iteratively to induce the effect of addition of subsequent layers to the assembly of layer-substrate. On the other hand, the thermal stress should be obtained by considering a decoupled process where, at first, the thermal field would be obtained by knowing the heat flux, the period of exposure of assembly to heat flux in each added layer, the initial temperature of assembly of layer-substrate assembly and consideration of effect of radiation and convection between the assembly and environment. By having thermal field during process, another step would be initiated to obtain the thermal stress based on the initially defined thermal field that has been obtained from previous heat transfer model. [20][18]

2.3.2. Single impact particle analysis

In the single particle impact step, the deposited material and the substrate are made of SS316, with defined material properties in table 3.

A two-dimensional axisymmetric FE model of a stainless steel 316 (SS316) particle impacting on a cylindrical SS316 substrate is developed. The particle impact is analyzed as a coupled thermal–displacement phenomenon under high strain rates. One of the assumptions is that particles do not interact between each other during the short time duration of impact. So, an independent single particle impact is a statistically representative event.[20][18]

The initial temperature of the particle is below its melting point. Thus, the impact, deformation and cooling stages are in solid state. [18] The model considers 90% of the kinetic energy being transformed into heat [27], with the remainder of the energy being spent as plastic deformation and rebound kinetic energy.[20]

Through explicit FE analysis calculates the future state of a system based on its current state, providing comprehensive historical information of the stress and strain fields during high velocity impact is possible. The mentioned information is worthy in the case of modeling highly dynamic events subjected to high strain rates and short periods of time, like impacts, collisions, or explosions.[33] [18]

Explicit formulation is adequate for analyzing short periods of time, however for longer time spans and repetitive impact it would be computationally costly. [33].Therefore, only a single impact is analyzed.

The response of the impacting particle and the underlying substrate under such loading conditions is strongly affected by the strain, strain rate, temperature, and microstructure of the material. [26] Therefore, an appropriate constitutive equation for definition of the material properties is essential for modelling such processes.

The proposed constitutive relation by Johnson and Cook is widely used in numerical models involving high strain rates and temperatures.[27][34][35]

The J–C model is stated as follows:[34] [35]

$$\sigma = [A + B \times (\bar{\varepsilon}^{pl})^n [1 + C \times \ln(\frac{\dot{\bar{\varepsilon}}^{pl}}{\dot{\varepsilon}_0})](1 - \hat{\theta}^m) \quad \text{Equation 2-1}$$

In Equation 2-1, $\bar{\varepsilon}^{pl}$ is the equivalent plastic strain, $\dot{\bar{\varepsilon}}^{pl}$ is the equivalent plastic strain rate, and A, B, C, m, n and $\dot{\varepsilon}_0$ are material parameters measured at or below the transition temperature. (A: Yield stress, B: Strain hardening, C: Strain rate sensitivity coefficient, m: Thermal softening parameter, n: Strain hardening exponent, $\dot{\varepsilon}_0$:Reference plastic strain rate) parameters measured at or below the transition temperature. softening is assumed to occur.

$\hat{\theta}$ is a non-dimensional temperature, defined by:

$$\hat{\theta} = \begin{cases} 0 & for \quad \theta < \theta_{transition} \\ \frac{(\theta - \theta_{transition})}{(\theta_{melt} - \theta_{transition})} & for \quad \theta_{transition} \leq \theta \leq \theta_{melt} \\ 1 & for \quad \theta \geq \theta_{melt} \end{cases} \quad \text{Equation 2-2}$$

The $\theta_{transition}$ in Equation 2-2, is the temperature above which thermal softening is assumed to occur. Since, in the example against which we have chosen to assess the validity of our model, the stainless-steel particles are below their melting point, we used the J–C model to describe the mechanical properties of the materials.

It should be reminded that Johnson-cook parameters for sprayed stainless steel are not available in the literature. So, the thermomechanical properties of the system were also assumed to be the same as that of bulk stainless steel.

The thermomechanical properties of SS 316 are listed in Table 3.

Table 3_ Thermomechanical properties of SS316 [18]

Temperature-independent properties			
Density[kg/m^3]	8031		
Specific heat [J/kg K]	457		
Latent Heat of Fusion[J/kg]	3.3e5		
Temperature-dependent properties			
Temperature[K]	Elastic modulus, [GPa]	Thermal conductivity [W/m K]	Thermal expansion coefficient [1/K]
298	193	15	1.60e-5
473	184	17	1.71e-5
873	154	19	1.8e-5
973	148	26	1.85e-5
1500	100	30	3e-5
1643	75	60	1.60e-5

J–C parameters of SS 316 are listed in Table 4. [36][37][38]

Table 4_ J–C parameters of SS 316 [18]

Johnson–Cook parameters	
A (Yield stress) [MPa]	388
B (Strain hardening coefficient) [MPa]	1901
C (Strain rate sensitivity)	0.02494
m (Thermal softening parameter)	0.6567
n (Strain hardening exponent)	0.8722
Transition temperature $\theta_{transition}$ [K]	298
Melting temperature θ_{melt} [K]	1643
Reference plastic strain rate $\dot{\varepsilon}_0$ [1/s]	1e-5

Cylindrical substrate dimensions are 1.5 mm radius and 1.5 mm height. The substrate dimensions compared to particle's dimensions are chosen to avoid edge effects. On the bottom edge of the substrate all Degrees of freedom are constrained (Encastre). In addition, on the left edge of the geometry, the axisymmetric axis of asymmetric model symmetry boundary conditions are specified on both particle and the substrate. Based on the requirement, different particle velocity and initial temperature is considered for the particle. Initial temperature of 298K is considered for the substrate. In Figure 23, the assembly of particle and substrate with distance of zero from each other are presented.[20][18]

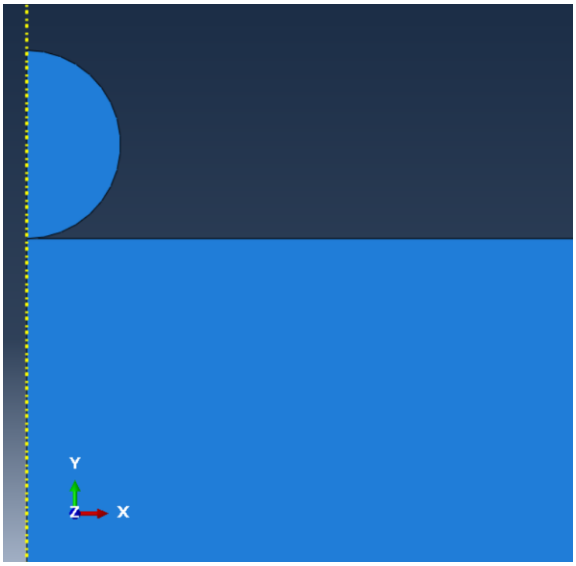

Figure 23_ Representation of the assembly of particle and substrate

A cylindrical coordinate system aligned with the substrate's central axis is employed as reference. Since the model is defined as a two-dimensional axisymmetric system, the stress tensor is composed of three main components: radial stress (in the direction of cylindrical substrate diameter), axial stress (in the direction of cylindrical and shear stress.

Due to the assumption of no-separation between the contacting nodes of the impinging particle and the substrate, debonding or rebounding are ruled out.

The requirement for a fine mesh with small elements to obtain detailed stress distributions leads to very short maximum allowable time increments which, in turn, result in a computationally intensive analysis. To have higher computational efficiency of the impact model, smaller elements were used only in the particle.

As simulation output, the resulting radial and axial residual stress distributions measured along the symmetry axis are computed after 400 ns of the onset of the impact. This time period is enough to allow for kinetic energy dissipation, particle spreading, substrate deformation and temperature stabilization.[18]

The Particle and substrate being meshed employing quadrangular linear coupled temperature-displacement elements or Three-node linear displacement and temperature elements used to discretize the particle and the substrate with pure Lagrangian method, show promising results for low temperature and velocity of impact of particle, which are comparable with results obtained by the reference. However, by increase in the mentioned parameters, due to extremely severe distortions in some elements specially in the particle, convergence will not be achieved.

In order to deal with this problem at first different sectioning and meshing strategies have been implemented based on personal observations and ways implemented in the papers with the objective of extracting stress state in single particle impact model. A number of these sectioning strategies are presented in the Figure 24.

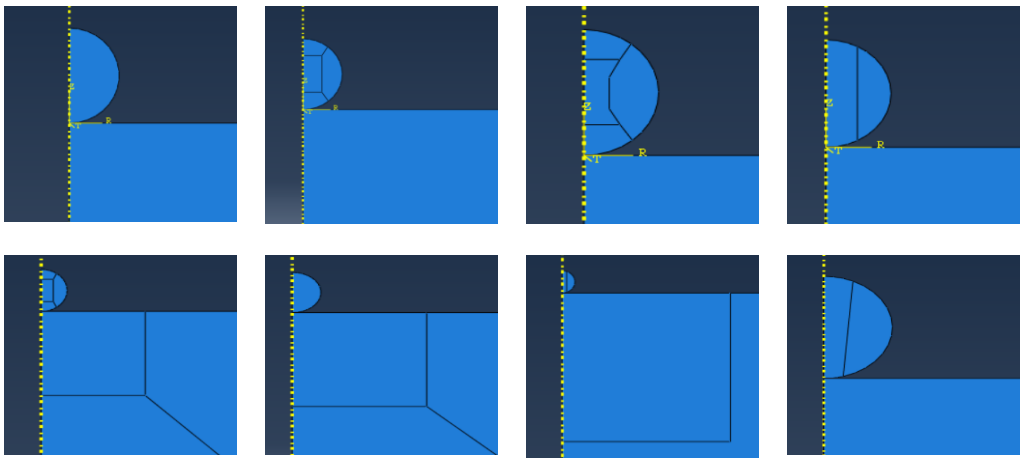

Figure 24_ Different used sectioning strategies

Through the use of paper published by Wen-Ya Li et al[28], and implementation of meshing strategy used in this paper(proportion between particle size and mesh size at contact area, as well as sections in the particle and substrate),and Arbitrary Lagrangian-Eulerian (ALE) analysis, in the main model for SS316, the attempt was to overcome to excessive distortions in some elements, and get the similar results as Oviedo et al[18] and Bansal et al.[20]

The modeling in order to achieve the results presented in this paper are presented hereafter:

In this paper the substrate as well as the impacting particle were made of Copper with the defined material properties (they are constant, not a function of temperature). The size of the substrate was 0.1*0.1 square millimeters with the seed size of 0.00048 mm at the contacting part. And the size of the particle was considered 0.02 mm with global mesh size of 0.0004 mm.

As reported by Wen-Ya Li et al[28], the completion of the job cannot be fulfilled if distortion control is not used.

In Figure 25, the comparison of the obtained results based on the parameters used by Wen-Ya Li et al [28], and the results reported by Wen-Ya Li et al [28] is presented.

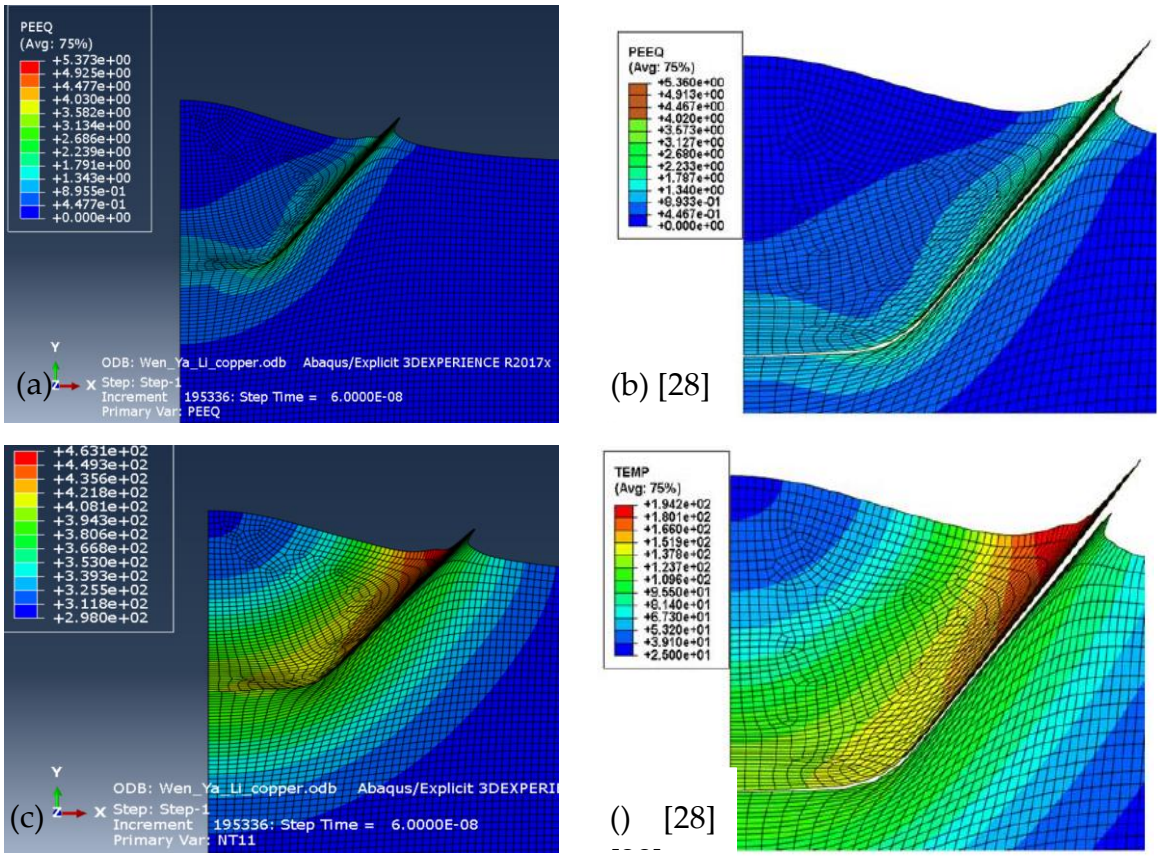

Figure 25_ (a): Obtained PEEQ based on paper, (b): PEEQ reported by the paper for distortion control of 0.1 and stiffness hourglass [28], (c): Temperature obtained (in Kelvin), (d): Temperature reported by the paper for distortion control of 0.1 and stiffness hourglass [28]

In the case of use of damage criterion, with JC damage, it is advised to use the slave surface of in the interaction as node region, however the obtained result is not at all reasonable. By changing the slave surface as surface region, the problem got solved and by choosing the limit of 2.4 for PEEQ for removal of element in field output similar results are obtained.

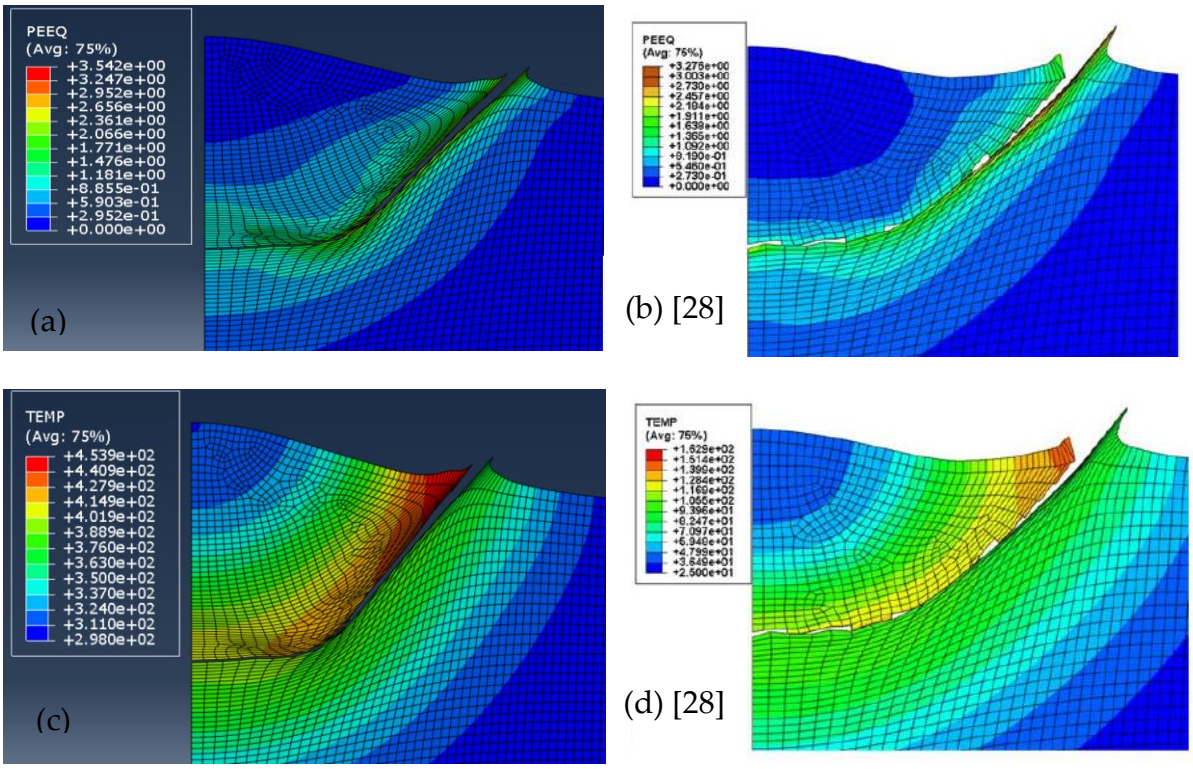

Figure 26_(a): Obtained PEEQ_ Damage Criterion, (b): Reported PEEQ_ Damage Criterion [28], (c): Obtained Temp_ Damage Criterion (Kelvin), (d): Reported Temp_ Damage Criterion [28] (Degrees of Centigrade)

Even though it was tried to obtain the same results as Wen-Ya Li et al [28], with their model parameters, due to unavailability of J-C damage parameters for SS316, finally for obtaining the stress field in the single particle impact analysis, element death method has not been used, as well due to some unrealistic material jet zone, the usage of ALE is avoided.

The implementation of the proportional mesh size between the particle and the substrate mentioned in this the work of Wen-Ya Li et al[28] enables the completion of the job for quasi high temperature and high velocity of particle, which beforehand was not possible due to over distortion in some elements in the particle. The comparison of the trend of radial and axial stress for particle temperature of 1600K, and particle

velocity of 500 m/s with the paper published by Oviedo et al [18], is presented in Figure 27.

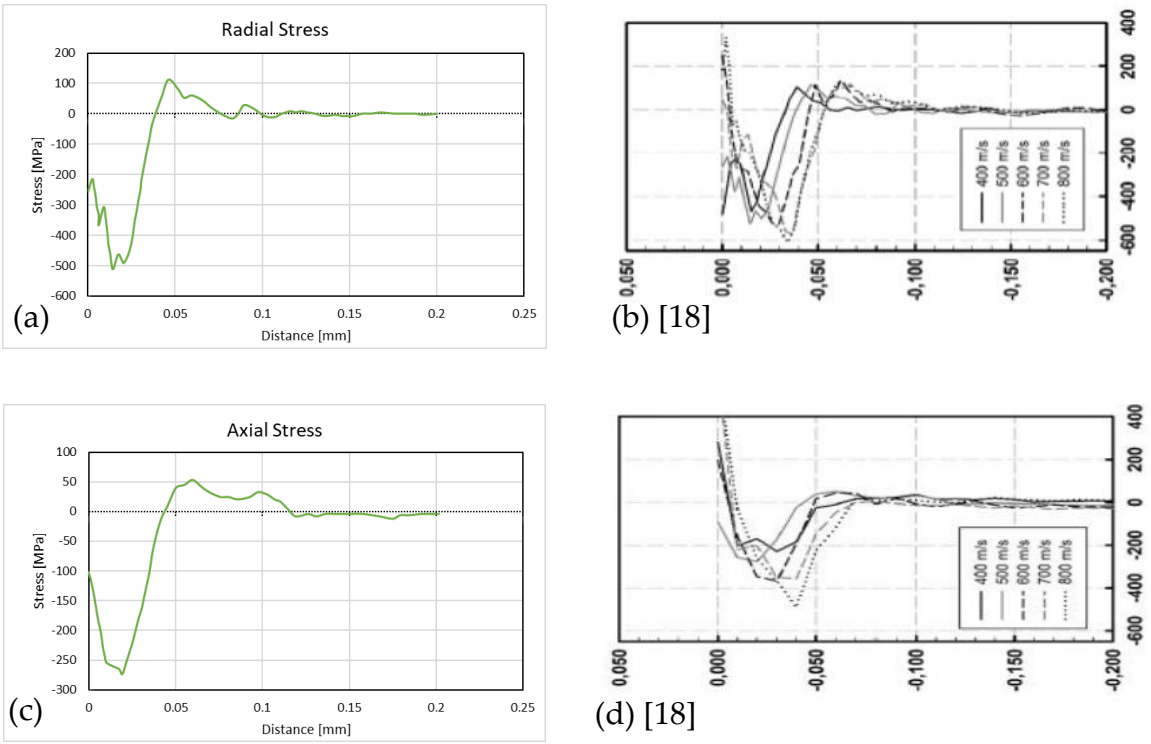

Figure 27_ (a): Obtained radial stress (S11) with particle temperature and velocity of 1600K and 500m/s, (b): Reported S11 for different impacting velocities and particle temp of 1600 K [18], (c): Obtained axial stress (S22) with particle temp and velocity of 1600K and temp of 1600, (d): Reported S22 for different impacting velocities and particle temp of 1600 K [18].

Even though comparable results for radial and axial stresses in the axis of axisymmetric geometry was obtained with respect to results presented by Oviedo et al [18]. the problem was not resolved for the impact velocity of 900 m/s and particle temperature of 1600K.

In the paper published by Rahmati et al [39], it was recommended for the sake of decrease of instability to describe the elastic behavior of particle with EOS (equation of state) and Shear Modulus. The EOS parameters of SS316 were obtained from Los Alamos laboratory. The EOS parameters of SS316 are mentioned in Table 5.

Table 5_ EOS parameters of standard materials [40]

Material	ρ_0 $[\frac{g}{cm^3}]$	C_0	s	γ_0
AL6061	2.703	5.288	1.3756	2.14
SS316	7.960	4.464	1.544	2.17
PMMA	1.186	2.65	1.494	

The similar problem, as excessive distortion in a number of elements in particle was the reason of not achieving convergence.

Based on the decision by W.Y. Li, et al [28] an initial distance between the particle and the substrate assembly was chosen, in combination with solutions already mentioned, but still the excessive distortion of small elements was the reason of non-completion of the job.

As mentioned by S. Bagherifard et al [41], one of the demanding aspects of high velocity impact simulations is the wave speed spread through the elements and the fluctuations of this wave which remain in the model preventing the possibility of having stable results. So in the 3D model of the single particle impact, the half infinite bottom-up elements have been used in the boundaries of the model in order to damp the wave fluctuations.

In the Figure 28, the implementation of preferred method by this paper [41] for the Explicit single particle impact of SS316 is presented. In (A), the assembly of particle and substrate, and in (B), the after-impact situation of the elements can be seen.

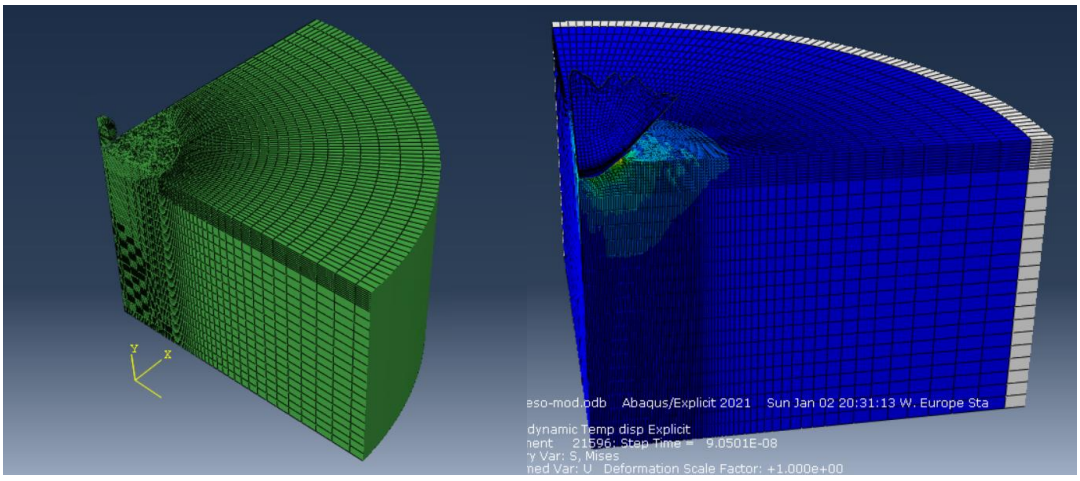

Figure 28_Representation of implementation of the method use in the paper published by Bagherifard et, al [41]

Non completion of job with no possibility of convergence due to excessive distortion of some elements in the particle was witnessed.

Then based on a Doctoral thesis entitled as Simulation of cold spray particle deposition by Paul Profizi [3], the Coupled Eulerian Lagrangian numerical approach (CEL) was implemented. This approach permits to avoid problems of excessive mesh distortion and unrealistic deformed shape which is a result of the physically enhanced modeling of fluid-like particle by the CEL particle model. Noting that the material jet still occurs at the substrate surface, but it does not affect the completion of calculation. [3]

In Figure 29, the remodeling of the Explicit single impact particle for Al particle-substrate assembly is presented with comparison to the results reported by Paul Profizi[3].

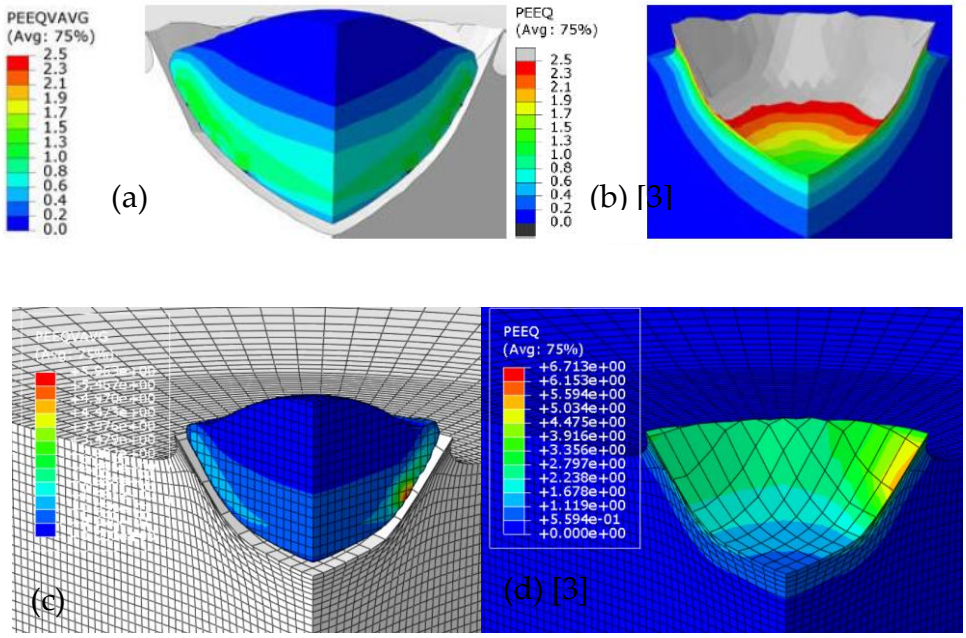

Figure 29_ Contours of (a) volume average equivalent plastic strain of Al particle and(b) equivalent plastic strain of Al substrate by using the CEL numerical approach at 700m/s, reported by the PHD thesis [3], (c) volume average equivalent plastic strain of Al particle and (d) equivalent plastic strain of Al substrate by using the CEL numerical approach at 700m/s, modeled [3]

As already mentioned, this approach permits to avoid problems of excessive mesh distortion and unrealistic deformed shape. The implementation of CEL approach for the particle-substrate assembly, would resolve the problem of non-convergence

already witnessed. The following succession of pictures in Figure 30, presents the evolution of mises stress during Explicit single particle impact for particle with the Temperature of 1600K and velocity of impact of 500m/s.

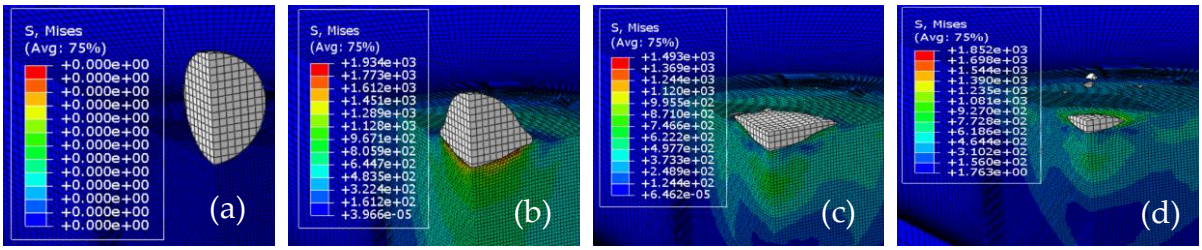

Figure 30_ Representation of history of evolution of mises stress during Explicit single particle impact with CEL method

2.3.3. Peening Stress prediction

Coatings is the consequence of several dynamic processes. A peening stress profile appears due to the impact of each particle that produce plastic deformation. Subsequently, thermal stresses are induced during the cooling down due to the thermal expansion mismatch. The subsequent deposition of layers of material and the balance of forces and moments through the thickness determine a profile of residual stresses.

As already mentioned, the computational cost of the explicit analysis does not justify modelling the coating process on a particle-by-particle impact basis. Further simplification based on an implicit methodology is required. So, layer by layer deposition for modeling the coating growth would be necessary. In the previous phrase, layer refers to several attached number of splats with the same thickness which can be obtained according to previously completed Explicit single particle impact step.

A two-dimensional axisymmetric FE model, employing the same reference cylindrical coordinate system of the single impact model, is developed assuming that the residual stress profile in both axial and radial directions under a single particle impact is repeatedly applied along the layer width. The overall representation of the model is shown in Figure 31.

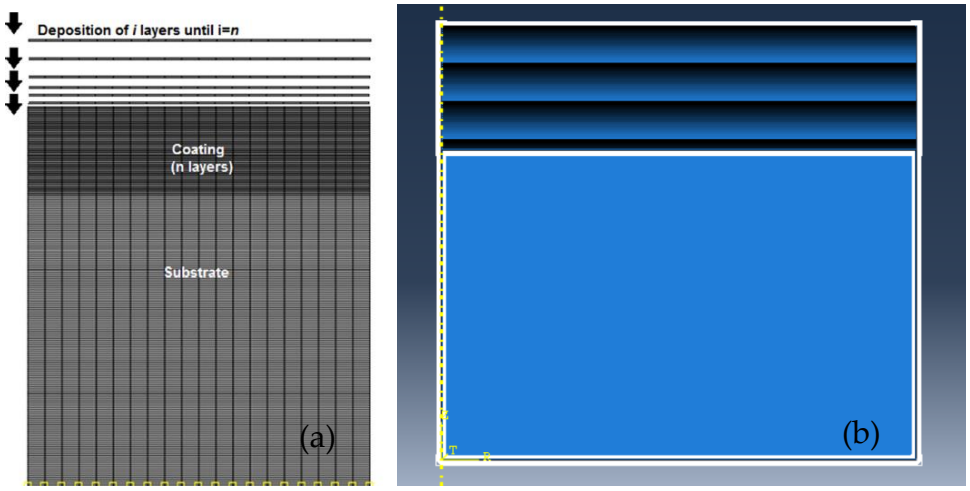

Figure 31_The overall representation of the layer deposition process[18]

The exemplary representation demonstrates extracted S11 (radial stress) and S22 (axial stress) from Explicit single particle impact in the axisymmetric axis of axisymmetric model in the substrate for the particle velocity of 500m/s and particle temperature of 1600 K is shown in Figure 32. The shown stress profiles should be tried to be induced in the implicit model for the assembly of one layer and the substrate. Then with generalization for the rest of the added layer (addition of stress for each layer after deposition of each layer), the evolution of peening stress during cold pray process for addition of 40 layers would be completed. It should be mentioned that the thickness of each added layer is obtained based on the final diameter of the deformed particle at the axisymmetric axis of axisymmetric part of Explicit single particle impact step.

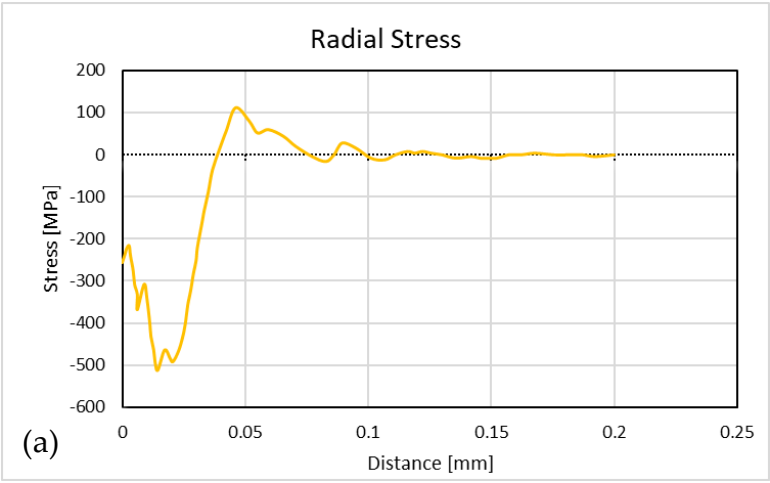

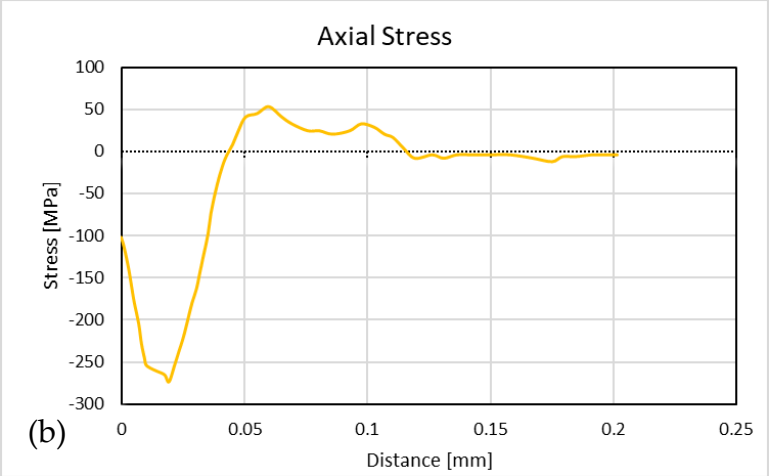

Figure 32_ (a): Radial stress as a function of distance from the top surface of substrate, (b): Axial stress as a function of distance from the top surface of substrate

Here after, different methods used for obtaining the peening stress are described.

It should be reminded that based on the descriptive name of the method, it is possible to know the loading condition and the applied area. (S refers to the substrate, and L refers to the added layers)

2.3.3.1. S-Axial Pressure-Radial Pressure-Predefined Radial Initial Stress

To induce the referred stress filed which is independent of radial position in the model, as is just a function of axial distance from the top surface of the substrate, initially sectioning in the assembly of substate- layers is used. The top 0.2 mm of the substrate is split in 40 parts (each section with the thickness of 5 microns, as well sectioning the added layer to 2 sections each with the thickness of 5 micron.). The mentioned sectioning lines would provide us with the possibility of applying radial, axial pressures, and definition of initial stress for the mentioned 40, 5micron thick sections in the top part of the substrate. It should be mentioned that for the sake of application of radial stress on the free edge of the axisymmetric model the DLOAD subroutine is used, as well the SIGINI subroutine has been used for the introduction of initial stress in the 40 sectioned parts in the top part of the substrate. The reason for the usage of only top 0.2 mm of the substrate for application of initial stress, radial and axial stress relies in the observation of the S11 and S22 obtained from Explicit single particle impact. As it is shown in Figure 32 (a)(b), the value of S11 and S22 at the depth higher than 0.2 mm in the substrate are negligible.

To obtain the desired stress field, radial pressure on the free edge of the model, axial pressures are applied on the horizontal section lines in the substrate, and initial stresses in the 40-layers created in the top part of the substrate, a corrective iterative process has been used.

The nature of this corrective approach which has been used by Oviedo et al[18] and Bansal et al[20] is explained here after:

given depth z, the residual stress from the explicit particle impact analysis$\sigma^{res}(z)$ can be approximately implemented in the layer deposition model by applying a load (or initial stress) of P_0= - $\sigma^{res}(z)$ to all elements along the radially outward line at that depth. To decrease the difference between the desired value (obtained stress from explicit single particle impact) and the stress state after equilibrium, the Equation 2-1 was implemented.

$$P_{j+1}(z) = P_j(z) + \alpha(\sigma^{res}(z) - \sigma^{FE}(z)) \qquad \text{Equation 2-1}$$

In Equation 2-1, $\sigma^{res}(z)$, refers to the desired stress either in the radial or axial direction. $\sigma^{FE}(z)$) is the response after equilibrium in the system, and the α being taken as -1. (However, for having less iteration, at first, α can be chosen bigger in value.)

The iterative process will continue till the following criterion reported in Equation 2-2 is satisfied:

$$\int_0^{z_r}\left(\sigma^{res}(z) - \sigma^{FE}(z)\right)dz \leq error \qquad \text{Equation 2-2}$$

The value of z_r , $error$ in order are considered 0.2mm and 0.02. this means that the difference between the areas under the target and the imposed stress-depth curves is within 10%.

1- Induction of S11 obtained from explicit single particle impact:

In order to induce radial stress, first the initial stresses are introduced to the 0.2 mm top sectioned part of the substrate. Obviously due to the presence of free edge the independence only with the application of initial stress in direction s11 and s33 cannot be achieved. So, in addition to the mentioned initial stress in the radial direction, the radial pressures on the free edge will be applied to decrease the free edge effect. The correction process for both applied radial initial stresses and radial pressures would be difficult. By observation, it was seen that far from the free edge, the overall effect is ruled by initial stress. So initially the radial stress obtained from explicit step will be introduced as predefined radial initial stresses in the sectioned top part of the

substrate. After completion of static step, with the help of ODB file, 11 paths far from the free edge will be created, the average of the stresses for corresponding nodes will be obtained. As already mentioned, using Equation 2-1 the correction of the introduced predefined radial initial stress will be done, till the error gets less than defined threshold of 10 percent. The representation of the applied initial stresses and evolution of error during iteration are presented in Figure 33.

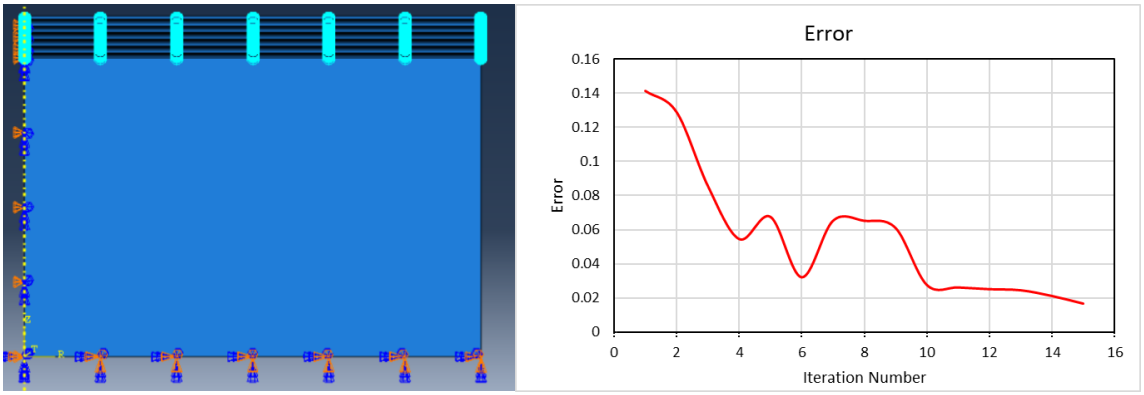

Figure 33_The representation of the applied initial stresses and evolution of error during iteration

As mentioned, the effect of free edge would be decreased by addition of radial pressures on top 0.2 mm of the right free edge of the substrate. In the same manner as the previous iteration for initial stresses, initially radial stress will be applied on the free edge. By definition of 3 paths near the free edge, the error though mentioned iterative approach will be decreased below threshold of 2%. The representation of the applied radial pressure is presented in Figure 34.

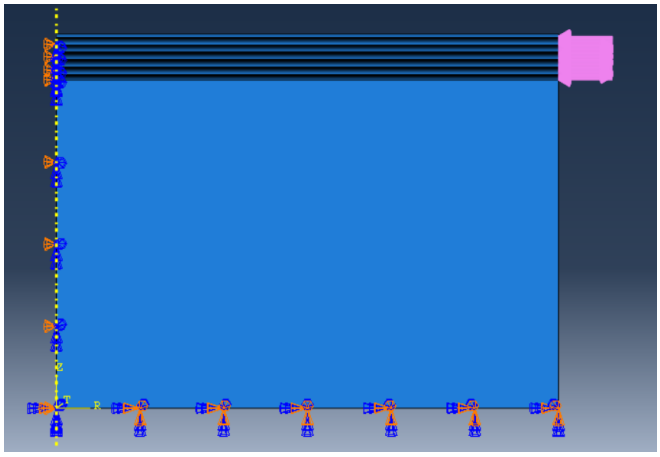

Figure 34_The representation of the applied radial pressure

In Figure 35, the stress state after application of radial pressures and predefined radial initial stresses are shown for radial and axial directions. As it can be seen in Figure 35 (A) and (B), the uniformity of the stress along radial direction and quasi-independence of stress profile from radial position in the substrate is guaranteed. As well, based on Figure 35 (C), it is obvious that the mentioned loading condition does not have considerable effect in axial stress state.

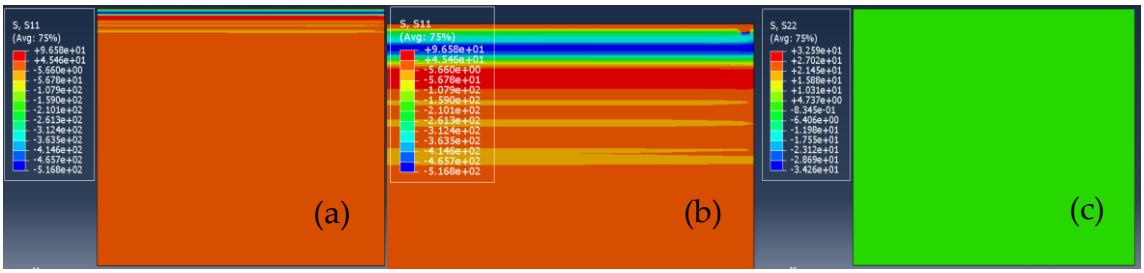

Figure 35_ Stress profiles after addition of corrected radial pressure on the right edge and corrected predefined radial initial stress in the top 0.2 mm of the substrate (a), (b): radial stress profile (c): axial stress profile

2. Induction of S22 obtained from explicit single particle impact:

In the same manner, the axially applied pressures would be corrected to obtain the desired axial stresses as described by explicit single particle impact. The only difference between correction in axial and radial pressure is that, in axial direct, the initial pressures are the differences of pressures to induce the desired axial stress profile, not the stresses read from explicit single particle impact themselves. To decrease the error lower than 10 percent, the difference between the average of nodes in 7 paths equally spaced in the top 0.2 mm of the substrate and the desired axial stress is taken into consideration. The representation of the applied axial pressures and the evolution of error during iterative process are presented in Figure 36.

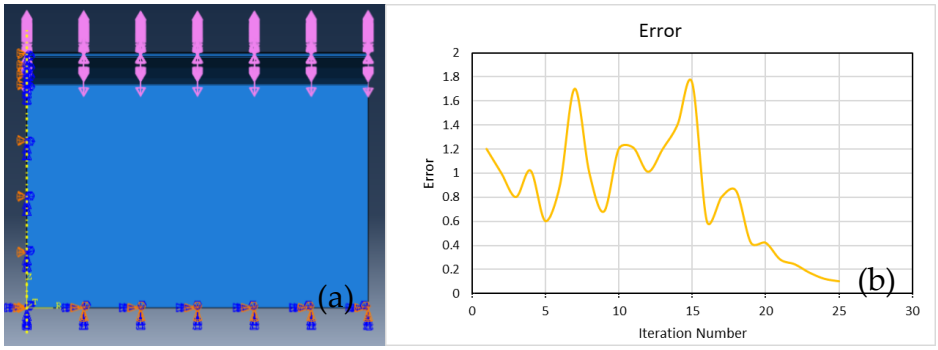

Figure 36_ The representation of (a): the applied axial pressures and (b): the evolution of error during iterative process

3. Simultaneous effect of found radial initial stress, axial and radial pressure

By having the simultaneous effect of corrected pressures in radial and axial direction and applied initial stresses, the induced stresses even though independent of the radial position in the substrate, the magnitudes due to mutual effects are higher.

4. Final correction in case of presence of all the loads

The effect of axial pressures on the radial direction was significant, but the effect of radial pressures and initial stresses in radial direction on the stresses in axial direction was negligible. So, another time the corrective iteration for the radial initial stresses and radially applied pressures was carried out.

By completing the iterative process another time, the desired radial and axial stresses representing peening stresses in one added layer are obtained. The mentioned stress field can be seen in Figure 37 (a)and (c), as well the axial and radial stresses along a specific path(the path is shown in Figure 37 (c), are presented in Figure 37 (b) and (d).

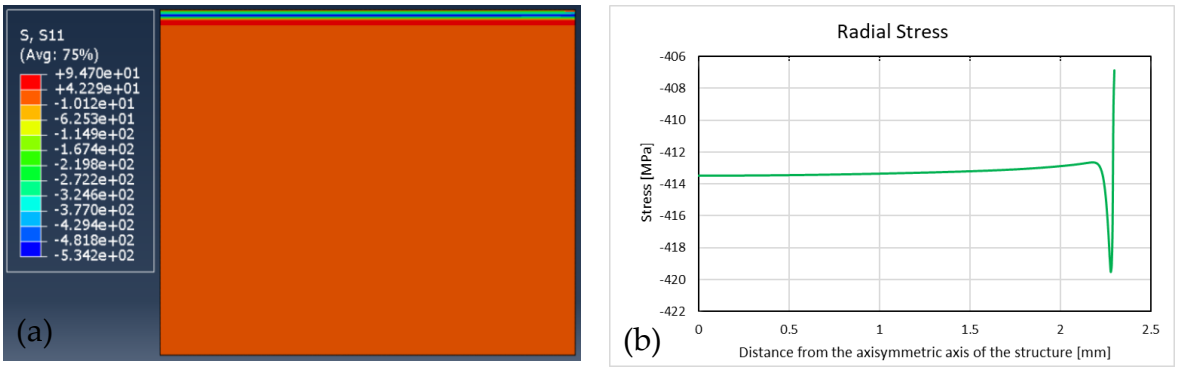

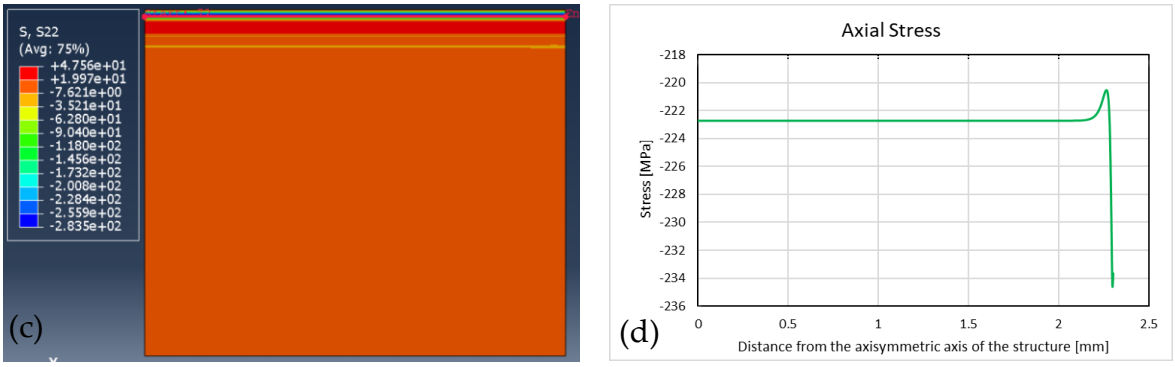

Figure 37_ After application of Radial, Axial pressure, and initial stresses (a): radial stress filed, (b): radial stress profile along the horizontal path, (c): axial stress field(d): axial stress along the horizontal path, The path is shown in (c)

With the implementation of the described method, we use initial stress in a part of substrate. But in the process of generalization (addition of subsequent layers), the evolution of the stress field cannot be seen, due to possibility of application of initial stress only in the initial step.

To deal with this difficulty, 40 jobs were created. Each job representing stress field after the corresponding added layer. (Ex: job no:2 shows the stress field after addition of layer number 2). Then with the help ODB file of these 40 jobs, axial and radial stresses were read from integration points and were written to the corresponding integration points in a general job with 40 steps, that was prepared to serve as a demonstrator.

Obviously to show the process of addition of layers, model change will be used to deactivate, and activate the layers whenever they are added on the initial substrate.

More information on the corrective process is provided hereby:

1- The initial pressure or initial stresses will be added by subroutine DLOAD and SIGNI.
2- The job will be submitted.
3- Text files containing data of each path will be saved.
4- The average of stresses at the nodes with the same distance from substrate top part will be obtained.
5- The satisfaction of threshold of error will be checked. (If criterion is satisfied, break the loop, otherwise continue the iteration)
6- The correction in the pressure or the initial stress will be done.

7- Another subroutine will be written with corrected values.
8- Another job will be created.
9- The new job will be submitted.
10- continue with step number 3.

The successive evolution of peening stress during layer deposition can be seen for a couple of layers in radial direction in Figure 38.

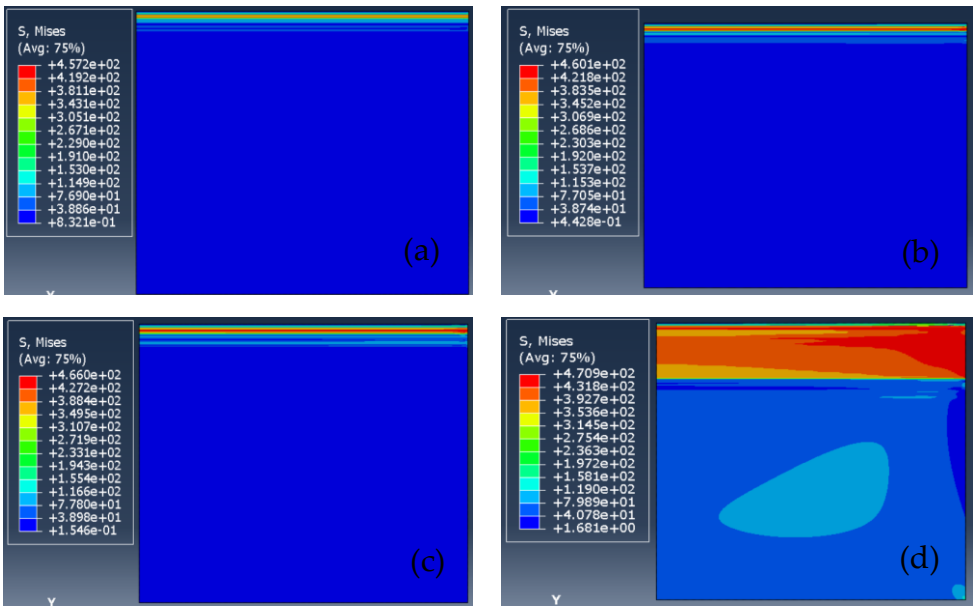

Figure 38_ The succession evolution peening stress during layer deposition, (a): stress state after deposition of 1st layer, (b): stress state after deposition of 2nd layer, (c): stress state after deposition of 3rd layer, (d): stress state after deposition of 40th layer

By comparing the results after the addition of 40 layers of SS316 on substrate made of SS316 with already mentioned dimensions, however the trend shows promising correspondence with the trend of radial and axial stresses reported by Oviedo et al[18], the amplitude of the obtained stresses based on the described method, have proven to be significantly higher.

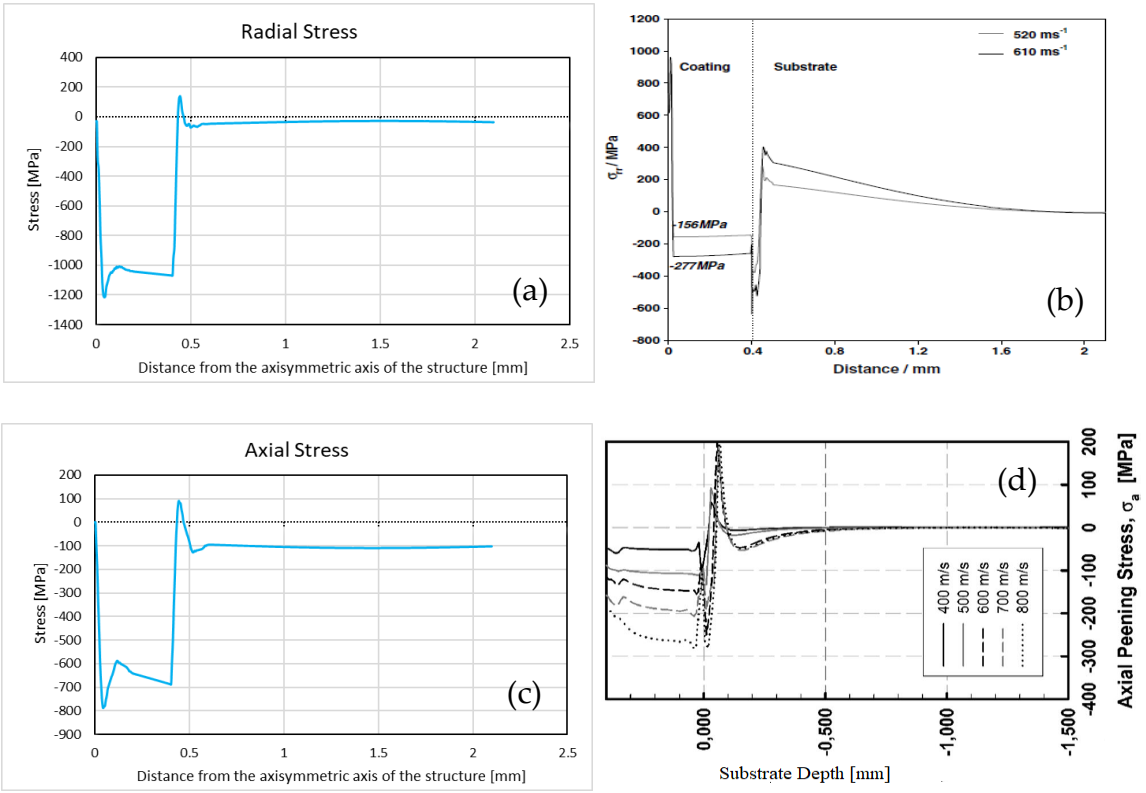

Figure 39_ Comparison of the stress trend between obtained residual stress and the reported stress, (a)(c): in order obtained radial and axial residual stress, (b)(d): in order reported radial and axial residual stress by Oviedo et al [18]

As already mentioned, the amplitudes of the obtained peening stresses are significantly higher than the amplitudes of the stresses reported by Oviedo et al[18]. In order to resolve this difficulty different methods have been used.

The used python code regarding this part can be checked in Peening Stress part of the Appendix.

2.3.3.2. S-Axial Pressure-Radial Pressure-Predefined Radial Initial Stress- time increase

This method is based on S-Axial Pressure-Radial Pressure-Predefined Radial Initial Stress method with minor changes. Stating the obvious, in a static analysis which is being used in the case of obtaining peening stress, the used duration of time is not important, as the solver applies the load in the form of ramp, increasing the loads form the 0 value to the allocated values. However, for the sake of reassurance, the duration of time in the last job representing the last step was increased by the multiplier factor of 40, to check any possible differences. As already well understood, no change has been witnessed.

2.3.3.3. S-Axial Pressure-Radial Pressure-Predefined Radial Initial Stress- step-number

This method is based on S-Axial Pressure-Radial Pressure-Predefined Radial Initial Stress method with minor changes. Obviously, the predefined initial stresses can be applied to the structure just in the initial step, however, it is possible to apply the mentioned axial and radial pressures, in their corresponding step, instead of being applied all at the same time. After completion of this model, no obvious changes in the obtained results have been noticed with respect to the results obtained by S-Axial Pressure-Radial Pressure-Predefined Radial Initial Stress method.

2.3.3.4. S-Axial Pressure-Radial Pressure-Predefined Radial Initial Stress- step-number- Model change

In the method referred as S-Axial Pressure-Radial Pressure-Predefined Radial Initial Stress- step-number, in the jobs corresponding the addition of J^{th} layer, the previous layers were present without any deactivation. (1 to J layer, even though the layers after layer J were deactivated). In this method in each steps model change and activation and deactivation of layers before layer number J are done. By completion of the process, the exact same results as previous methods have been obtained.

2.3.3.5. S-Axial pressure with/without Predefined Initial Radial+ Load amplitude-40 steps (Comparison in the axial direction only)

This method is based on the S-Axial Pressure-Radial Pressure-Predefined Radial Initial Stress- step-number- Model change, as the number of steps is 40, and the loads are applied at their corresponding step. (For the sake of comparison only the application of predefined initial radial stress is applied or not applied). The sole difference is the use of amplitude in the applied loads in the form of ramp defined with 4 points.

The comparison between the extracted axial stress from single particle impact analysis and the induced axial stress after addition of first layer with application of axial pressures in the substrate and with/without the presence of the predefined initial radial stress in the substrate is presented in Figure 40.

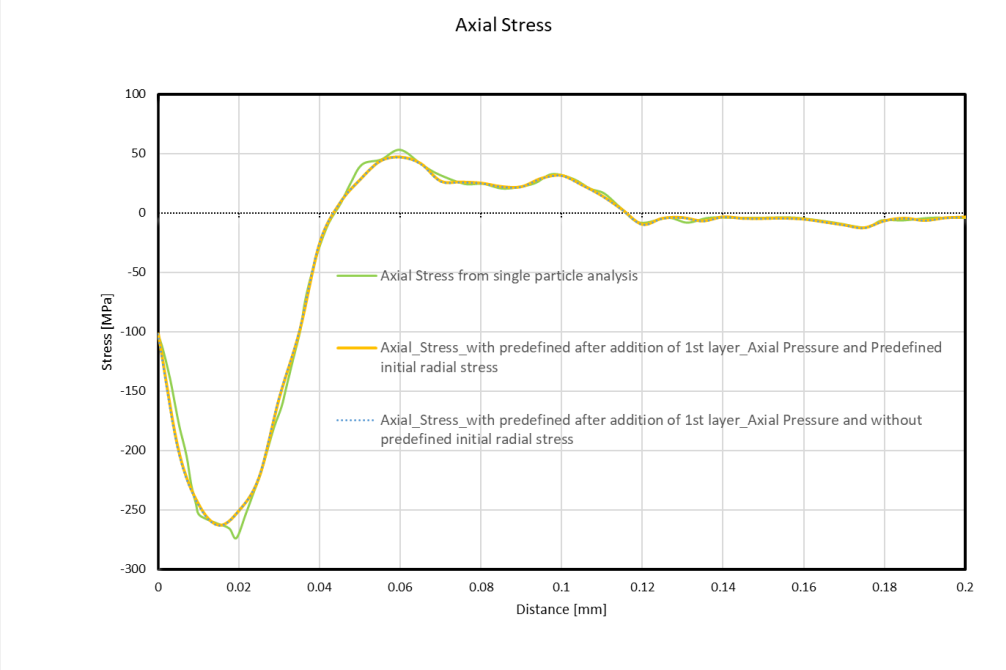

Figure 40_The comparison between the extracted axial stress from single particle impact analysis and the induced axial stress after addition of first layer with application of axial pressures in the substrate and with/without the presence of the predefined initial radial stress in the substrate

The comparison of axial stress after deposition of 40 layers with different conditions is presented in the Figure 41.

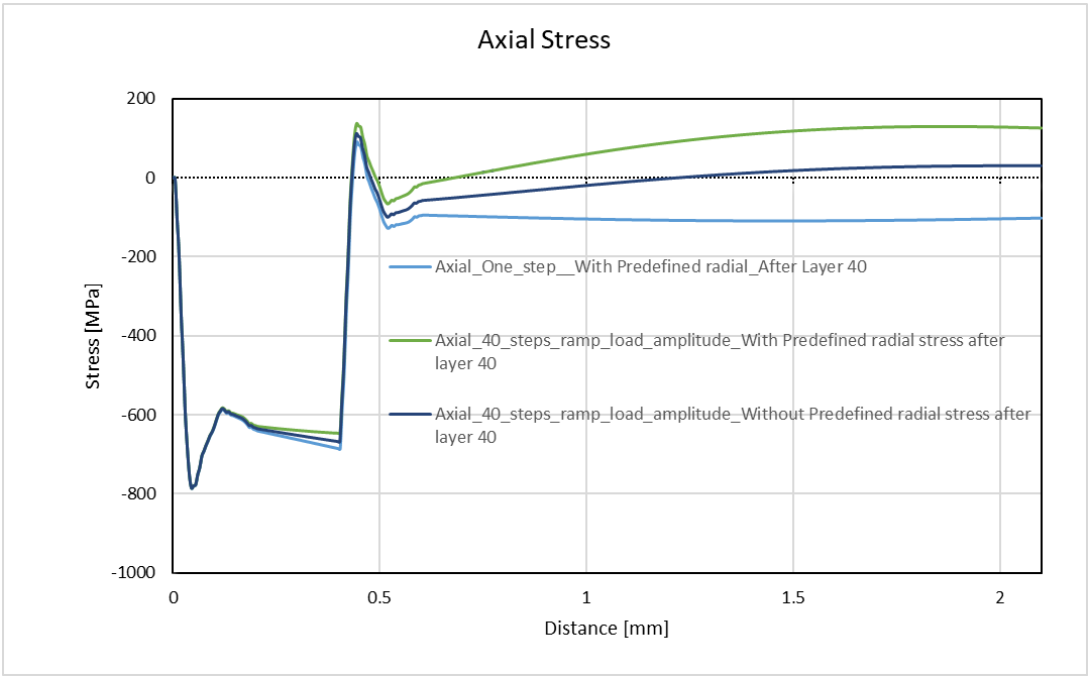

Figure 41_ Representation of the comparison of the obtained axial stress after deposition of 40 layers with different conditions: 1- One step_ with axial pressure and predefined initial radial

stress, 2- 40 steps_ with axial pressure and load amplitude, 3- 40 steps_ with axial pressure and load amplitude_ with predefined radial initial stress

2.3.3.6. S- (S-Axial Pressure -Predefined Radial Initial Stress) as initial-Axial pressure

This method as well uses the same procedure used by S-Axial Pressure-Radial Pressure-Predefined Radial Initial Stress with some profound differences in the generalization (layer addition process) of applied loads with addition of layers. The steps to implement this method are described hereby:

1- First the job representing the addition process of layer one gets completed which complied to the extracted stresses profile in the axis of axisymmetric structure in single particle impact analysis by implementation of the iterative corrective approach mentioned before. (So, the stress profile after addition of first layer is obtained)
2- For job number 2, or to be more specific the step representing addition of second layer, the generalized predefined stress for 2 layers, is added to the structure of model 2, as well, axial, and radial pressures needed for induction of first layer stresses are added. (Just 1 pairs of sets of axial and radial pressures are applied)
3- The result obtained from step 2, will be applied in a copy of model 2, as predefined initial radial and axial stresses, with addition of the same axial and radial pressures used in step one, with a shift in the zone of application for considering the thickness of newly added layer (layer number 2) (At the end of this step, results after addition of layer 2 are obtained)
4- Now in this step, we go to step number 2, providing the detailed for next step by increasing all the indices by +1.
5- Then we go to step 3, increasing all the indices by +1

By obtaining the results for 40 layers and comparing the results with the results reported by Oviedo et al [18], no promising results were obtained, as in the case of axial stress, no compliance has been witnessed, and no distinguishable separation line between the stresses of added layers and substrate has been seen. In addition, even though in radial direction the boundary between added layers and substrate was obvious, the abrupt increase of amplitude of the stress due to presence of axial pressure, did not let the trend to be comparable to Oviedo et al [18].

2.3.3.7. L-Predefined initial radial, axial and in plane shear stress

Instead of application of radial, axial pressures, and initial stresses in the radial direction in the substrate right below each of the added layers, which was previously described mentioned in S-Axial Pressure-Radial Pressure-Predefined Radial Initial Stress method, the initial stress in the radial direction (s11, S33), axial direction (s22), and in plane shear stress (s12) has been applied to each of the deposited layers with the thickness of 10 micron. Even though this method, has proven to have less control over the profile of imposed stress in the substrate, it has shown to be a worthy method, as the difficulties during the development of the model with the previous model has been resolved.(mentioned difficulty refers to the lengthy process of having 40 jobs representing 40 steps of material deposition, then the reading and writing each variables to another ODB file which has served as a demonstrator).

In this method, even though the overall trend of induced residual stress seems like the reported stress trends, the amplitude is significantly higher. In addition, there is considerably less control to induce the residual stress for the first, as well the uniformity seen in the radial direction, and independence of the stresses from the radial position cannot be seen.

2.3.3.8. S-Axial pressure, L- Predefined initial radial and axial stress

The initial stresses in the radial direction (s11, S33), axial direction (s22) has been applied to each of the deposited layers, and axial pressure have been applied right below the added layer to better induce the stress profile obtained by Single particle impact. The advantage of this method with respect to L-Predefined initial radial, axial and in plane shear stress method is that, it can better induce desired stresses for the first layer, as well it is easier to implement with respect to S-Axial Pressure-Radial Pressure-Predefined Radial Initial Stress method.

Even though the below mentioned radial and axial stresses for 1 and 10 layers are not modeled with the same parameters as the paper, it has proven to be not effective neither in obtaining the amplitudes nor the trends of the stress field in the axis of the axisymmetric assembly of substrate-added layers. The obtained radial and axial residual stress after addition of 1^{st} and 10^{th} layers are presented in Figure 42.

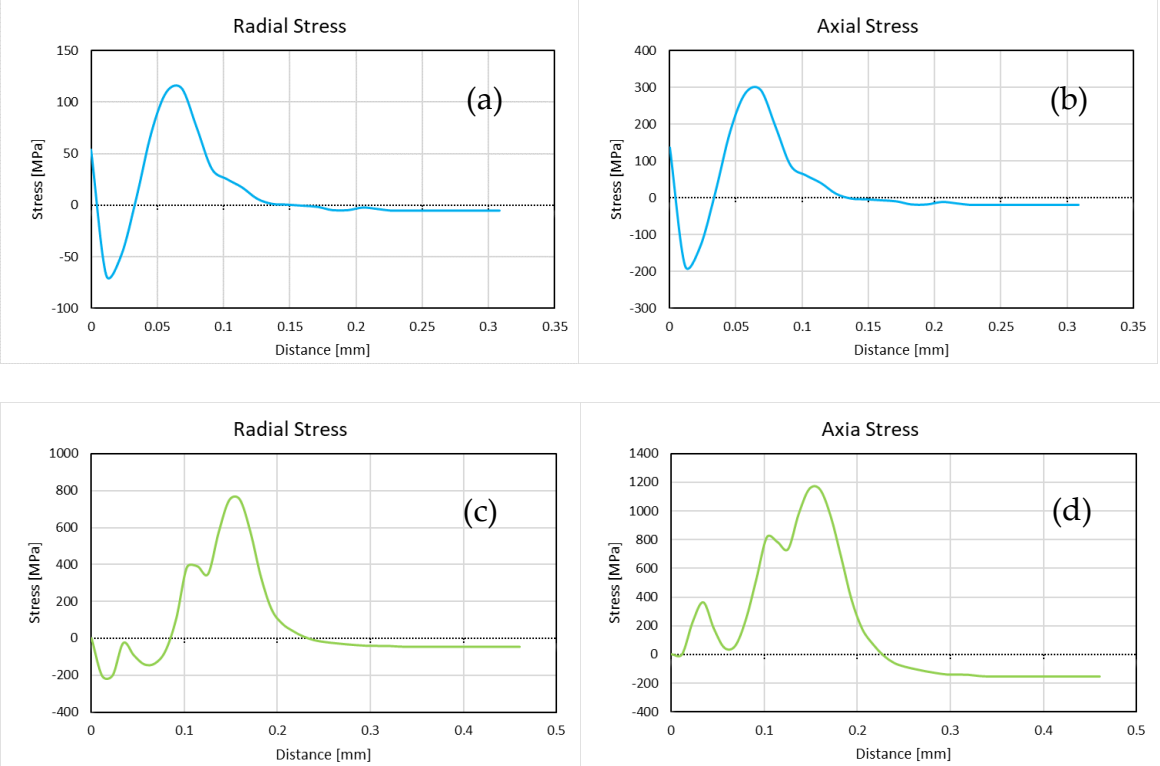

Figure 42_ (a), (b): In order obtained radial and axial residual stress after deposition of 1st layer, (c), (d): in order obtained radial and axial residual stress after deposition of 10th layer

2.3.3.9. S-Predefined initial radial stress, Axial displacement

In this method, the combination of the radial initial stress and displacement in the edges of the created layers are used for application of displacement, with the same corrective iterative approach already described, however this method has proven to be not useful and having the same problem in being able to detect the true amplitude of the stresses. The obtained residual stress after depostion of fist as well as 82nd layers in radial and axial direction are presented in Figure 43, in the radial and axial direction. (Not for the same parameters, however the amplitude expectation was not fulfilled)

As it can be seen, the stress amplitude in the coating in radial and axial direction are equal to zero, the the abrupt changes are due to high difference between the values obtained by the elements at the viciny of each other for the same node.(As the difference of stress for the common edge for 2 elements is significantly high, the software does not get average of the stresses, but shows both the stresses for the same node.)

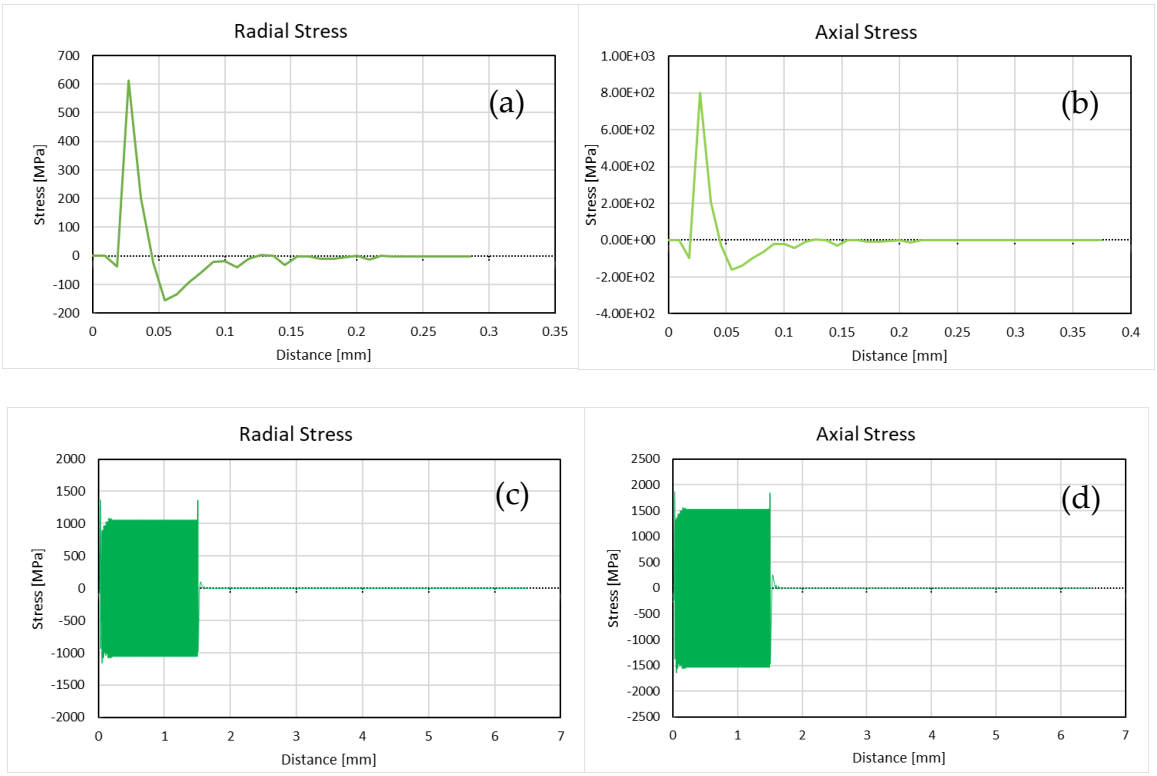

Figure 43_ Figure 41_ (a), (b): In order obtained radial and axial residual stress after deposition of 1st layer, (c), (d): in order obtained radial and axial residual stress after deposition of 82nd layer

2.3.3.10.S_Predefined radial initial stress, A to R and R to A transformation

In this method, only initial stress (radial predefined stresses in the sectioned parts will be added to induce the desired radial stress profile extracted from single particle impact analysis. As referred by Bansal et al[20], the axial distribution would not be approximated by axial pressure distribution, and for the purpose of iteration only, the axial stress profile is previously transformed into a radial stress distribtion through the

$\sigma_r = -\frac{\sigma_a}{\nu}$ Equation 2-

$\sigma_r = -\frac{\sigma_a}{\nu}$ Equation 2-4

where σ_r is the transformed residual stress in the radial direction, σ_a the residual stress in the axial direction and ν is the Poisson ratio that for SS316 is 0.33.

Then the transformed radial residual stress would be induced with the help of previously described iterative corrective approach. By having the transformed axial stress profile and radial stress profile, the generalization for addition of 40 layers has been done.

It should be mentioned that for obtaining the axial stress profile for 40 added deposition layers, the previously mentioned equation should be used in the backward direction.

The induced radial stress based on the radial stress extracted from single particle impact analysis is presented in the Figure 44. The resulting radial stress after the addition of 40 layers is carried out in 2 manners which involves averaging and generalization or generalization and then averaging.

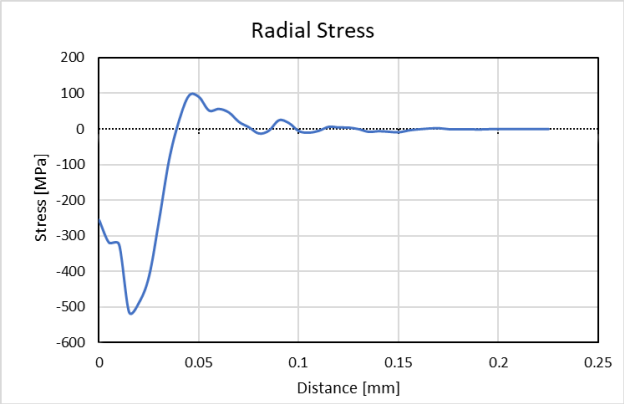

Figure 44_ Induced radial stress profile after addition of first layer

The case of generalization and averaging proved to be not a proper method, as it cannot distinguish even the separation boundary of substrate and added layers of material. Even though the method with succession of averaging and then generalization, can distinguish the separation part of substrate- layers, the obtained amplitude for radial stress is not in compliance with the results provided by Oviedo et al. [18] The obtained residual stress in radial direction after addition of 40 layers, with 2 already mentioned manners (Averaging+ Generalization or Generalization+ Averaging) are presented in Figure 45.

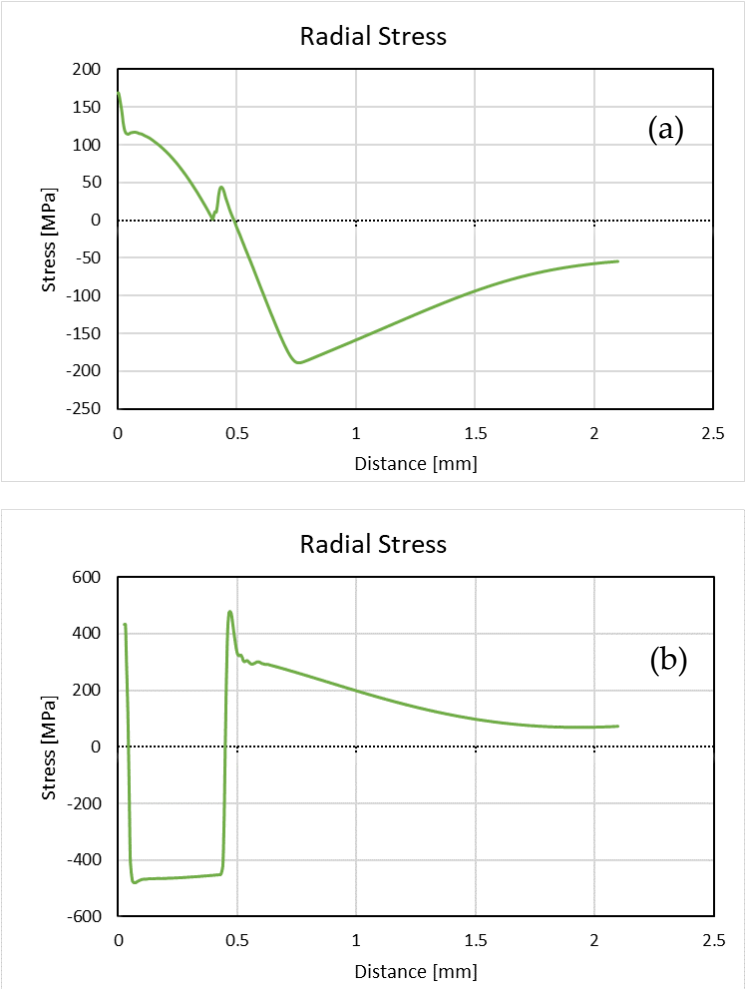

Figure 45_ Representation of induced radial residual profile after addition of 40 layers, (a): with generalization + averaging, (b): with averaging + generalization

In the axial direction with the mentioned method, the obtained axial residual stress after addition of the 40 layers is presented in Figure 46.

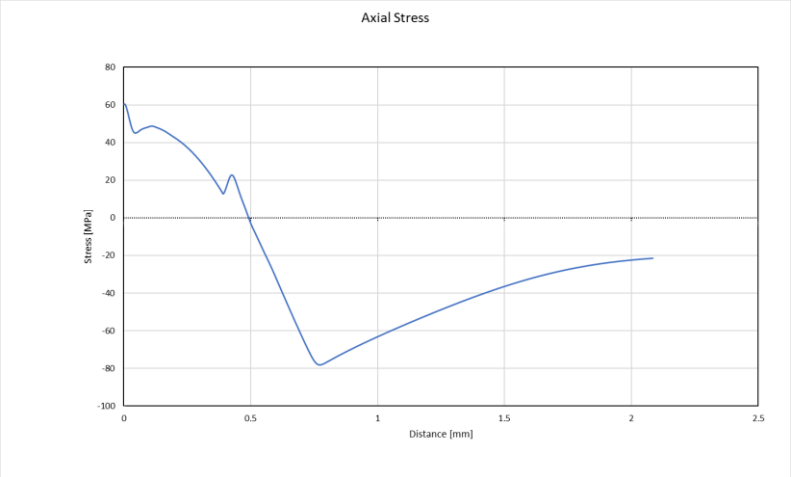

Figure 46_ Representation of induced axial residual profile after addition of 40 layers

Obviously in this method the amplitude of the compressive stress in the added layers in the radial direction is significantly higher with respect to the results reported by Oviedo et al. [18] In the case of radial direction no correspondence to the axial residual stress reported by Oviedo et al [18] after deposition of 40th layer is seen.

2.3.3.11.S_Axial pressure to get result in radial direction

In this method, it was tried to induce the radial stress with the help of axial pressures, which has proved to be not effective, as the amplitude of the obtianed radial stress, was not even closely comparable.

2.3.3.12.S_(Predefined radial initial stress, A to R and R to A transformation) as intial+reference value

In method which is basically baesed on the method proposed as S_Predefined radial initial stress, A to R and R to A transformation, with the difference that, after acquisition of the predefined-initial radial stresses in the top 0.2 mm of the substrate, they are supposed to be applied in the corresponding step, representing the duration of addition of that specifc layer. One of the first ideas to implemend this method was simply having equal number of models as the added layers, and by running the analysis for the previous steps then applying the results of previous steps as predefined field in the successive model. At the same time application of the predefined initial radial stresses responsible for induction of effect of the next added layer. However, as the common area between the predefined initial radail stresses and the predefined state would be interfearig. To deal with this issue the following steps were used.

1- Application of predefined initial radial stresses responsible for induction of radial stress after addition of first layer similar to the radial stress profile extracted from single particle impact model.
2- Making a path on the axisymmetric axis of the assembly
3- Reading the radial stress profile ast the mentioned path
4- Making another model with the presence of the next added layer
5- Application of the summation of the read stress and the predefined initial stresses responsible for induction of effect of layer number one, as predefined initial stresses.
6- Go to the step 2 repeat the steps till the addition of the last layer.

The obtined results show that this method could not obtain the comparable amplitudes in comparison to the results reported by Oviedo et al. [18]

2.3.3.13.S+L_Predefined radial initial stress (Just radial direction)

This method is based on the S_Predefined radial initial stress, A to R and R to A transformation with the difference that, it would serve only for acquisition of residual stress in the radial direction.

In this method with the help of mentioned iterative corrective approach in S-Axial Pressure-Radial Pressure-Predefined Radial Initial Stress, the predefined radial initial stresses responsible for induction of residual radial stress extracted from single particle impact analysis are obtained. The predefined initial radial stress added in the substrate is based is the absolute value of the average of the evolution of radial stress in the central node of the impacting particle in the single particle impact analysis.

In Figure 47 , the comparison of the desirable radial stress extracted from single impact particle analysis and the induced radial residual stress after addition of first layer is presented.

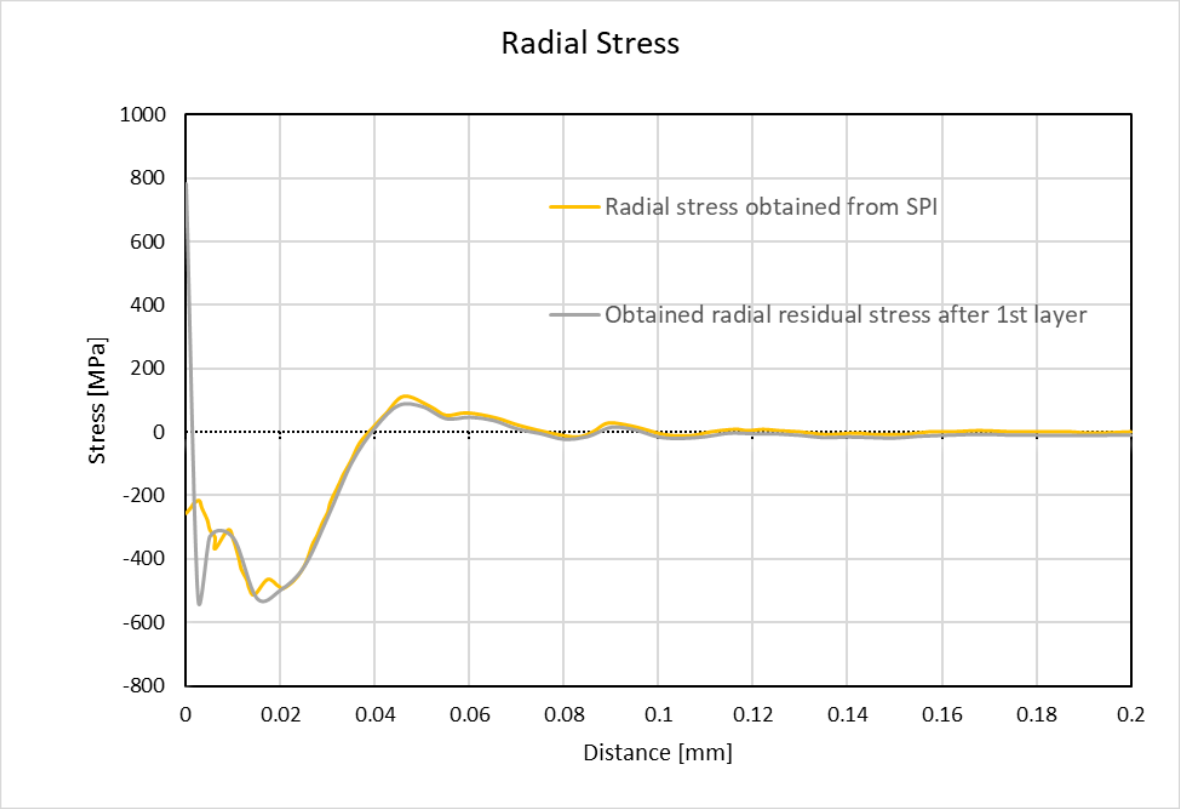

Figure 47_ Comparison of the extracted radial stress from single particle impact analysis and the obtained radial residual stress after addition of the first layer

Then the generalization of addition of the mentioned load would conclude in the acquisition of the induced radial residual stress after addition of 40th layer. The obtained residual stress in the radial direction after deposition of 40th layer is presented in Figure 48.

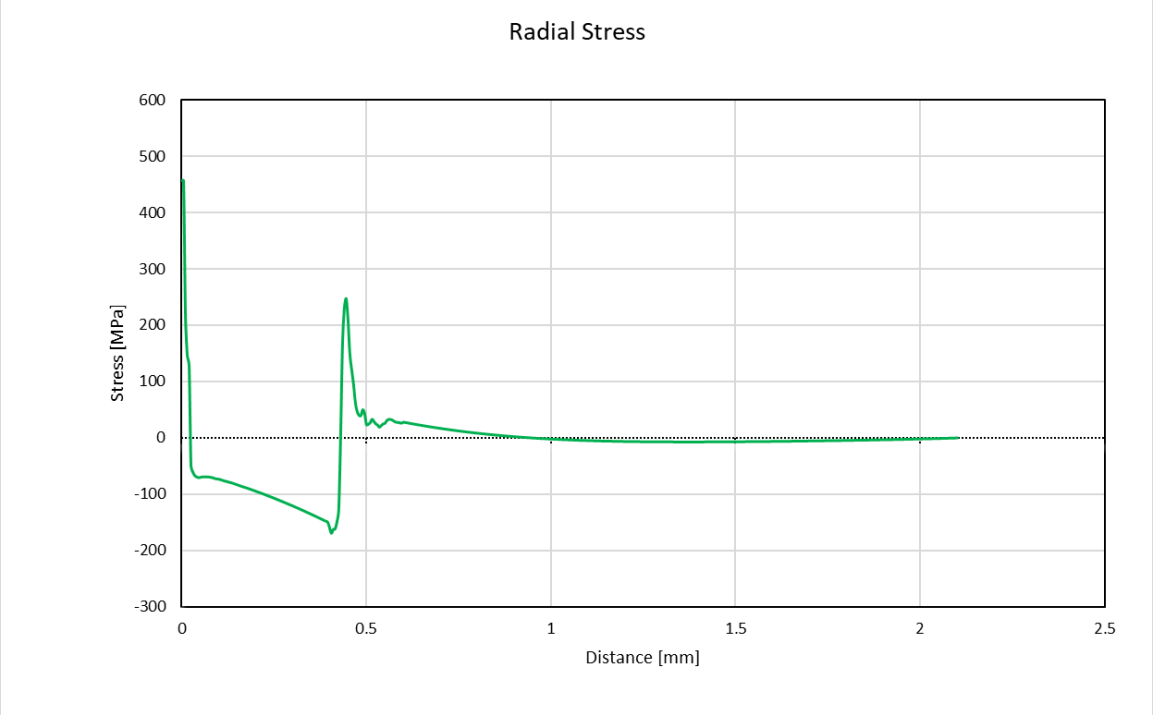

Figure 48_ Representation of induced radial residual profile after addition of 40 layers

The obtained result seems promising as presents close correspondence to the reported radial residual stress by Oviedo et al. [18]

2.3.3.14.S_ Predefined radial initial stress S22 as S11(Just axial direction)

This method is based on the S+L_Predefined radial initial stress (Just radial direction) with the difference that no predefined initial stress is applied in the added layers, and the axial stress extracted from single particle impact analysis is treated as radial stress, and finally the final obtained radial stress for 40 layer, represents the residual stress in the axial direction.

The Comparison of the obtained axial residual stress (radial stress which presents the axial stress) and the axial stress extracted from single particle impact analysis is presented in Figure 49

Figure 49_ The Comparison of the obtained axial residual stress (radial stress which presents the axial stress) and the axial stress extracted from single particle impact analysis

With the generalization of the added predefined initial stress, the induced radial residual stress which represents the residual stress in the axial direction after addition of 40 layers is obtained. The representation of the obtained axial residual stress after addition of 40th layer is presented in Figure 50.

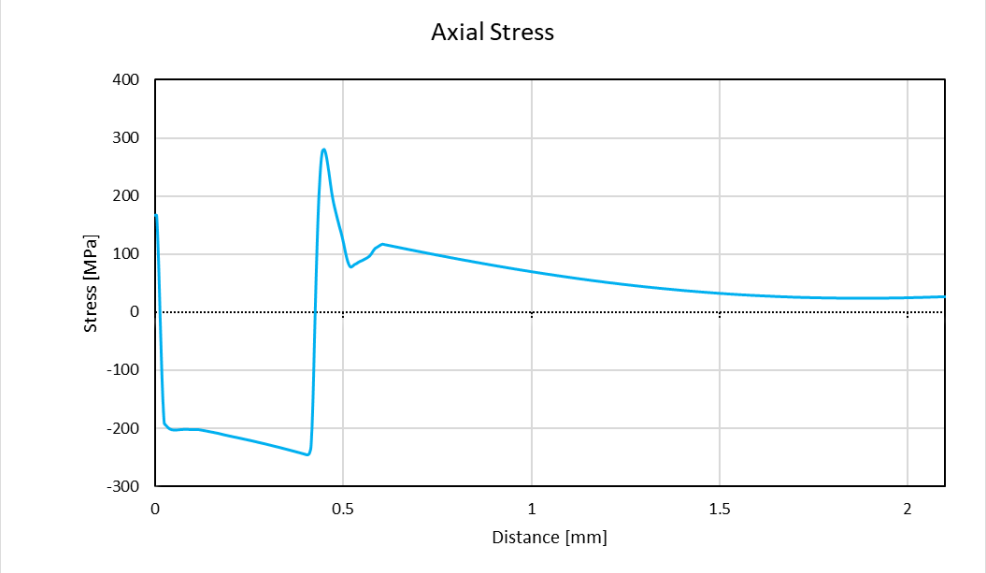

Figure 50_ The representation of the obtained axial residual stress after addition of 40th layer

2.3.3.15.S+L-Predefined Radial Initial stress (Just axial direction)

This method is based on the S_ Predefined radial initial stress S22 as S11(Just axial direction) with a modification. In this method, except for the application of predefined radial initial stress in the top part of the substrate, based on the time history of the evolution of the axial stress in the central node of the particle in single particle impact analysis, predefined radial initial stress is applied in the added layers.

In Figure 51 , the comparison of the axial stress profile extracted from single particle impact analysis and the induced axial stress after addition of the first layer is presented.

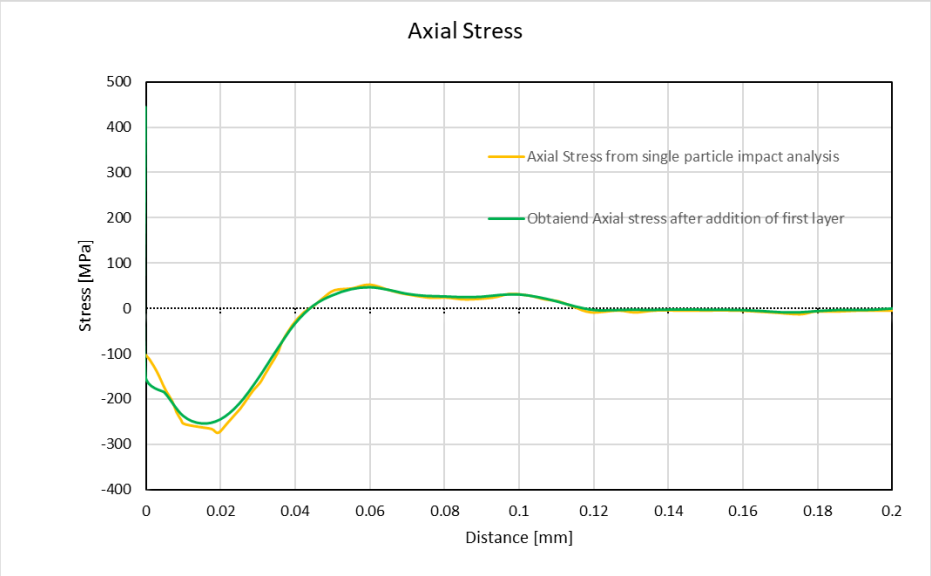

Figure 51_ Representation of the comparison of the axial stress profile extracted from single particle impact analysis and the induced axial stress after addition of the first layer

Through the generalization (successive layer addition process by repetition of the applied loads), the axial stress profile through the assembly of substrate-40 added layers are obtained. The obtained axial stress profile after addition of the 40th layer is presented in Figure 52.

Figure 52_ Representation of the obtained axial stress profile after addition of the 40th layer

2.3.3.16.S-Axial Pressure-S+L-Radial Pressure-Predefined Radial Initial Stress

With some minor modifications in the 1 layer stress profile of S-Axial Pressure-Radial Pressure-Predefined Radial Initial Stress method, is possible to obtain not only the stress trend in the assembly of substrate-layer, also closer amplitudes of stress with respect to the results presented by Oviedo et al[18] and Bansal et al. [20]

The modification regards addition of predefined initial radial and axial stress in the added layers based on the time history of the stresses in the center of accelerated particle in the explicit sinlge particle impact analysis. After deletion of the first part of the stress history in the radial and axial direction in the central node of particle, the absolute value of the averaged stresses in the radial direction and axial directions in order, were applied as predefined initial radial and axial stresses in the added layers. The Figure 53 (a),(b), in order, shows the obtained radial and axial stress profiles after addition of 1st layer.

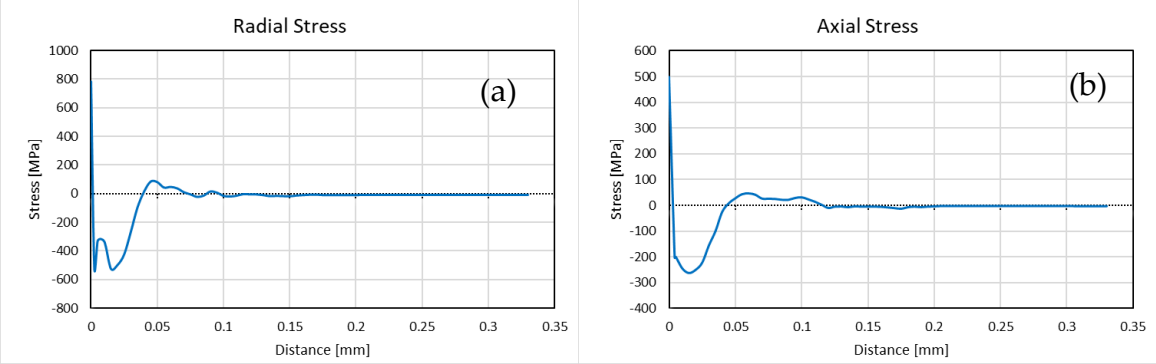

Figure 53_ Representation of the (a), (b) in order, obtained radial and axial stresses after deposition of first layer

Then by repetition of application of the loads used for inducing stresses in the substrate after addition of one layer, final peening radial and axial stresses in the assembly of substrate -layer, with 40 added layers was obtained.

The Comparision of the obtained radial and axial stresses with reported radial and axial stresses is presented in Figure 54.

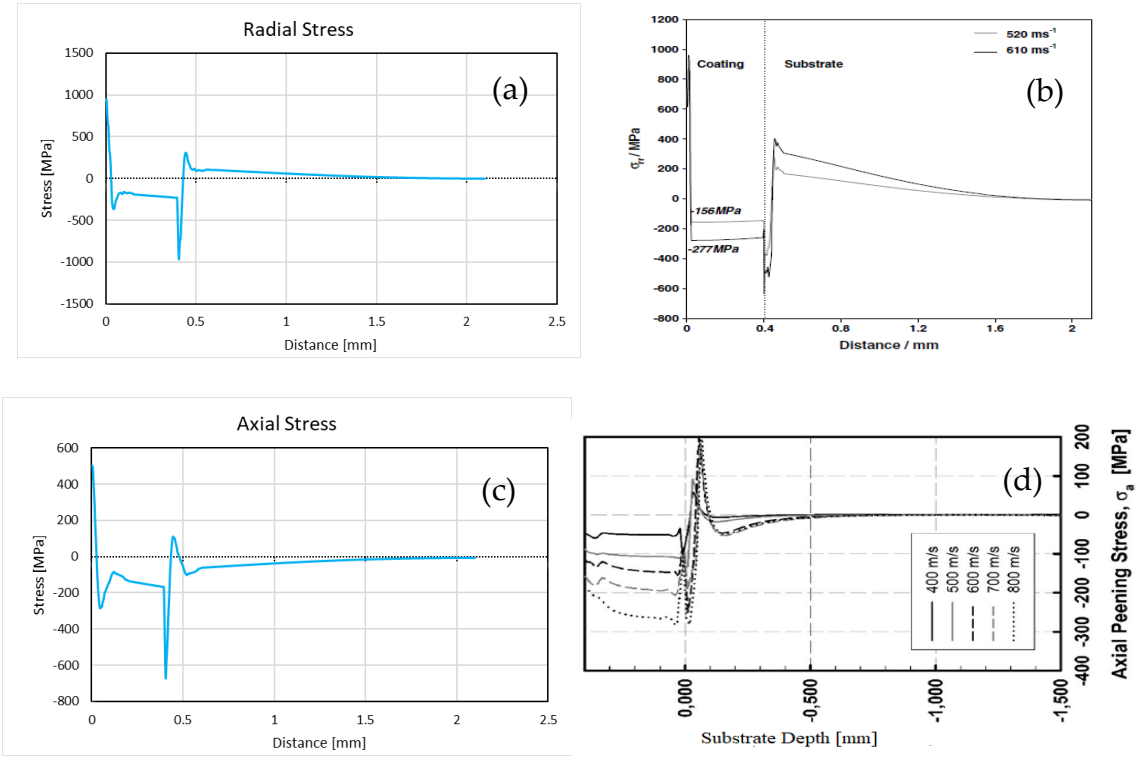

Figure 54_ The Comparison of stress profiles, (a), (c): in order, obtained radial and axial stresses after addition of 40th layer, ((b), (d): in order, reported radial and axial stress profiles after addition of 40th layer based on Oviedo et al [18]

Even though the stress profile is comparable with paper, through the use of experimental parameters, the method proves to be ineffective in obtaining the stress amplitude correctly.

2.3.4. Thermal stress

The generated thermal stress during coating deposition is predicted using a nonlinear, sequentially coupled, thermomechanical FE analysis performed in two stages. In the first stage, a heat transfer analysis is performed to obtain the thermal history of the specimen. The time-dependent temperature distribution being repeatedly applied for each layer to accumulate the final residual stress distribution.[18][20]

A two-dimensional axisymmetric FE model, employing the same reference cylindrical coordinate system of the single impact model is developed. The overall representation of the layer deposition process is shown in Figure 55.

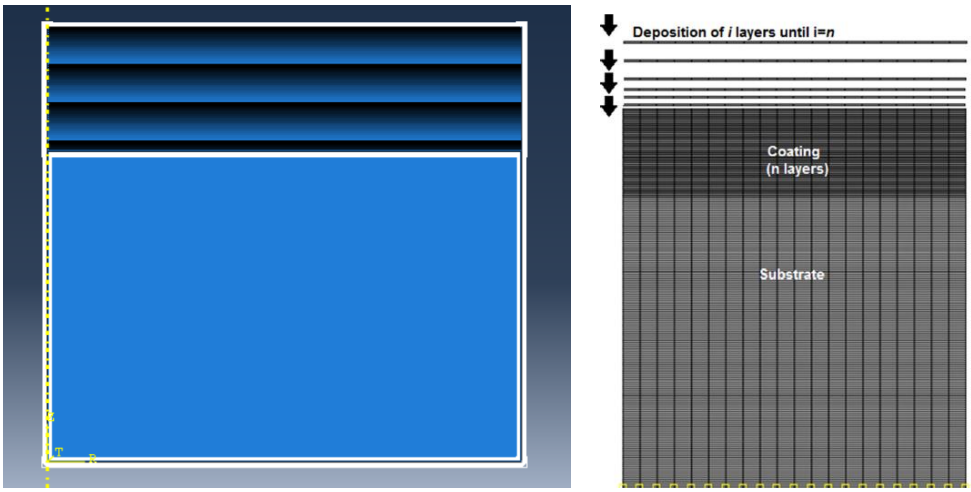

Figure 55_ The overall representation of the layer deposition process [18]

Heat transfer analysis uses four-node linear diffusive heat transfer elements. The stress analysis uses four-node bilinear, reduced integration axisymmetric stress elements with hourglass control. Temperature dependency of the conductivity is modelled.

The total duration of the process is 4 seconds, each layer deposition takes 0.1s, in total the time needed between laying each consecutive layer is 0.1 seconds.

To model heat transfer between the gas jet and the coating surface, a surface thermal load of 1 MW/m2 was applied during a time period of 40 ms.[18] This period was

estimated from the traverse velocity of the spray gun and corresponds to the time required by the spray gun to pass over a spray zone of approximately 30 mm. [20] [18]

For application of these mentioned heat flux on the top surface of the substrate, 40 amplitudes (with 4 points) were defined. It should be mentioned that the area under the defined amplitudes used for application of heat fluxes is exactly 0.04 seconds. The Representation of applied loads as well as 2 examples of the heat flux amplitudes are shown in Figure 56.

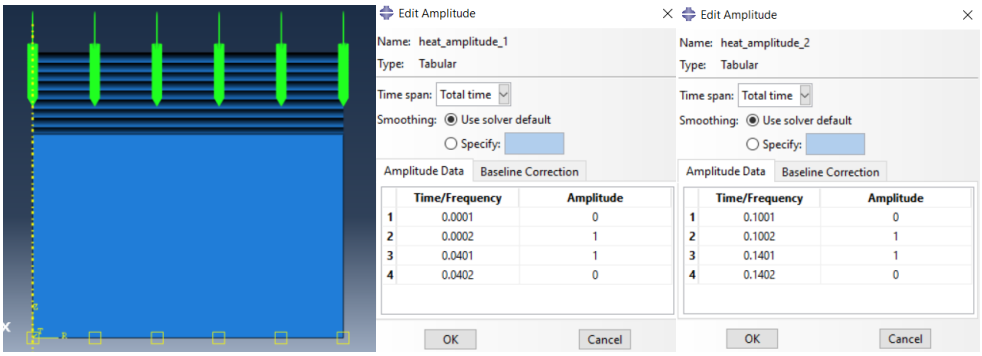

Figure 56_ The representation of applied loads as well as 2 examples of the heat flux amplitudes

As already mentioned in the process of obtaining peening stress during coating deposition, the thickness of each added layer based on the explicit single particle impact step was 10 microns. In addition, the cooling curve of a 10 microns thick splat for several deposition temperatures are presented in figure. The mentioned deposition temperature as an initial temperature in the heat transfer step was applied as shown in Figure 57.

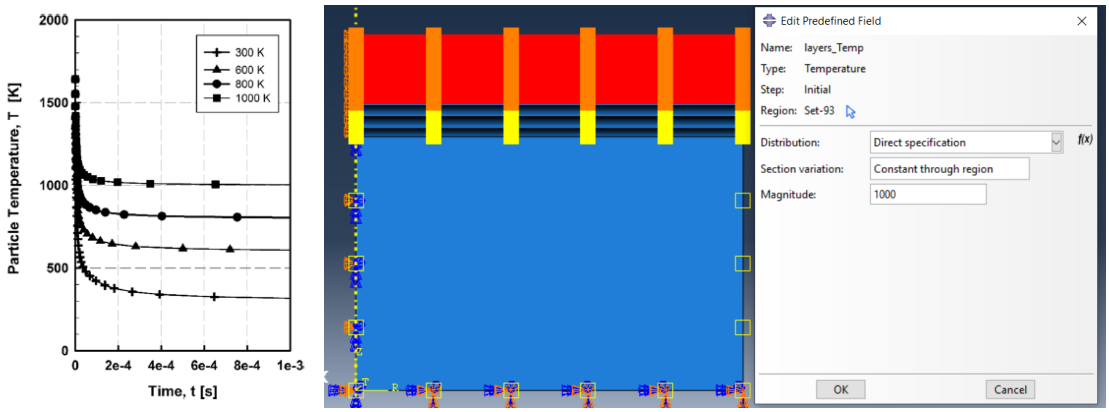

Figure 57_The history of deposition temperature as a function of time and initial particle temperature, and its application as initial temperature for the newly added layer in model

To show the appearance of each deposited layer, model change was incorporated. Following figure contains representation of model change of a couple of layers and the used code.

	Name	Initial	activation_1	activation_2	activation_3
✔	Int-model-change-2-1		Created	Modified	Propagated
✔	Int-model-change-2-2		Created	Modified	Propagated
✔	Int-model-change-3-1		Created	Propagated	Modified
✔	Int-model-change-3-2		Created	Propagated	Modified

(a)

```
for i in range(2,40+1):
    mdb.models['Model-1'].ModelChange(activeInStep=False, createStepName=
        'activation_1', includeStrain=False, name='Int-model-change-'+str(i)+'-1', region=
        mdb.models['Model-1'].rootAssembly.sets['Layer-'+str(i)+'-1'])
    #
    mdb.models['Model-1'].ModelChange(activeInStep=False, createStepName=
        'activation_1', includeStrain=False, name='Int-model-change-'+str(i)+'-2', region=
        mdb.models['Model-1'].rootAssembly.sets['Layer-'+str(i)+'-2'])
for i in range(2,40+1):
    mdb.models['Model-1'].interactions['Int-model-change-'+str(i)+'-1'].setValuesInStep(
        activeInStep=True, stepName='activation_'+str(i))
    mdb.models['Model-1'].interactions['Int-model-change-'+str(i)+'-2'].setValuesInStep(
        activeInStep=True, stepName='activation_'+str(i))
```

(b)

Figure 58_ Representation of (a): model change of a couple of layers, (b): the used simple python code

Cooling of the coated specimen by natural convection, and radiation between the assembly of deposited layers-substrate and the surroundings are also modelled. The natural convective heat transfer coefficient of air around the cylinder (the assembly of added layers and the substrate) with the average temperature of 310 K, ambient temperature of 298K is calculated as 12.0009 (W/m^2C).[42] Emissivity coefficient of the structure depends on the temperature, and more importantly on the quality of the exposed surface.[43] For polished SS316 at 232 degrees of centigrade, the emissivity is 0.57, and at the temperature of 949 degrees of centigrade, the emissivity is 0.66, so the use of 0.59 seems reasonable.

The newly exposed top surface of assembly of substrate-deposited layers, only during deposition of newly added deposited layer and the time needed to start the new layer, will experience heat exchange with surrounding air. The representation of the added interactions in the structure, examples of activation, deactivation of convection and radiation interactions between the structure and the ambient in order are presented in Figure 59.

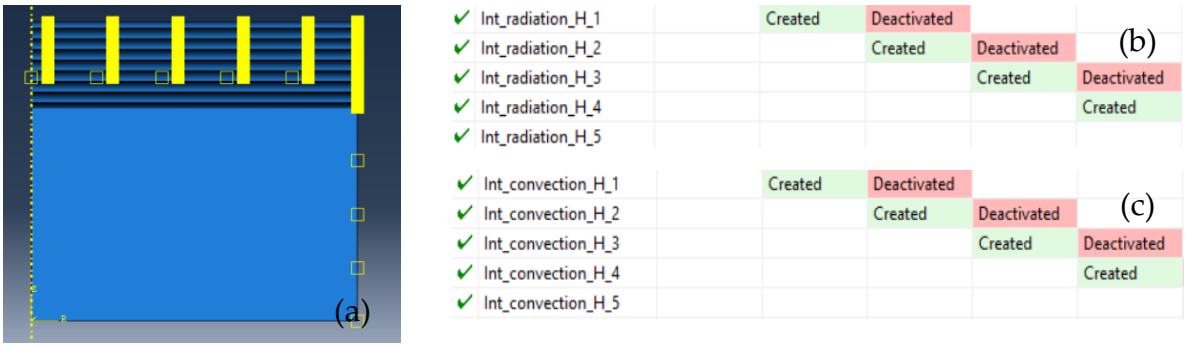

Figure 59_ Representation of, (a): interactions of newly exposed top surface of substrate and environments, (b): natural convection between newly exposed top surface and air, (c): radiation between newly exposed top surface and air

Unlike the heat exchange at the newly exposed top surface of the substrate, the periphery of the cylindrical assembly of substrate-deposited layers is exposed to the environment in the whole process duration. So, there is no need to deactivation of the convection and radiation interactions in the initial steps when the layers are not added, as that function is done with the presence of model change interaction. The representation of the added interactions in the structure, examples of activation of convection and radiation interactions between the structure and the ambient in order are presented in Figure 60.

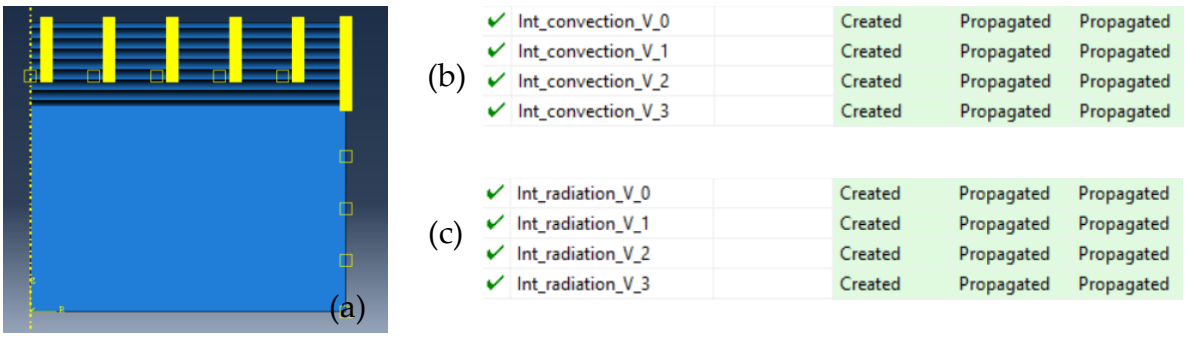

Figure 60_ Representation of, (a): interactions between periphery of the assembly and environment, (b): natural convection between periphery of the assembly and environment, (c): radiation between periphery of the assembly and environment

The codes regarding acquisition of thermal field can be seen in the Thermal Stress part of the Appendix.

The Figure 61 shows the evolution of thermal field during addition of first layer in successive increments.

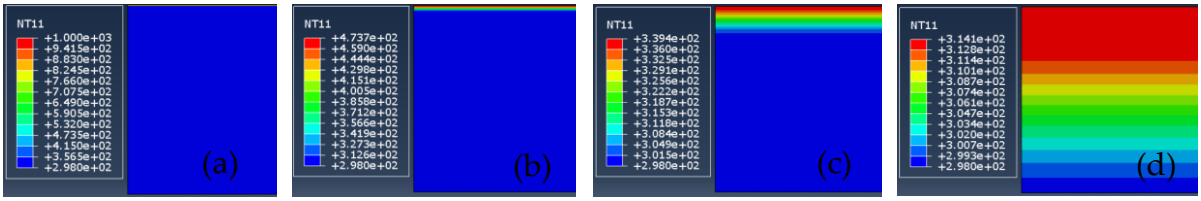

Figure 61_ Evolution of thermal field during addition of first layer in successive increments (a to d)

The obtained temperature history during the layer deposition process, serves as initial temperature in another model to obtain the induced thermal stress in the assembly of deposited layers-substrate. The Figure 62Figure 61 shows the evolution of the induced stress filed during addition of first layer in successive increments.

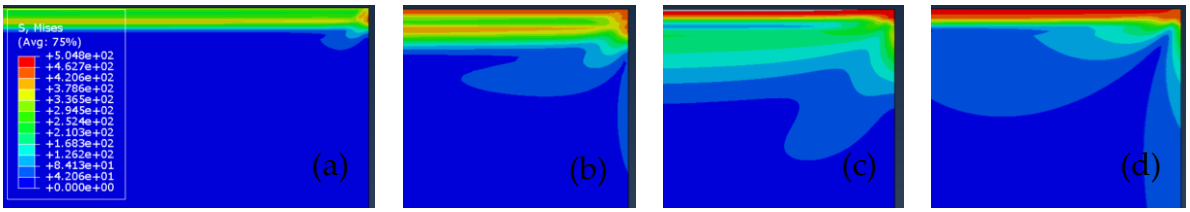

Figure 62_ Evolution of the induced stress field during addition of first layer in successive increments (A to D)

By comparing the obtained and reported radial residual thermal stress by Oviedo et al [18], after addition of 40 layers of SS316 on the substrate made of SS316, good correspondence between results is seen. The comparison of mentioned results is reported in Figure 63.

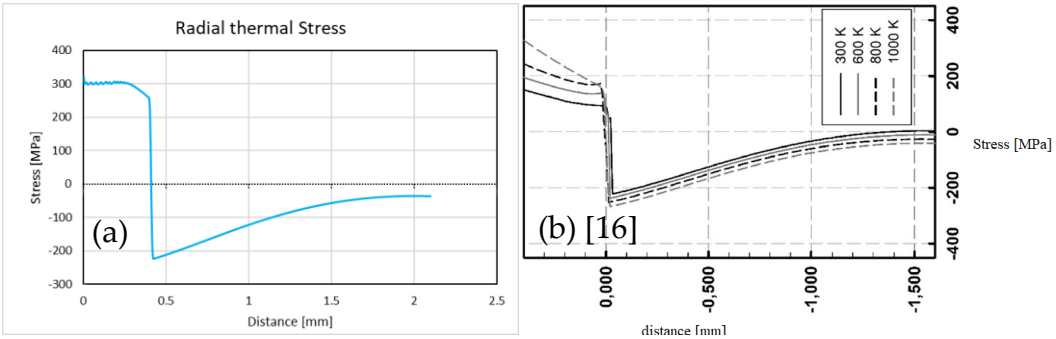

Figure 63_ Comparison of radial thermal stress profile in the axis of axisymmetric structure after deposition of 40 layers, (a): Obtained radial thermal stress, (b): Reported radial thermal stress based on Oviedo et al [18]

3 Experimental process

This chapter includes detailed report regarding the used deposition, measurement process, equipment, and exact dimensions of the used samples.

3.1. Equipment used for deposition process

3.1.1. Impact Innovations spray systems 5/8

The schematics of the Coldspray Additive manufacturing have been presentated in Cold spray equipment part.

The used cold spray system was Impact Spray System 5/8, which is composed of the 5/8-gun, control unit, the control software, the air- and water-cooling system for the nozzle and the air-cooling system for powder feeder. System's maximum operating pressure and temperature are 50 bar 1100 degrees of centigrade, with heating power of 40KW. [44] The Impact Innovations GmbH spray systems 5/8 and the 5/8 gun itself can been seen in Figure 64.

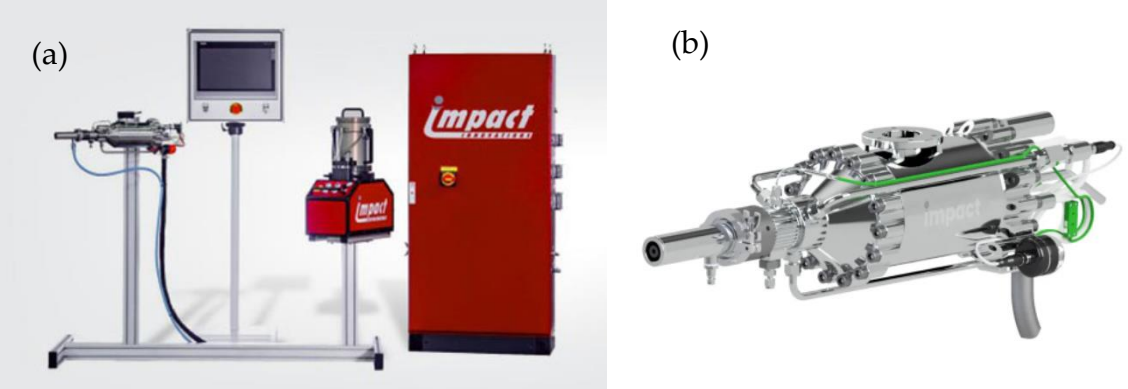

Figure 64_ Representation of (a): Impact Innovations GmbH spray systems 5/8, (b): 5/8 gun [44]

In Figure 65, the impact spray system 5/11 can be seen, which has higher capacity with respect to the system currently under use in Politecnico di Milano, however, the working principle is the same. The gas used by Impact Innovations GmbH is nitrogen, that is stored in a pressure vessel. when the gas is needed, it would be heated up to cause evaporation. A pump compresses the nitrogen and forces the gas through complex pipe geometries to cause further heating effect. When the gas reaches the control unit, the flow splits up. A part of it (blue flow of gas) is sent directly to the gun, where it is heated. Afterwards, the process gas is injected in the nozzle where it mixes up with the powder flow. The remaining gas (green flow of gas) is sent to the powder feeder, playing the role of carrier gas. To avoid backflow of powder, the powder is injected upstream the nozzle throat at a pressure higher than the pressure of process gas. It is worth mentioning that when the equipment is turned on, the aspiration and

filtration system collects powders and gas, so to maintain clean the chamber and collect particles for a possible reuse.[44]

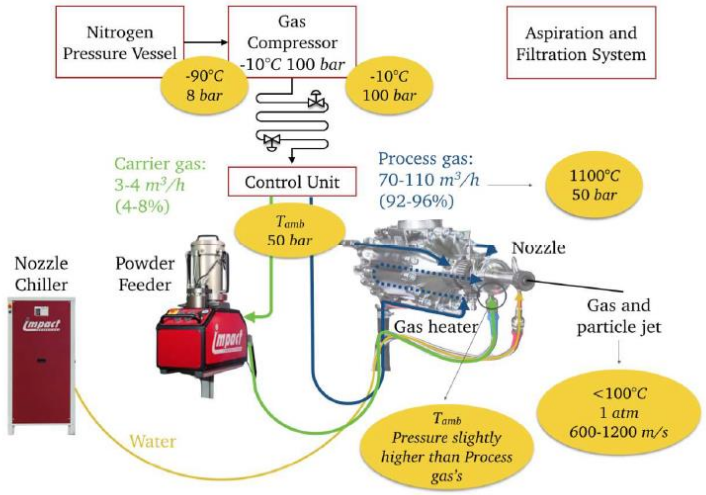

Figure 65_ The scheme of the gas path from storage to the nozzle of an Impact Spray System 5/11 [44]

3.1.2. KUKA KR 16 3 robot

The nozzle movement is possible with the help of a robotic arm. The used robot system is KUKA KR 16 3 robot, which is a 6-axis robot arm. It offers a 16 kg payload and 1611 mm reach. The repeatability of the KUKA KR 16 3 robot is 0.05 mm.[45] The robot system consists of:

1- Robot arm
2- Robot controller
3- Connecting cables
4- Teach pedant `

The representation of the KUKA KR 16 3 parts is shown in Figure 66.

Figure 66_ Representation of the robot system parts [45]

3.2. Sample preparation

The substrate is made of stainless steel 316, with the nominal dimension of 30×30×5 cubic millimeters, that were cut from a sheet with the thickness of 5 mm, and simply brushed afterwards with no specific preprocessing.

For experimental part, 20 samples have been prepared with the referred nominal dimensions. The average actual dimensions of the samples are as (29.20±3.23) × (29.78±1.39) × (5.031±0.025) cubic millimeters. Detailed information regarding dimensions of each sample is referred in Sample dimension part of Appendix.

3.3. Deposition process

The experimental work consists of deposition of grade 316 stainless steel on substrate made of grade 316 stainless steel: 1st test, with deposition of 1 layer, 2nd test with deposition of 2 layer with bidirectional scanning strategy, the 3rd test, with deposition of 2 layers with cross-hatching scanning strategy, 4th test, with deposition of 10 layers with cross-hatching scanning strategy, and 5th test with deposition of 10 layers with bidirectional scanning strategy. The detail of parameters of each test is mentioned in Table 6. The change of thickness and the duration of deposition for each sample are mentioned in Table 7.

The deposition process of the mentioned samples has been done in University of Politecnico di Milano. The used cold spray system was Impact Spray System 5/8, and the used robotic arm was KUKA KR 16 3 robot.

Table 6_ Experimental deposition parameters

Test Number	1	2	3	4	5
Sample Number	1	2	15	16	10
Deposition Strategy	-	BI	CH	CH	BI
Number of Layers	1	2	2	10	10
Process Gas Pressure [Bar]	35				
Process Gas Temperature [Celsius]	700				
Deposition offset (step) [mm]	1.2				
Off spray Distance[mm]	13				
Standoff Distance[mm]	30				

Table 7_ Sample thickness change and duration of deposition for each sample

Test Number	1	2	3	4	5
Initial Thickness	5.03	5	5.05	5.05	5.05
Final Thickness	5.27	5.42	5.44	6.5	6.5
Deposition Thickness [mm]	0.24	0.42	0.39	1.45	1.45
Time of Process [s]	24	37	37	191	191

The samples after layer depositions are shown in Figure 67.

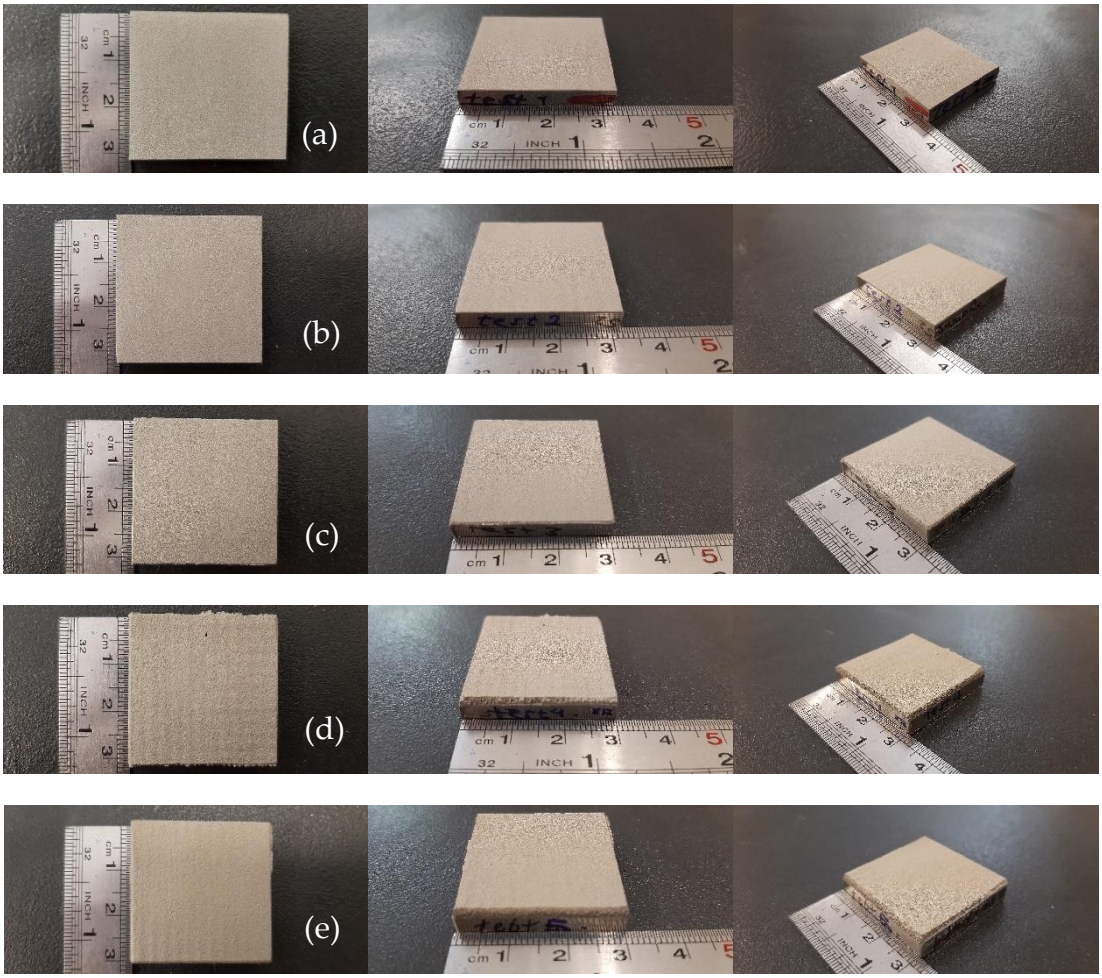

Figure 67_ Representation of deposited sample, (a): sample no 1, (b): sample no 2, (c): sample no 3, (d): sample no 4, (e): sample no 5

3.4. Residual stress determination with X-ray diffraction

Residual stress/strain values are among the most widely measured parameters. Among the different methods implemented for strain/stress determination, X-ray diffraction (XRD)-based techniques play a crucial role as these methods are phase specific, noncontact. In addition, these techniques simultaneously obtain other information like crystallographic orientation, presence of other phases, composition.[46] In x-ray diffraction residual stress measurement, the strain in the crystal lattice is measured, and the residual stress responsible for production of the strain is calculated, with the assumption of a linear elastic distortion of the crystal lattice.

Usability of mechanical methods and nonlinear elastic methods to residual stress determination are limited. Mechanical methods are limited by assumptions concerning the nature of the residual stress field and sample geometry. Mechanical methods, being necessarily destructive, cannot be directly checked by repeat measurement. As well, Spatial and depth resolution are orders of magnitude less than those of x-ray diffraction.[47]

X-ray diffraction residual stress measurement can be used for crystalline, relatively fine-grained materials that produce diffraction for any orientation of a sample surface, as to determine the stress, the strain in the crystal lattice must be measured for at least two known orientations relative to the sample surface.

The used samples can be metallic or ceramic, if a diffraction peak of suitable intensity and free of interference from neighboring peaks produced in the high back-reflection region with the radiations available.[47]

3.4.1. Principles of X-Ray Diffraction Stress Measurement

The diffraction of a monochromatic beam of x-rays at a high diffraction angle (2θ) from the surface of a stressed sample for two orientations of the sample relative to the x-ray beam is shown in the following figure. The angle ψ, represents the orientation of the sample surface. Ψ is the angle between the sample surface normal and the bisector of incident and diffracted beam.

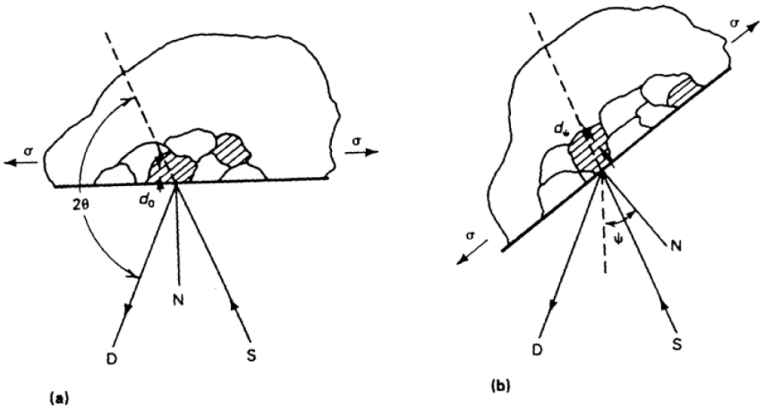

Figure 68_ Principal of X-ray diffraction measurement [47]

Diffraction occurs at an angle 2θ, which is defined by Bragg's Law: n λ = 2d sin θ, n in this equation is an integer showing the order of diffraction, λ is the wavelength of x-ray, d is the crystal planes lattice spacing, and as already mentioned θ is the diffraction angle. Any change in the lattice spacing, d, results in a corresponding shift in the diffraction angle 2θ.[47]

Figure 68 (a) shows the sample in the ψ = 0 orientation. Poisson's ratio contraction as a conclusion of presence of tensile stress, reduces lattice spacing, and consequently increasing slightly the diffraction angle 2θ. By rotation of sample with the value of ψ, as shown in the Figure 68 (b), the tensile stress present in the surface increases the lattice spacing over the stress-free state and decreases 2θ. Calculation of the present stress in the sample is possible by measuring the change in the angular position of the peak of diffraction for at least two sample orientations.[47]

X-ray diffraction stress measurement is limited to the surface of the sample. Electropolishing can be used to expose new surfaces for measurement. A condition of plane stress is assumed in the exposed surface layer. a stress distribution described by principal stresses σ1 and σ2 exists in the plane of the surface, and no perpendicular stress is assumed to the surface. However, a perpendicular strain component to the surface exists because of the Poisson's ratio contractions.[47]

The used techniques are the single-angle technique, or single-exposure Technique, Two-Angle Technique. The sin2ψ technique, The Marion-Cohen technique, and Full-Tensor Determination. [17]

3.4.2. The main components of a diffractometer

The main components of a diffractometer are presented hereafter:[48]

1- X – ray generator
2- Cathodic tube
3- X – ray detector
4- Goniometer
5- Sample positioning and movement system
6- Cooling system
7- Data acquisition software

The schematic of x – ray diffractometer is shown in Figure 69.

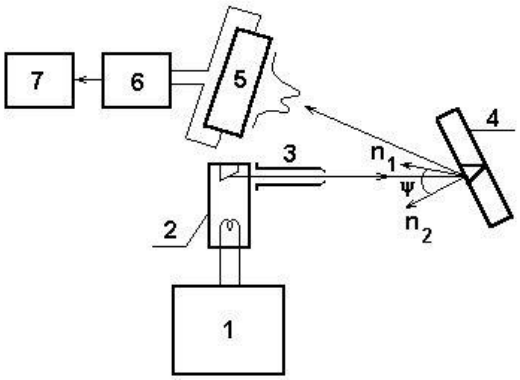

Figure 69_ The schematic of x-ray diffractometer: (1) high voltage source, (2) X - Ray tube, (3) collimator, (4) sample, (5) detector, (6) electronics, (7) computer [48]

3.5. Experimental measurement equipment

In this work the aim is to measure the residual stress profile along the thickness of the samples extracted from the cold sprayed deposition. The measurement of the stress in the deposited sample has been done in Politecnico di Milano.

3.5.1. AST X-Stress 3000 portable X-ray diffractometer

Residual stress measurements were performed using AST X-Stress 3000 portable X-ray diffractometer, with X XTronic 0.22 r 1969 – 2010, sin2(ψ) method, was used at a diffraction angle (2θ) of 152.3 with a total of 5 tilts in the range of −45° to 45° along 3 rotations of 0°, 45° and 90°. The used X-ray diffractometer is shown in Figure 70.

Figure 70_ AST X-Stress 3000 portable X-ray diffractometer

3.5.2. Struers Lectros-5 electrolytic polishing machine

In depth measurements were performed via layer-by-layer electropolishing. Electropolishing allows material removal without introducing residual tensions on the surface as opposed to traditional methods such as milling and turning.

Electropolishing is done using Struers LectroPol-5 on a circular area with a diameter of 1 square centimeter using an electrolytic solution of 94% CH3COOH, 6% HClO4 at a voltage of 20V. A Mitutoyo micrometer (IDCH0530/05060) Precisely quantifies the quantity of material removed at each step. Struers electro polisher and Struers control unit as main parts of the used electropolishing instrument are shown in order in Figure 71 (a)(b).

Figure 71_ Electropolishing instruments. (a): Struers electro polisher, (b): Struers control unit[49]

The micrometer used during electropolishing process to measure the polished thickness is shown in Figure 72.

Figure 72_ Mitutoyo micrometer (IDCH0530/05060)

3.6. Measured depths in samples

In order, depths used for residual stress measurement and the date of measurement by XRD diffractometer for sample no 1 to 5 are reported in Table 8, Table 9, Table 10, Table 11, and Table 12.

Table 8_ Depths used for residual stress measurement in sample no 1

Test1-SS316-CS-1L			
Step	Nominal Depth [μm]	Real Depth [μm]	Date of Measurement
1	0	0	21.04.22
2	-20	-20.1	22.04.22
3	-60	-61.3	22.04.22
4	-100	-99.7	22.04.22
5	-120	-119.5	26.04.22
7	-150	-149.8	27.04.22
8	-180	-180.2	28.04.22
9	-210	-210.4	6.05.22

Table 9_ Depths used for residual stress measurement in sample no 2

Test2-SS316-CS-2L-BI			
Step	Nominal Depth [μm]	Real Depth [μm]	Date of Measurement
1	0	0	21.04.22
2	-20	-20	22.04.22
3	-60	-60.8	22.04.22
4	-90	-89.6	26.04.22
5	-120	-119.7	27.04.22
7	-150	-150.8	27.04.22
8	-180	-180.4	28.04.22
9	-210	-213.4	28.04.22
10	-240	240.3	5.05.22
11	-270	270.4	5.05.22

12	-300	301.2	6.05.22

Table 10_ Depths used for residual stress measurement in sample no 3

Test3-SS316-CS-2L-CH			
Step	Nominal Depth [μm]	Real Depth [μm]	Date of Measurement
1	0	0	21.04.22
2	-20	-21	22.04.22
3	-60	-61.8	22.04.22
4	-90	-90.6	26.04.22
5	-120	-120.1	27.04.22
7	-150	-151.1	27.04.22
8	-180	-179.7	28.04.22
9	-210	-210.2	28.04.22
10	-240	-240	5.05.22
11	-270	-270.4	5.05.22
12	-300	-301.9	6.05.22

Table 11_ Depths used for residual stress measurement in sample no 4

Test4-SS316-CS-10L-CH			
Step	Nominal Depth [μm]	Real Depth [μm]	Date of Measurement
1	0	0	21.04.22
2	-20	-23.2	22.04.22
3	-60	-72	26.04.22
4	-90	-91.6	27.04.22
5	-120	-122.7	27.04.22

7	-150	-152.5	27.04.22
8	-180	-181.1	28.04.22
9	-210	-210.7	28.04.22
10	-240	-240.2	5.05.22
11	-270	-270.1	5.05.22
12	-300	-299.7	6.05.22

Table 12_ Depths used for residual stress measurement in sample no 5

Test5-SS316-CS-10L-BI			
Step	Nominal Depth [μm]	Real Depth [μm]	Date of Measurement
1	0	0	22.04.22
2	-20	-20	22.04.22
3	-60	-60.6	22.04.22
4	-90	-90.7	26.04.22
5	-120	-119.2	27.04.22
7	-150	-149.7	27.04.22
8	-180	-179.8	28.04.22
9	-210	-210.2	28.04.22
10	-240	-242.4	5.05.22
11	-270	-273	6.05.22
12	300	-299.6	6.05.22

In the case of high errors, the measurements for the corresponding depth have been repeated with higher exposure time or/and higher number of tilts.

3.7. Measurement results

As already mentioned, to obtain the residual stress profile in depth of the assembly of substrate-deposited layer, electropolishing has been used. It should be reminded that after electropolishing, in depth measurement, and acquisition of the residual profile in depth, in order to take into consideration, the stress relaxation effect due to layer removal in electropolishing, they are corrected based on Moore Evan's Theory. The measured equivalent radial residual stresses in the samples are presented in **Error! Reference source not found.**.

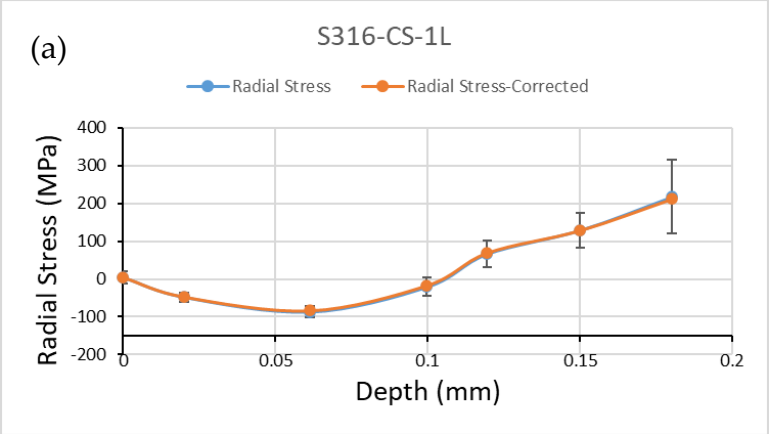

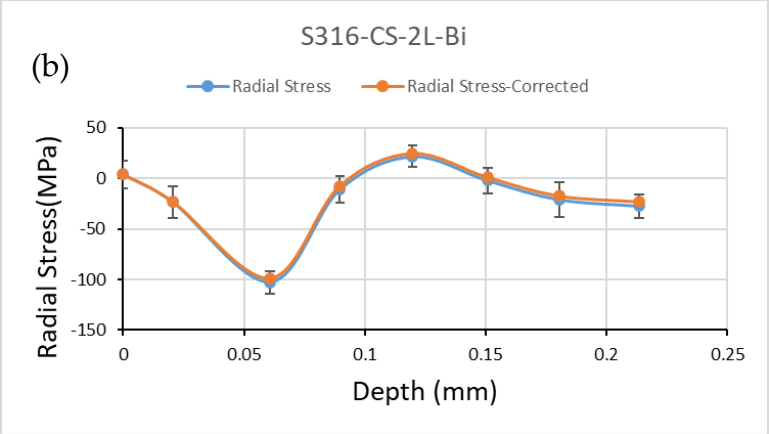

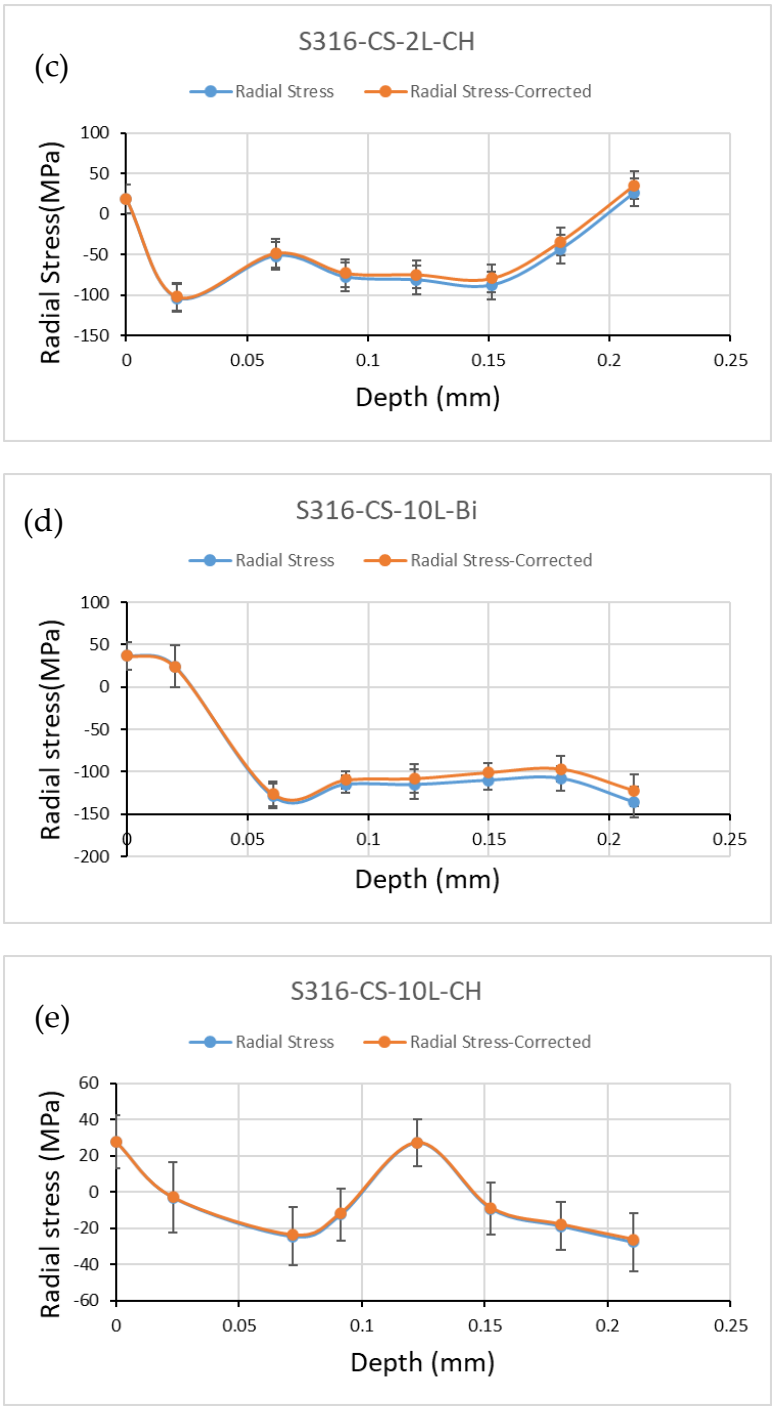

Figure 73_ The equivalent measured radial and equivalent corrected radial stress in order in (a): S316-CS-1L, (b): S316-CS-2L-Bi, (c): S316-CS-2L-CH, (d): S316-CS-10L-Bi, (e): S316-CS-10L-CH

4 The comparison of the numerical method with the experimental process

As already mentioned in Table 6, the Process Gas Temperature was 700 degrees of Celsius, and the Process Gas Pressure was 35 bar. The powders with the mean diameter size of 30 micron are supplied by the mass rate of 20 gr/min. By use of KSS software and providing the software with the spray parameters, the software provides us with diagrams that reflect the temperature and pressure and flow rate for the gas, and temperature and velocity for the particles based on their diameter. Based on the parameters mentioned already, the particles will be accelerated with the velocity of 591 m/s, and the temperature of 458 degrees of centigrade. By getting the input and impact temperatures of the gas from KSS, the calculation of the Nusselt number distribution across radial coordinate of the nozzle (which depends on gas material, parameters, nozzle design, thermal boundary conditions, etc) is done. Then based on the parameters for nitrogen at impact temperature and reference size of the sample which was 3 cm the heat transfer coefficient was calculated and subsequently the heat flux was obtained.

Table 13_ Experimental Modeling parameters

The Heat Flux	403971 W/m^2
Total time of addition of each layer	0.492936 s
Total heating time in each layer	0.23104 s

In Table 13, experimental modeling parameters are mentioned. As the thickness of the added layer in the case of Test number 5 (10-layer, Bidirectional strategy) is 1.5 mm, based on the thickness of the splat of the particle on the substrate with the thickness of 18.2 micron, the considered number of added layers in the modeling would be 82 ($1500/18.2 \approx 82$). The mentioned thickness of each layer is obtained based on the Explicit single particle impact analysis.

4.1. Single particle impact analysis

In the same manner as already described in Single impact particle analysis in chapter Developing Numerical method to predict residual stress in 2D, In the first step, an axisymmetric single particle impact model, with defined geometry of the substrate (Being large enough to avid the edging effect), particle size, velocity and temperature of the substrate and particle, has been considered.

A two-dimensional axisymmetric FE model of a stainless steel 316 (SS316) particle impacting on a cylindrical SS316 substrate is developed. As in the previous chapter explained, the single particle impact is analyzed as a coupled thermal–displacement phenomenon under high strain rates. Based in the assumption of short duration of impact, the particles do not interact with each.[20][18]

The model considers 90% of the kinetic energy being transformed into heat [27],with the remainder of the energy being spent as plastic deformation and rebound kinetic energy.[20] In this step Lagrangian method has been used, as the deformation of the elements were not significantly severe, and no need to implementation Arbitrary Lagrangian Eulerian method (ALE) or Coupled Eulerian Lagrangian method(CEL) has been sensed.

The response of the impacting particle and the underlying substrate under such loading conditions is strongly affected by the strain, strain rate, temperature, and microstructure of the material[28]. Therefore Johnson-Cook constitutive law for definition of the material properties is used.

The material properties are already mentioned in

Table 3 and Table 4, in chapter Developing Numerical method to predict residual stress in 2D. Cylindrical substrate dimensions are 1.5 mm radius and 1.5 mm height. The substrate dimensions compared to particle's dimensions are chosen to avoid edge effects. On the bottom edge of the substrate all Degrees of freedom are constrained (Encastre), as well on the left edge of the geometry-the axisymmetric axis of asymmetric model-, symmetry boundary conditions are specified on both particle and

the substrate. In addition, initial temperature of 298K is considered for the substrate. The assembly of the substrate and the particle is presented in Figure 74.

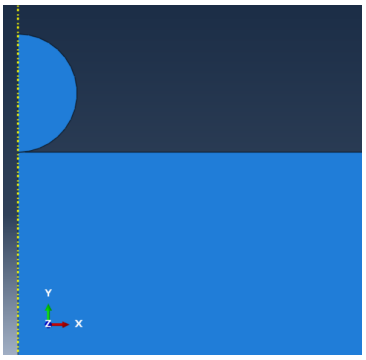

Figure 74_ Representation of the assembly of particle and substrate

As simulation output, the resulting radial and axial residual stress distributions measured along the symmetry axis are computed after 400 ns of the onset of the impact. This time period is enough to allow for kinetic energy dissipation, particle spreading, substrate deformation and temperature stabilization.[18]

The Radial and axial stresses in the axis of the axisymmetric structure in the substrate in order are reported in Figure 75.

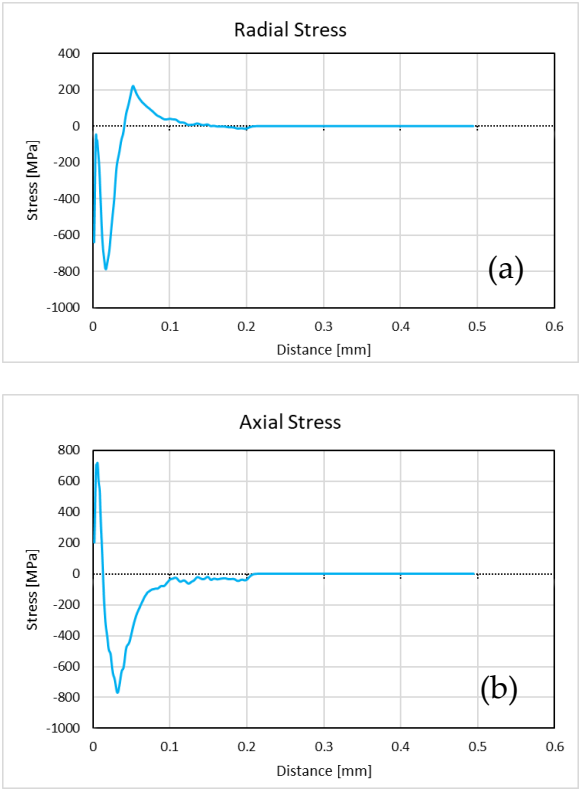

Figure 75_(a), (b): in order, radial and axial residual stress in the axisymmetric axis of the cylindrical substrate in the single particle impact analysis

4.2. Peening stress

As already mentioned, the dimensions of the cubic substrate were approximately 30×30×5 cubic millimeters.

The possibility of implementation of the mentioned geometry in 2D was not possible. In order to deal with this difficulty and avoid the use of 3D model, the substrate is considered as a cylinder with the radius of 15 mm and the thickness of 5mm.

It is possible to check the thickness of the added layers in each test. Based on the test number 5 (10-layer with Bidirectional Scanning strategy), the thickness of the deposited layers is approximately 1.5 mm.

By considering the dimension of the cylinder, initially an axisymmetric model with the radius of 15 mm and the thickness of 6.5 mm is created. Then based on the thickness of the splat of deposited particle on the substrate, obtained from single particle impact model, the model is sectioned. Initially for obtaining loads able to produce radial and axial stress in the substrate, the layers which are not still deposited are deactivated with the help of Model Change. The Representation of the assembly of the substrate-added layers and sectioning strategy is shown in Figure 76.

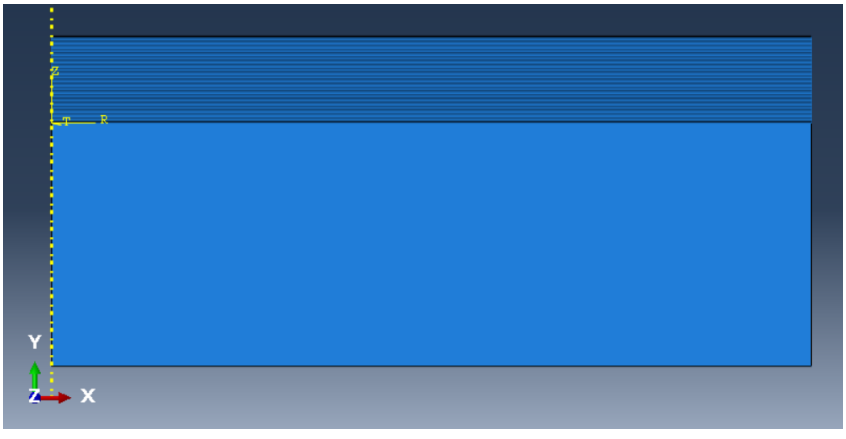

Figure 76_ Representation of the assembly of the substrate- added layers and sectioning strategy

4.2.1. S-Axial Pressure-S+L-Radial Pressure-Predefined Radial Initial Stress

This method is the last method described in the chapter **Error! Reference source not found.** section Peening Stress prediction, which could successfully reach the results reported by Oviedo et al[18] for deposition of SS316 on the substrate made of SS316.

For obtaining the pressures and initial stresses responsible for inducing the desired stress state prescribed by single particle impact after addition of first layer, the main mindset behind the method, relies on the idea of application of vertical pressures, and predefined radial initial stresses, right below the added layer up to the depth of 200 micron .The reason for considering only the first top 200 micron of the substrate for application of the mentioned loads is based on obtained stresses the single particle impact model shown in Figure 75 ,as stresses approach the value of 0 MPa surpassing depth of 200 micron.

Having based on the single particle impact, the thickness of the splat of added material as 18.2 micron, the 200 microns in the substrate right below the first added layer is split to 22 parts with the thickness of 9.1. The consideration of use of the thickness of 18.2 microns is avoided, to have more control in producing the desired stress trend obtained by the single particle impact analysis.

As already described in part Peening Stress prediction in chapter **Error! Reference source not found.**, the used iterative corrective approach, tries to define an error criterion which gives us a quantitative value to show the ability of the loads in reaching the desired axial and radial stress trends in single particle impact analysis shown in Figure 75.

By doing so, the value of the pressures applied on the edge of the added sections in the particles and radial initial stresses applied at the defined sections could be obtained.

The comparison between stresses based on single particle impact analysis and the obtained radial and axial stresses in order in radial and axial directions are presented in Figure 77.

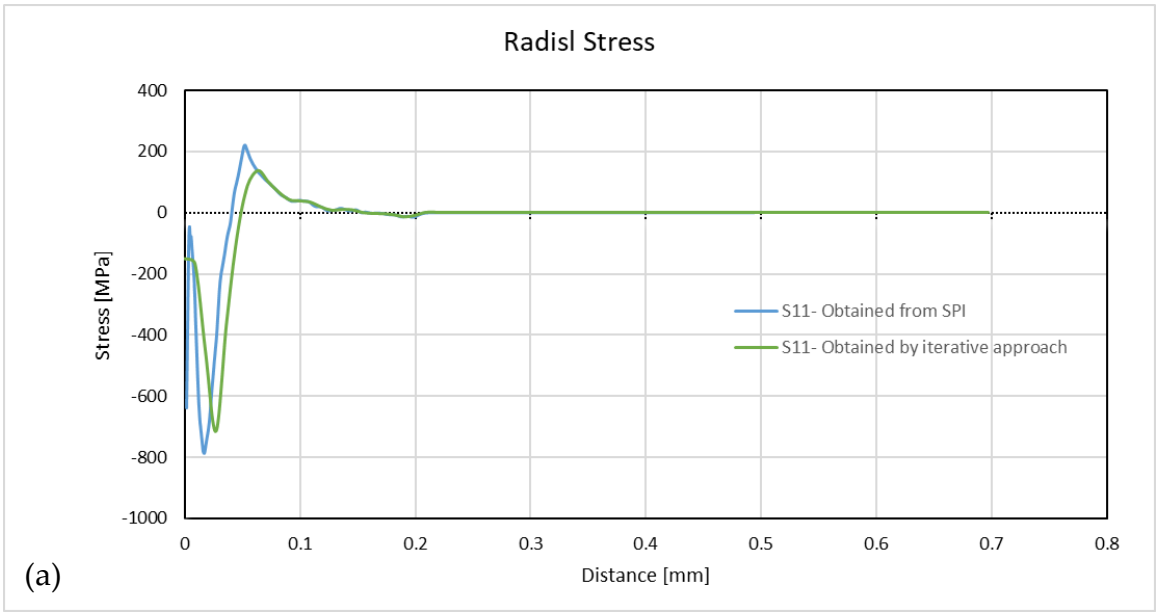

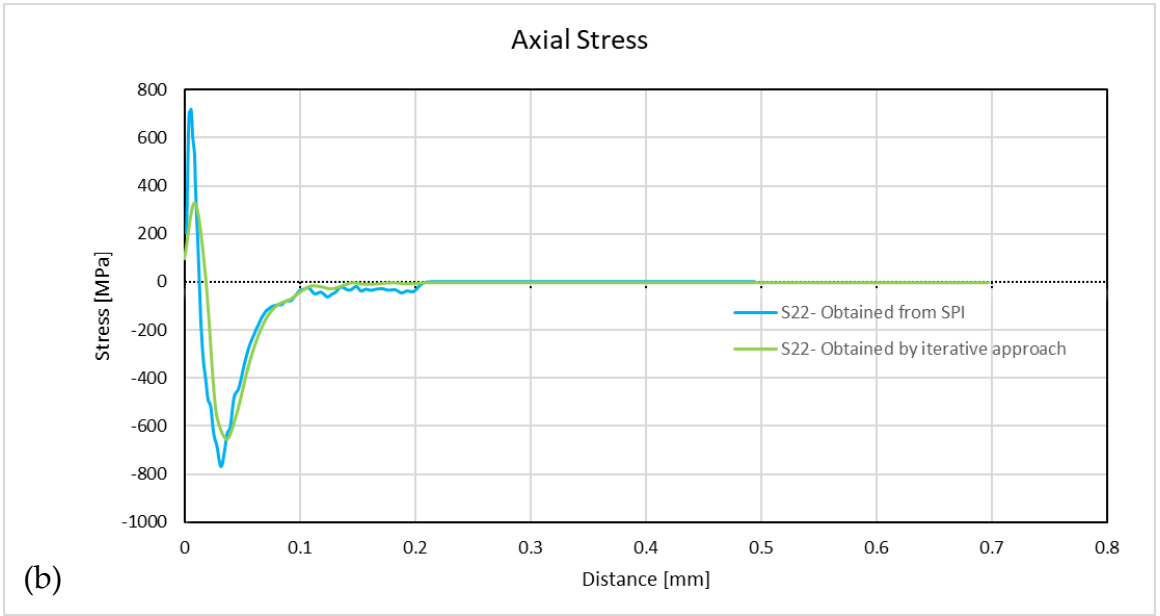

Figure 77_ Comparison between the stress profile between the result of single particle impact model and the obtained stress trend from iterative corrective approach in the substrate after deposition of 1st layer with the thickness of 18.2 micron in (a): radial direction, (b): axial direction

Now by knowing the radial initial stresses in the defined sections and the applied axial pressures on the defined edges of the mentioned sections, the residual stress after addition of first layer with the thickness of the splat of particle (Obtained from single particle impact), is obtained.

The repetition of addition of these loads for each added layer, would result in the acquisition of the stress field after addition of n^{th} layer. As the thickness of the added layers for test number 5 was approximately 1500 micron, and the thickness of the obtained splat from single particle impact was 18.2 microns, number of added layers in the model roughly would be 82.

As already mentioned, the applied loads for acquisition of stress field after addition of n^{th} layer would be possible through the use of a simple piece of code. In this code, for example for the case of axial loads: the pressures for obtaining axial stress are used as a list, then by shifting these loads and repetitive summation of loads, a list containing 82 lists, will be obtained. The last list contains 186 pressures, that by being applied as the section edges, will obtain the axial stress field.

The exact same process would be repeated for obtaining a list containing total of 185 initial radial stress values that would be applied to the already defined sections. For this part a simple code is used which can be found in Generalization phase part of the Appendix.

After the generalization phase, and the completion of the modelling for the mentioned method for addition of 82 layers representing addition of 1.5 mm thickness of the added material, the obtained residual radial stress profile is presented in Figure 78.

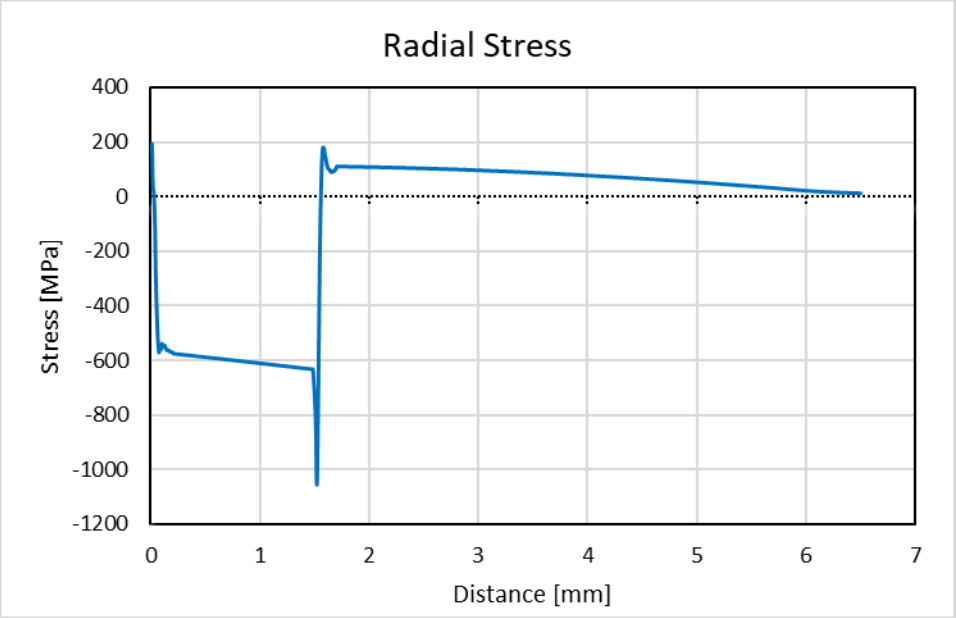

Figure 78_Obtained residual stresses after addition of 82 layers, based on experimental parameters in radial direction

Unfortunately, the stress amplitudes in the radial and axial directions are noticeably high which is not comparable to the experimental results. It should be mentioned the effect of thermal stress is included in the stress profile reported in Figure 78.

4.2.2. S+L_Predefined radial initial stress (Just radial direction)

In this method with the help of mentioned iterative corrective approach in S-Axial Pressure-Radial Pressure-Predefined Radial Initial Stress, the predefined radial initial stresses responsible for induction of residual radial stress extracted from single particle impact analysis are obtained. The predefined initial radial stress added in the substrate is based is the absolute value of the average of the evolution of radial stress in the central node of the impacting particle in the single particle impact analysis.

The comparison between stresses based on single particle impact analysis and the obtained radial stresses is presented in Figure 79.

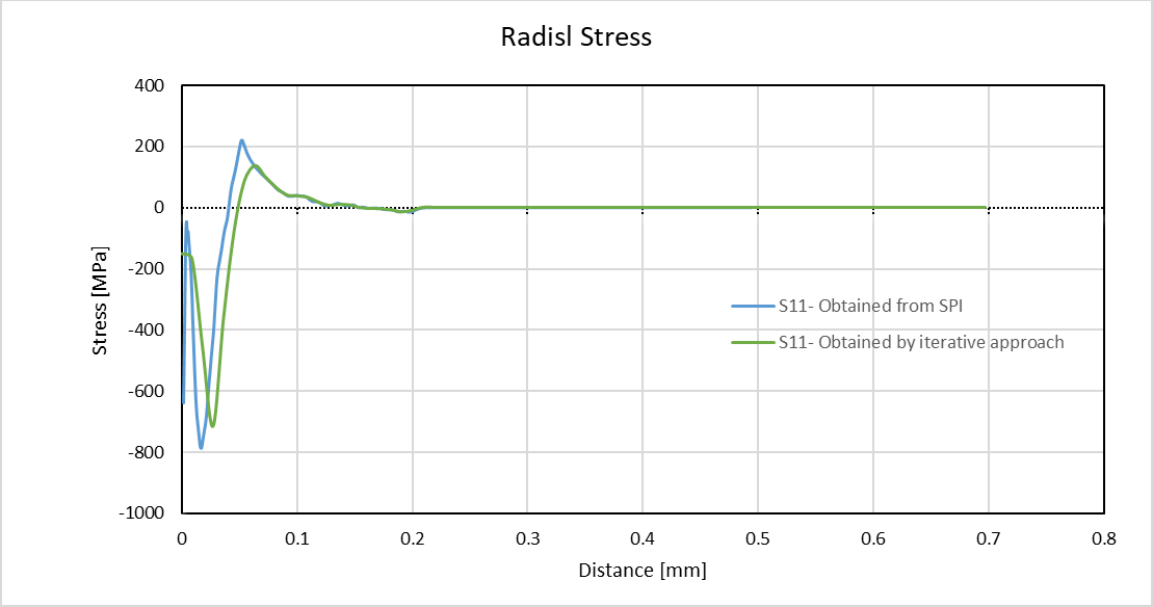

Figure 79_ Comparison between the stress profile between the result of single particle impact model and the obtained stress trend from iterative corrective approach in the substrate after deposition of 1st layer with the thickness of 18.2 micron in radial direction

By generalization of the layer addition for 1.5 mm of thickness the total stress would be obtained. Reminder in the, the total stress is presented in Figure 80, which as well includes the effect of thermal stress.

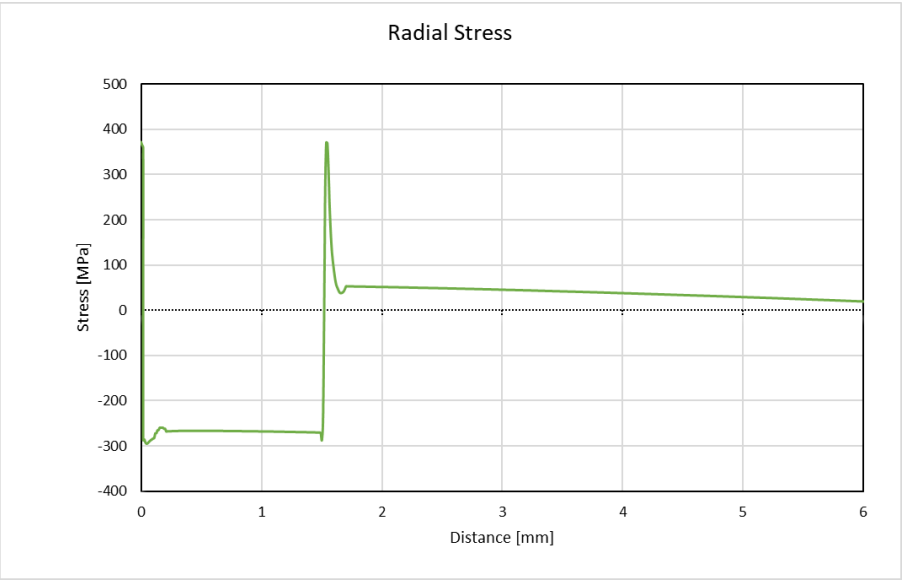

Figure 80_ Obtained total radial residual stress after addition of 1.5 mm of layer deposition

4.3. Thermal Stress based on experimental parameters

The generated thermal stress during coating deposition is predicted using a nonlinear, sequentially coupled, thermomechanical FE analysis performed in two stages. In the first stage, a heat transfer analysis is performed to obtain the thermal history of the specimen. The time-dependent temperature distribution being repeatedly applied for each layer to accumulate the final residual stress distribution.[18][20]

A two-dimensional axisymmetric FE model, employing the same reference cylindrical coordinate system of the single impact model is developed. It is worth mentioning that exact sectioning strategy as in the case of geometry used for acquisition of peening stress is maintained here in order to have compatible meshes. The representation of the assembly of substrate- added layers is shown in Figure 76.

heat transfer analysis uses four-node linear diffusive heat transfer elements. The stress analysis uses four-node bilinear, reduced integration axisymmetric stress elements with hourglass control. Temperature dependency of the conductivity is modelled.

To model heat transfer between the gas jet and the coating surface, a surface thermal load of 403971 W/m2 was applied during a time period of 0.23104 s.[18] This period was estimated from the traverse velocity of the spray gun and corresponds to the time required by the spray gun to pass over a spray zone of approximately 50 mm.

For application of these mentioned heat flux on the top surface of the substrate, 82 amplitudes (with 4 points) were defined. It should be mentioned that the area under the defined amplitudes used for application of heat fluxes is exactly the needed duration of time.

Based on the amplitude defined, the heat flux is active, just in specific period, before the addition of the subsequent layer. Even though, by definition of the amplitudes, there is no need to deactivate the heat fluxes in the following steps, the heat fluxes in the subsequent step are deactivated based on personal preference.

Then the initial temperature of 298 k is applied for the substrate, and initial temperature of 641.85 K for the added layers. In addition, the boundary condition of temperature of 298 K at the bottom part of the assembly of substrate-added layers, is added. In Figure 81, in order, the zones used for addition of initial temperature in the substrate and the layers are shown.

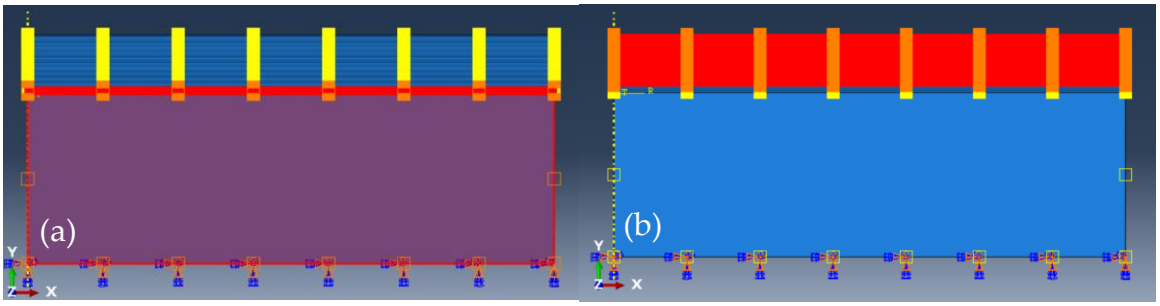

Figure 81_ Representation of the added initial temperature in order in, (a): in the substrate, (b): in the added layers

Instead of changing the conductivity in the each added layer to have the addition of layers, model change is used. All the added layers in the first step are deactivated, and in proper step, they are activated.

It should be mentioned that as the thickness of sections in the assembly in order to obtain the peening stress was 9.1 microns, each of the added layers with the thickness of 18.2 microns are divided in two parts. (For example, the two sections of layer 3 are named as layer_3-1 and layer_3-2 and in the case of model change, Int-3-1 and Int-3-2).

Cooling of the coated specimen to the ambient temperature by natural convection, and radiation between the assembly of deposited layers-substrate and the surroundings are modelled.

The natural convective heat transfer coefficient of air around the cylinder (the assembly of added layers and the substrate) with the average temperature of 310 K, ambient temperature of 298K is calculated as12.0009 (W/m^2C).[42]

Emissivity of the structure depends on the temperature, and more importantly on the quality of the exposed surface, based on the references, for polished SS316 at 232 degrees of centigrade, the emissivity is 0.57, and at the temperature of 949 degrees of centigrade, the emissivity is 0.66, so the value being used as 0.59 seems reasonable.[43]

The newly exposed top surface of assembly of substrate-deposited layers, only during deposition of newly added deposited layer and the time needed to start the new layer, will experience heat exchange with the surrounding. But The periphery of the cylindrical assembly of substrate-deposited layers is exposed to the environment in the whole process duration. More detailed explanation degrading the used

interactions and defined edges can be seen in part Thermal stress of chapter **Error! Reference source not found.**.

The thermal history during the addition of 82nd layer (The last added layer) of the thermal analysis is represented in Figure 82 (a), (b), (c), each representing consecutive increment in the last step.

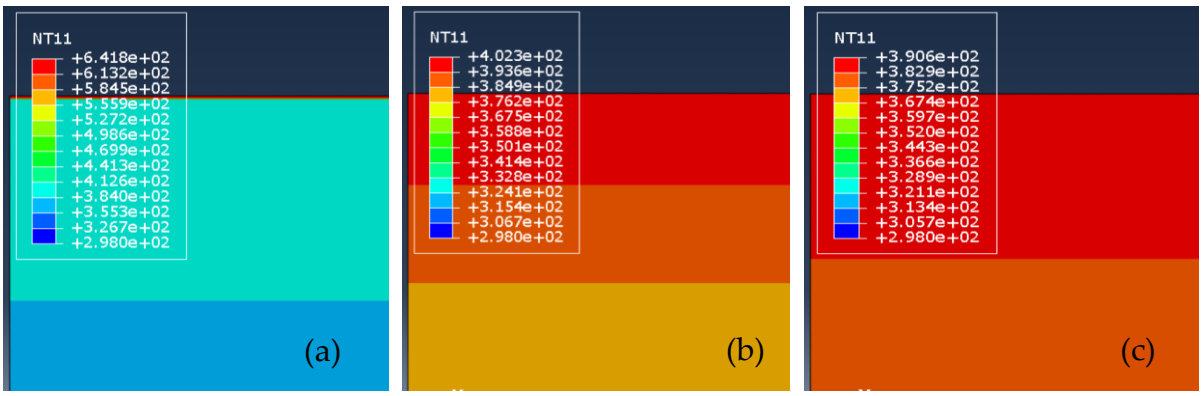

Figure 82_ Evolution of thermal field after addition of 82nd layer (Units are in Kelvin), (a), (b), (c): representing consecutive increments in the 82nd step

By application of the obtained thermal field as initial temperature in an implicit model, the thermal residual stress is obtained. In Figure 83, the evolution of thermal stress during addition of 82nd layer is represented. (a), (b), (c) representing consecutive increments in the last step of the analysis.

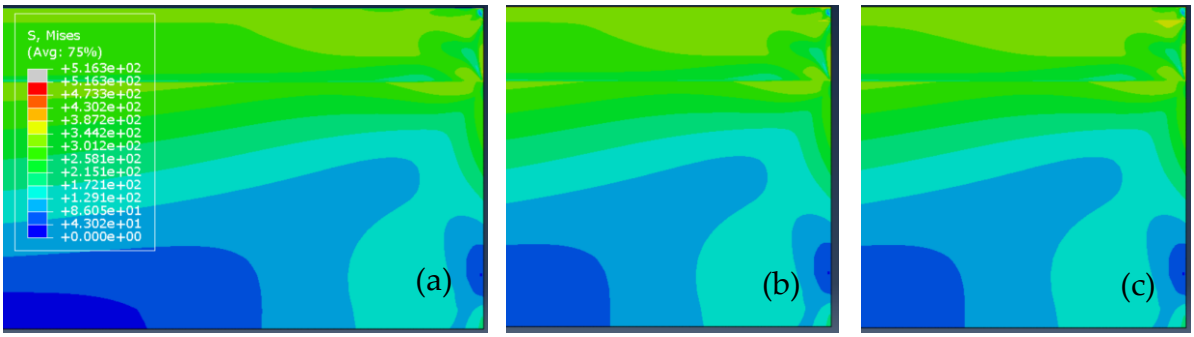

Figure 83_ Evolution of thermal field after addition of 82nd layer (Units are in MPa), (a), (b), (c): represent consecutive increments in the 82nd step

In Figure 84, the thermally induced radial residual stress in axis of the axisymmetric structure is presented.

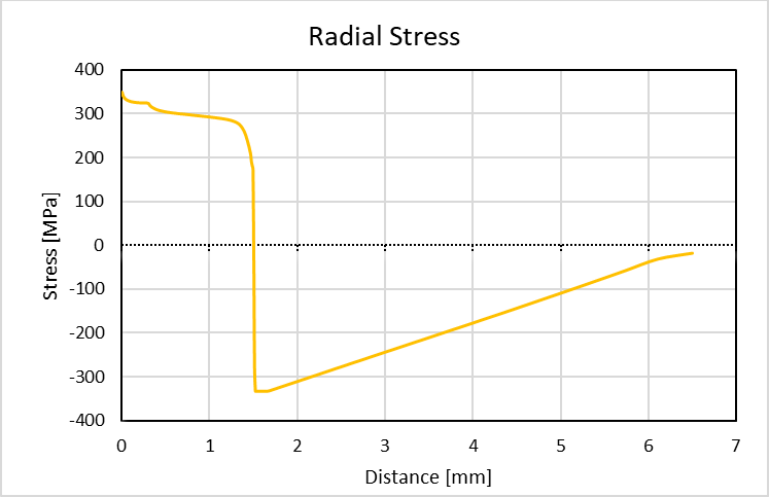

Figure 84_ Representation of the thermally induced radial residual stress after the addition of 82nd layer

4.4. Comparison of the results

In the same manner described in S+L_Predefined radial initial stress (Just radial direction) peening stresses and total stresses in the radial direction for the 1- layer test and 2-layer bidirectional tests are obtained. Based on the thickness of the added layers and the thickness of the particle in the single particle impact analysis, the mentioned experimental tests are modeled in order by addition of 13 and 23 layers on the substrate.

In Figure 85, in order radial thermal stresses, radial peening stresses and radial total stresses after addition of 13, 23 and 82 layers are represented. Obviously based on Figure 85, the stress relaxation effect is noticeable after consideration of the thermal effect.

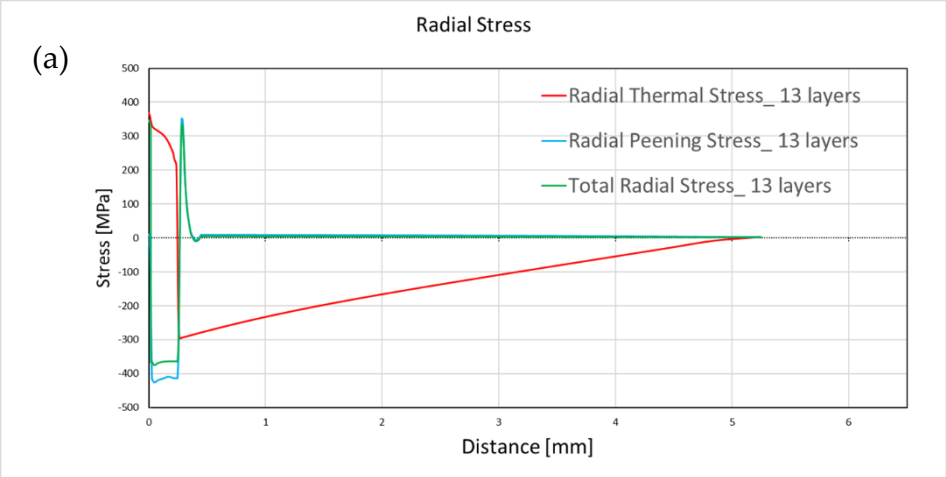

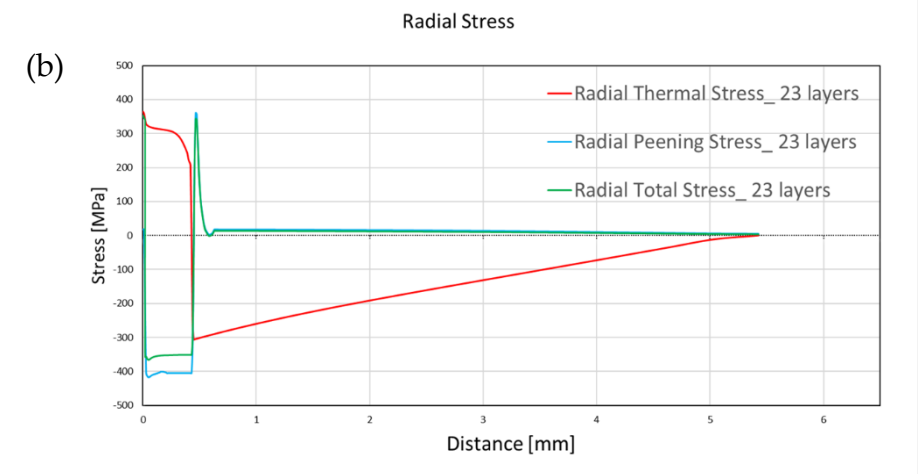

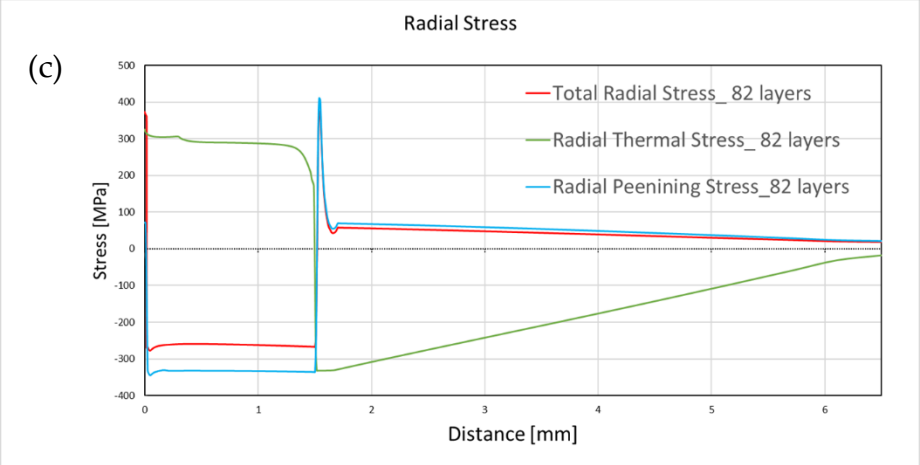

Figure 85_ Representation of the radial thermal stresses, radial peening stresses, and radial total stresses after addition of (a): 13 layers, (b): 23 layers and (c): 82 layers

In Figure 86, in order comparison of the radial thermal stresses, radial peening stresses and radial total stresses after addition of 13 layers, 23 layers, and 82 layers on the substrate are presented. Based on the Figure 86, even though the amplitude of the stresses' change by addition of the layers, the radial thermal stresses, radial peening stresses, and radial total stresses for all the models including 13, 23, and 82 layers follow the same trends.

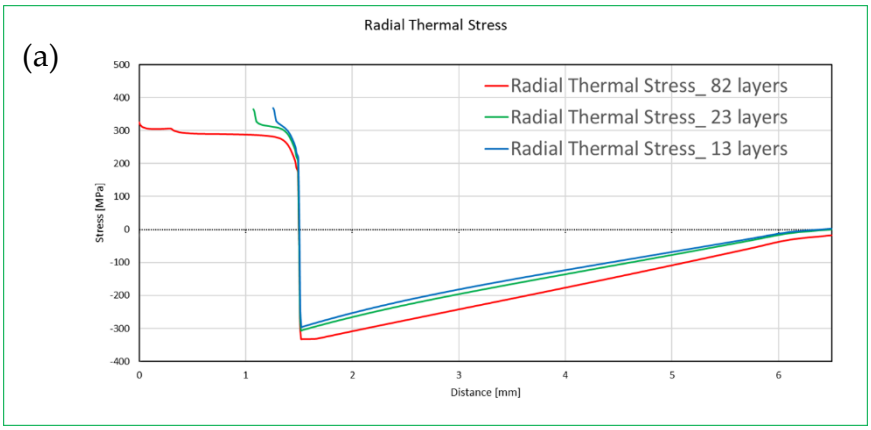

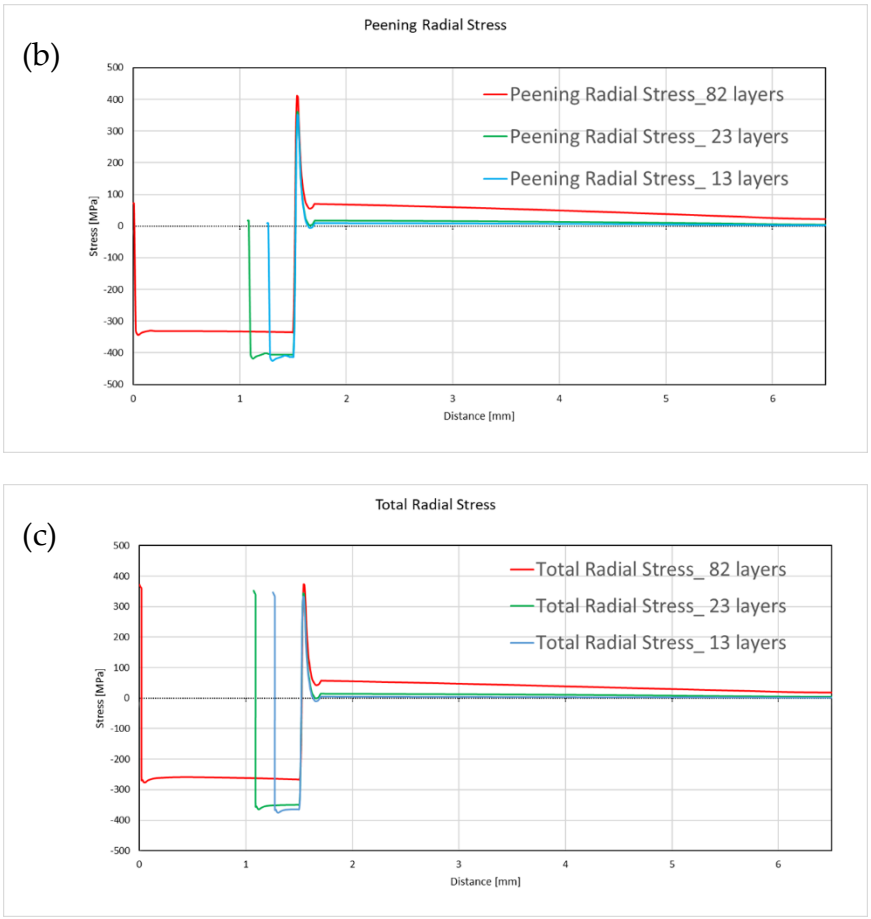

Figure 86_ Representation of comparison of the (a): radial thermal stresses, (b): radial peening stresses and(c): radial total stresses after addition of 13 layers, 23 layers, and 82 layers on the substrate

In Figure 87, in order the comparison of the obtained total radial stresses and the measured total stresses after addition of 13, 23, and 82 layers are represented.

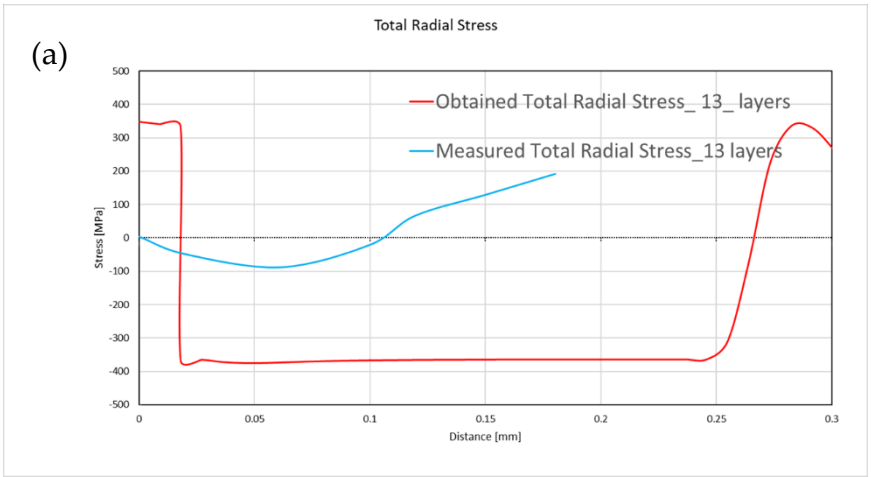

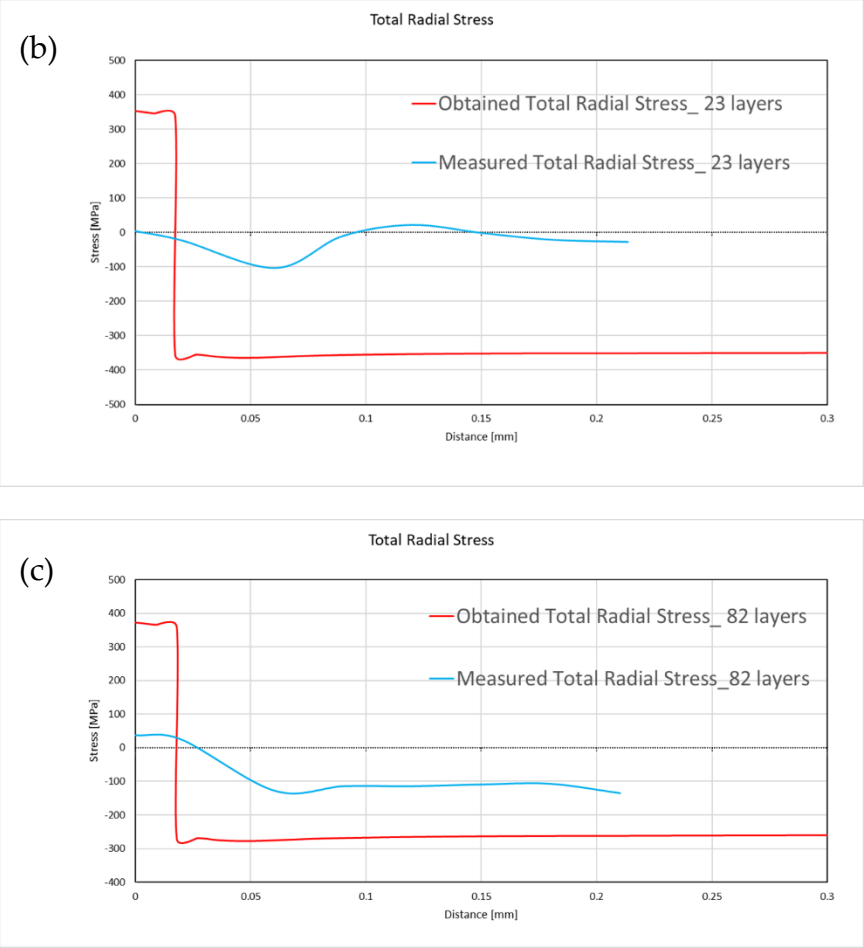

Figure 87_ Representation of comparison of the obtained total radial stresses and the measured total stresses after addition of (a): 13 layers, (b): 23 layers, and (c): 82 layers

5 Conclusion

The major purpose of this project is to obtain in plane induced residual stress trend during layer deposition with the help of cold spray additive manufacturing.

The cold gas dynamic spraying (CGDS) process is referred as cold spray. In cold spray process, preheated particles with temperatures lower than material's melting temperature with impacting velocities higher than critical velocities bombardon the substrate by a carrier gas. In this process, development of higher particle velocities has been continued by simultaneous decrease of heat input. So, deformation of particles even in the solid state would be possible which guarantees good bonding even in partial particle melting. The accelerated particles upon exit from the nozzle experience significant amount of deformation followed by bonding between the substrate and the particles. The succession of the impact and following deformations, will conclude in the layer addition process. Even though avoidance from high-temperature oxidation, phase change, evaporation, melting, crystallization, debonding, gas release, strict substrate surface preparation and other accompanying difficulties related to traditional thermal spraying methods with cold spray process can be achieved, successive addition of deposited layer would contribute to the accumulation of significant amount of residual stress. As the main concentration of the thesis project, a numerical model based on previously developed models for stress trend evaluation during high velocity impact techniques is developed which has proven to be able to obtain the in-plane stress trend during cold spray additive manufacturing. In the developed method, initially the peening stress after the addition of the first layer is induced based on the extracted stress trend from an explicit axisymmetric displacement-thermal analysis of single particle impact. The peening stress in the first layer is induced by application of loads which were iteratively corrected till the moment an error criterion representing the difference of the induced stresses and the extracted stresses from single impact particle analysis is less than a specific threshold. Through the checked methods, two of which have been better able to obtain complaint results as the reported ones: S+L_Predefined radial initial stress (Just radial direction) and S-Axial Pressure-S+L-Radial Pressure-Predefined Radial Initial Stress. Having the loads responsible for the induction of stress after addition of first layer and generalization of the loads for addition of higher layers, the total peening stress during process is obtained.

Thermal stress distribution due quenching and post cooling is obtained by an uncoupled thermal- mechanical analysis. Initially the temporal thermal field with the presence of convection and radiation, and conduction through the added layer sand substrate is obtained. Then the obtained thermal temporal field is used in an implicit model to obtain the residual stress due quenching and post cooling.

The experimental part consists of deposition of grade 316 stainless steel on substrate made of grade 316 stainless steel: 1st test, with deposition of 1 layer, 2nd test with deposition of 2 layer with bidirectional scanning strategy, the 3rd test, with deposition of 2 layers with cross-hatching scanning strategy, 4th test, with deposition of 10 layers with cross-hatching scanning strategy, and 5th test with deposition of 10 layers with bidirectional scanning strategy. The deposition has been carried out at the university of Politecnico di Milano with Impact Innovations spray systems 5/8, and head guidance by KUKA KR 16 3 robot. And residual stress measurements were performed using AST X-Stress 3000 portable X-ray diffractometer within depth measurement done by layer-by-layer electropolishing. The mentioned model (S+L_Predefined radial initial stress (Just radial direction)) is used for modeling the process for addition of coating for 1 layer, 2 layers and 10 layers. Even though the amplitudes of the radial peening stresses, radial thermal stresses, and radial total stresses change by further layer addition, the overall trends are the same.

Compariosn of the results with available models develped for other thermal spray technologies showed a very good match. When considerably increasing the number of the layers and thus the deposit thickness to get closer to AM applications of cold spray, the results showed a less quantitative agreement with the experimentally measured data, despite correctly predicting the evolution trend of the stresses.

Some of the future work would include:

- The usage of multi particle impact analysis as the root for acquisition of the peening stress.
- The usage of better generalization method for addition of the layers. Instead of addition of the initially obtained corrected loads over and over, based on the multi particle impact analysis, an extrapolation can be obtained to be used in the generalization phase. (Checking the trend of stress after the succession of impacting particles, as the addition of stress will not be constant as considered in this project and a multitude of papers concentrating on evaluation of residual stresses during high velocity impact techniques.)

- The use of temperature dependent heat transfer coefficient during process for better acquisition of the thermal stress.
- In this project due to unavailability of the Johnson-cook parameters and thermomechanical properties for sprayed stainless steel in the literature, the deposited material is treated the same as the bulk material. These simplifications contribute to the error in the obtained results. The material behavior of the deposited material to be considered different from the bulk material of the substrate to have more realistic results.

Bibliography

[1] K. Taylor, B. Jodoin, J. Karov, Particle loading effect in cold spray, J. Therm. Spray Technol. 15 (2006) 273–279. https://doi.org/10.1361/105996306X108237.

[2] T. Stoltenhoff, H. Kreye, H.J. Richter, An analysis of the cold spray process and its coatings, J. Therm. Spray Technol. 11 (2002) 542–550. https://doi.org/10.1361/105996302770348682.

[3] P. Profizi, Development of a Numerical Model of Single Particle Impact with Adhesion for Simulation of the Cold Spray Process, (2016) 1–154.

[4] M.F. Smith, Comparing cold spray with thermal spray coating technologies, Cold Spray Mater. Depos. Process Fundam. Appl. 1911 (2007) 43–61. https://doi.org/10.1533/9781845693787.1.43.

[5] A. Papyrin, K. Corporation, Coldsp Y, (2001) 49–51. www.ktech.com.

[6] History of cold spray, (n.d.). https://coldspray.com/the-history-of-cold-spray-technology/.

[7] V.M.F. Papyrin Anatolii, V. Kosarev,K.V. Klinkov, A. Alkhimov, Cold Spray Technology, n.d.

[8] H. Singh, T.S. Sidhu, S.B.S. Kalsi, Cold spray technology: Future of coating deposition processes, Frat. Ed Integrita Strutt. 22 (2012) 69–84. https://doi.org/10.3221/IGF-ESIS.22.08.

[9] impact company, Impact instruction manual, n.d.

[10] H. Wu, X. Xie, M. Liu, C. Verdy, Y. Zhang, H. Liao, S. Deng, Stable layer-building strategy to enhance cold-spray-based additive manufacturing, Addit. Manuf. 35 (2020) 101356. https://doi.org/10.1016/j.addma.2020.101356.

[11] J. Villafuerte, Current and future applications of cold spray technology, Met. Finish. 108 (2010) 37–39. https://doi.org/10.1016/S0026-0576(10)80005-4.

[12] F. Gärtner, T. Stoltenhoff, T. Schmidt, H. Kreye, The cold spray process and its potential for industrial applications, J. Therm. Spray Technol. 15 (2006) 223–232. https://doi.org/10.1361/105996306X108110.

[13] R. Ghelichi, S. Bagherifard, D. Macdonald, I. Fernandez-Pariente, B. Jodoin, M. Guagliano, Experimental and numerical study of residual stress evolution in cold spray coating, Appl. Surf. Sci. 288 (2014) 26–33. https://doi.org/10.1016/j.apsusc.2013.09.074.

[14] D. Boruah, B. Ahmad, T.L. Lee, S. Kabra, A.K. Syed, P. McNutt, M. Doré, X. Zhang, Evaluation of residual stresses induced by cold spraying of Ti-6Al-4V on Ti-6Al-4V substrates, Surf. Coatings Technol. 374 (2019) 591–602. https://doi.org/10.1016/j.surfcoat.2019.06.028.

[15] V. Luzin, K. Spencer, M.X. Zhang, Residual stress and thermo-mechanical properties of cold spray metal coatings, Acta Mater. 59 (2011) 1259–1270. https://doi.org/10.1016/j.actamat.2010.10.058.

[16] Y.C. Tsui, T.W. Clyne, An analytical model for predicting residual stresses in progressively deposited coatings: Part 1: Planar geometry, Thin Solid Films. 306 (1997) 23–33. https://doi.org/10.1016/S0040-6090(97)00199-5.

[17] G. Shayegan, H. Mahmoudi, R. Ghelichi, J. Villafuerte, J. Wang, M. Guagliano, H. Jahed, Residual stress induced by cold spray coating of magnesium AZ31B extrusion, Mater. Des. 60 (2014) 72–84. https://doi.org/10.1016/j.matdes.2014.03.054.

[18] F. Oviedo, A. Valarezo, Residual Stress in High-Velocity Impact Coatings: Parametric Finite Element Analysis Approach, J. Therm. Spray Technol. 29 (2020) 1268–1288. https://doi.org/10.1007/s11666-020-01026-5.

[19] E. Lin, I. Nault, O.C. Ozdemir, V.K. Champagne, A. Nardi, S. Müftü, Thermo-Mechanical Deformation History and the Residual Stress

Distribution in Cold Spray, J. Therm. Spray Technol. 29 (2020) 1424–1436. https://doi.org/10.1007/s11666-020-01034-5.

[20] P. Bansal, P.H. Shipway, S.B. Leen, Residual stresses in high-velocity oxy-fuel thermally sprayed coatings - Modelling the effect of particle velocity and temperature during the spraying process, Acta Mater. 55 (2007) 5089–5101. https://doi.org/10.1016/j.actamat.2007.05.031.

[21] L. Li, L. Yan, W. Cui, Y. Chen, T. Pan, X. Zhang, A. Flood, F. Liou, Predictive model for thermal and stress field in selective laser melting process-Part I, Procedia Manuf. 39 (2019) 539–546. https://doi.org/10.1016/j.promfg.2020.01.414.

[22] L. Li, L. Yan, Y. Chen, T. Pan, X. Zhang, W. Cui, A. Flood, F. Liou, Predictive model for thermal and stress field in selective laser melting process-Part II, Procedia Manuf. 39 (2019) 547–555. https://doi.org/10.1016/j.promfg.2020.01.416.

[23] N.S. Development, D. Additive, M. Process, Numerical Simulation Development and Computational Optimization for Directed Energy Deposition Additive Manufacturing Process, Materials (Basel). (2020).

[24] F.E. Bock, J. Herrnring, M. Froend, J. Enz, N. Kashaev, B. Klusemann, Experimental and numerical thermo-mechanical analysis of wire-based laser metal deposition of Al-Mg alloys, J. Manuf. Process. 64 (2021) 982–995. https://doi.org/10.1016/j.jmapro.2021.02.016.

[25] A. Gouldstone, ON SIMULATION OF MULTI-PARTICLE IMPACT INTERACTIONS IN THE COLD SPRAY PROCESS, (2016) 2–4.

[26] M. Grujicic, C.L. Zhao, W.S. DeRosset, D. Helfritch, Adiabatic shear instability based mechanism for particles/substrate bonding in the cold-gas dynamic-spray process, Mater. Des. 25 (2004) 681–688. https://doi.org/10.1016/j.matdes.2004.03.008.

[27] B. Yildirim, S. Muftu, A. Gouldstone, Modeling of high velocity impact of spherical particles, Wear. 270 (2011) 703–713. https://doi.org/10.1016/j.wear.2011.02.003.

[28] W.Y. Li, C. Zhang, C.J. Li, H. Liao, Modeling aspects of high velocity impact of particles in cold spraying by explicit finite element

analysis, J. Therm. Spray Technol. 18 (2009) 921–933. https://doi.org/10.1007/s11666-009-9325-2.

[29] H. Assadi, F. Gärtner, T. Stoltenhoff, H. Kreye, Bonding mechanism in cold gas spraying, Acta Mater. 51 (2003) 4379–4394. https://doi.org/10.1016/S1359-6454(03)00274-X.

[30] satbroadcasts, (n.d.). http://www.satbroadcasts.com/news,85,EIRP_values_for_Ku_band_EIRP_vs_dish_size_comparison.html (accessed March 25, 2021).

[31] G. Bae, Y. Xiong, S. Kumar, K. Kang, C. Lee, General aspects of interface bonding in kinetic sprayed coatings, Acta Mater. 56 (2008) 4858–4868. https://doi.org/10.1016/j.actamat.2008.06.003.

[32] I. Smojver, D. Ivančević, Bird strike damage analysis in aircraft structures using Abaqus/Explicit and coupled Eulerian Lagrangian approach, Compos. Sci. Technol. 71 (2011) 489–498. https://doi.org/10.1016/j.compscitech.2010.12.024.

[33] G. Qiu, S. Henke, J. Grabe, Application of a Coupled Eulerian-Lagrangian approach on geomechanical problems involving large deformations, Comput. Geotech. 38 (2011) 30–39. https://doi.org/10.1016/j.compgeo.2010.09.002.

[34] ABAQUS Inc, Analysis Theory Manual version Abaqus 6.11, I (n.d.).

[35] G.R. Johnson, W.H. Cook, A Computational Constitutive Model and Data for Metals Subjected to Large Strain, High Strain Rates and High Pressures, Seventh Int. Symp. Ballist. (1983) 541–547.

[36] M.J. Azizpour, D. Sajedipour, H.M. Majd, M.R.T. Birgani, M. Rabiae, Impact Temperature in Splat and Splat-Substrate Interface in HVOF Thermal Spraying, World Acad. Sci. Eng. Technol. - Int. Sci. Index. 6 (2012) 576–578. http://waset.org/publications/15835/impact-temperature-in-splat-and-splat-substrate-interface-in-hvof-thermal-spraying.

[37] T.C. Totemeier, Effect of high-velocity oxygen-fuel thermal spraying on the physical and mechanical properties of type 316 stainless steel, J. Therm. Spray Technol. 14 (2005) 369–372. https://doi.org/10.1361/105996305X59440.

[38] C. Xxii, DOTTORATO DI RICERCA IN Meccanica dei materiali e processi tecnologici Neutronic Analysis for ITER CXRS Diagnostic Upper Port-Plug, (2010).

[39] S. Rahmati, A. Ghaei, The use of particle/substrate material models in simulation of cold-gas dynamic-spray process, J. Therm. Spray Technol. 23 (2014) 530–540. https://doi.org/10.1007/s11666-013-0051-4.

[40] Los Alamos Lab, (1996).

[41] R. Ghelichi, S. Bagherifard, M. Guagliano, M. Verani, Numerical simulation of cold spray coating, Surf. Coatings Technol. 205 (2011) 5294–5301. https://doi.org/10.1016/j.surfcoat.2011.05.038.

[42] T. natural convective heat transfer coefficient of air around the Cylinder, No Title, (n.d.). https://thermal.mayahtt.com/tmwiz/convect/natural/horiz-cylinder/horiz-cylinder.htm.

[43] SS316 emmitivity, (n.d.). https://www.omega.co.uk/literature/transactions/volume1/emissivitya.html.

[44] Impact Innovation, Impact Innovatopn Cold Spray System, (n.d.). https://impact-innovations.com/en/products/.

[45] K.R. GmbH, KUKA System Software 8.3, (2015) 491.

[46] P. Taylor, I.C. Noyan, T.C. Huang, B.R. York, Critical Reviews in Solid State and Materials Sciences Residual stress/strain analysis in thin films by X-ray diffraction Residual Stress/Strain Analysis in Thin Films by X-ray Diffraction, Crit. Revients Solid State Mater. Sci. (2011) 37–41.

[47] P.S. Prevey, X-Ray Diffraction Residual Stress Techniques, Mater. Charact. (2018) 380–392. https://doi.org/10.31399/asm.hb.v10.a0001761.

[48] J.T.A. V Monin, Nondestructive control of residual stress state of weld regions by x-ray diffraction methods, (n.d.). https://www.ndt.net/article/v05n04/monin/monin.htm.

[49] struers, Electrolytic-Preparation with STrers, (n.d.). https://www.struers.com/en/Products/Electrolytic-Preparation.

A Appendix

A.1. Sample dimension

In Table 14, the dimensions of used samples during experimental part can be seen, through which just 5 of them with less deviation from the desired dimension of 30×30×5 cubic millimetres have been chosen for deposition process.

Table 14_ Representation of the dimensions of the used samples

samples	d1-min	d1-max	d1-mean	d2-min	d2-max	d2-mean	d3
1	30.5	30.7	30.6	28.5	28.9	28.7	5.03
2	30.4	30.5	30.45	31.6	31.9	31.75	5
3	31.9	32	31.95	31.9	32	31.95	4.97
4	31.8	31.9	31.85	32.9	33	32.95	5.04
5	32.1	32.3	32.2	28.9	29.1	29	5.04
6	28.5	28.6	28.55	27.9	28	27.95	4.98
7	29.6	29.6	29.6	27.9	28	27.95	5.04
8	28	28	28	28.7	28.8	28.75	5.05
9	28	28	28	27.8	28.1	27.95	5.04
10	28	28.1	28.05	27.6	27.7	27.65	5.04
11	27.6	27.7	27.65	297.7	298.8	29.85	5.04
12	3.01	30.2	16.605	30.1	30.3	30.2	5.05
13	30.1	30.1	30.1	30.1	30.4	30.25	5.05
14	30.2	30.3	30.25	30	30.2	30.1	5.01
15	30.1	30.2	30.15	30.1	30.2	30.15	5.05
16	30.2	30.2	30.2	30.1	30.2	30.15	5.05
17	30	30.2	30.1	30.1	30.1	30.1	5.01
18	30	30.1	30.05	30.1	30.1	30.1	5.01
19	29.6	29.8	29.7	30	30	30	5.06

20	29.9	30.1	30	30	30.2	30.1	5.06

B Appendix

B.1. Peening Stress

As already mentioned, the stress profile is already extracted from the axis of axisymmetric structure in explicit coupled displacementt-thermal analysis of single impact particle. Then with the help of an iterative corrective approach, and with the help of the methods already described in Peening Stress prediction part of chapter Developing Numerical method to predict residual stress in 2D, the loads responsible for induction of mentioned stress profile would be found. Then being generalized to obtain the stress profile during the cold spray process.

B.1.1. Axial Stress

In S-Axial Pressure-Radial Pressure-Predefined Radial Initial Stress method, the axial pressures are responsible for induction of axial stress trend in the substrate.

To obtain the axial pressure applied at the top 0.2 mm of the substrate right below the added layer, the following procedure will be followed.

Mesh size is not consistent on the axis of axisymmetric structure in single particle impact, so firstly, an interpolation should be done, and obtain the stresses at the suitable coordinates, used in the following steps.

xmode220_list refers to the coordinates being used for reading stresses in the ODB file.

xp220_list refers to the coordinates in which the stresses are read from single particle model.

S220_list refers to the stresses in the xp220_list coordinates from single particle impact ODB file.

The following part refers to the interpolation done to obtain the stresses in the suitable coordinates from the results extracted from single particle impact.

```
ST220= []
p=0
ST220.append(s220_list [0])
for i in range (2,41+1):
   for j in range (1, len(s220_list)):
```

```
    if (xp220_list[j-1]>xmode220_list[i-1]>xp220_list[j]):
        p=poly1d(polyfit([xp220_list[j-1], xp220_list[j]],[s220_list[j-1],s220_list[j]],1))
        ST220.append(p(xmode220_list[i-1]))
```

Defining the edges with the help of the already sectioned part is possible is described in the following piece of piece of code.

```
for num in range (1,41):
  mdb.models['s22'].rootAssembly.Surface(name='Surf-L'+str(num), side1Edges=
    mdb. models['s22'].rootAssembly.instances['Sub+Layer-1'].edges.findAt(((
    0.575, 1.7-((num-1)*0.005), 0.0), )))
```

Afterwards, by having the axial stress profile from single particle impact ODB file, the responsible loads for inducing the mentioned profile as first guess were obtained.

```
ST220m=[]
Sm. append (ST220[0])
for i in range (1, len(ST220)):
 ST220m. append(-ST220[i-1] +ST220[i]+0.0000001)
```

ST220m here refers to the modified ST220 as first guess for the applied axial pressures on the predefined horizontal edges in the 0.2 mm top part of the substrate.

Then the loads will be defined by knowing ST220m and the predefined horizontal edges as 'Surf-L'+str(num).

```
for i in range (1,40+1):
   mdb. models['s22']. Pressure(amplitude=UNSET, createStepName='step',
      distributionType=UNIFORM, field='', magnitude=s22Load[i-1], name='Load-
'+str(i), region=
      mdb. models['s22']. rootAssembly.surfaces['Surf-L'+str(i)])
```

The job is run and completed.

The ODB file is opened, and a couple of paths are defined to be used for averaging corresponding results for higher accuracy:

```
o3 = session.openOdb(name='file.address.odb')
session.viewports['Viewport: 1'].setValues(displayedObject=o3)
session.viewports['Viewport: 1'].makeCurrent()
session.viewports['Viewport: 1'].odbDisplay.display.setValues(plotState=(
  CONTOURS_ON_UNDEF, ))
############ the same path should be defiend
session.viewports['Viewport: 1'].view.setValues(nearPlane=6.62149,
```

```
    farPlane=9.5912, width=0.471231, height=0.283124, viewOffsetX=-0.822098,
    viewOffsetY=0.674144)
session.viewports['Viewport: 1'].view.setValues(nearPlane=6.61823,
    farPlane=9.59446, width=0.470999, height=0.282985, viewOffsetX=-0.791323,
    viewOffsetY=0.557147)
firstpoint_list=[18501,18572,18649,18700,18771,18833,18897]
secondpoint_list=[950,879,20626,20677,20748,20810,20874]
for i in range(1,7+1):
    session.Path(name='Path-'+str(i), type=NODE_LIST, expression=(('SUB+LAYER-1',
(firstpoint_list[i-1],
        secondpoint_list[i-1], )), ))
```

Then the averaging is done on the defined paths' data which were already saved as txt file.

```
x11_list=[]
s11_list=[]
for i in range(1,7+1):
    import os
    path='D:\Thesis_Abaqus\PHD-thesis-Al\pressure_read from ovideo'
    os.chdir(path)
    file=open('XYDataS11_'+str(i)+'_'+str(num)+'.txt','r')
    f=file.readlines()
    lis11=[]
    for line in f:
        reading=line.split()
        lis11.append(reading)
    for i in range(len(lis11)-1,-1,-1):
        if len(lis11[i])==0:
            del lis11[i]
    lis11=lis11[2:]
    x11_lis_ex=[]
    s11_lis_ex=[]
    for j in range(0,len(lis11)):
        x11_lis_ex.append(float(lis11[j][0]))
        s11_lis_ex.append(float(lis11[j][1]))
```

```
    counter=0
    for i in range(0,len(x11_lis_ex)):
        if (0.001>x11_lis_ex[i]>-0.001):
            counter=counter+1
    SSUM=0
    SAV=0
    if (counter>1):
        s11_liss_ex=[]
        for j in range(1, counter+1):
            SSUM=SSUM+s11_lis_ex[j-1]
        SAV=SSUM/counter
        x11_liss_ex=x11_lis_ex[counter-1:]
        s11_liss_ex.append(SAV)
        for i in range(counter,len(x11_liss_ex)+1+counter-2):
            s11_liss_ex.append(s11_lis_ex[i])
    else:
        s11_liss_ex=s11_lis_ex
        x11_liss_ex=x11_lis_ex
    x11_list. append(x11_liss_ex)
    s11_list. append(s11_liss_ex)

s11_avg=[]
x11_avg=x11_list[0]
for j in range(1,41+1):
    V=0
    for i in range(1,7+1):
        V=s11_list[i-1][j-1]+V
    s11_avg.append(V/7)
K1=0
for i in range(2,41+1):
    K1=K1+abs(ST110[i-1]-s11_avg[i-1])
K=K1*mesh_size
```

If the K is lower than a threshold the iteration won't be continued, otherwise the value of the vertical pressures are updated based on the difference between the read results and the corresponding stresses read form single particle impact analysis.

B.1.2. Radial Stress

In S-Axial Pressure-Radial Pressure-Predefined Radial Initial Stress method, the radial stress is induced through the use of predefined radial initial stress in the top 0.2 mm of the substate right below the added layer.

Mesh size is not consistent on the axis of axisymmetric structure in single particle impact, so firstly, an interpolation should be done, and obtain the stresses at the suitable coordinates, used in the following steps.

xmode110_list refers to the coordinates being used for reading stresses in the ODB file.

xp110_list refers to the coordinates in which the stresses are read from single particle model.

S110_list refers to the stresses in the xp110_list coordinates from single particle impact ODB file.

The following part refers to the interpolation done to obtain the stresses in the suitable coordinates from the results extracted from single particle impact.

It should be mentioned that the effect of the radial pressures added on the free edge of the 2D model is local, and the overall stress field is ruled by the added predefined initial radial stresses in the 0.2 mm top part of the substrate.

```
ST110=[]
p=0
ST110.append(s110_list [0])
for i in range (2,41+1):
  for j in range (1, len(s110_list)):
    if (xp110_list[j-1]>xmode110_list[i-1]>xp110_list[j]):
      p=poly1d(polyfit([xp110_list[j-1], xp110_list[j]],[s110_list[j-1],s110_list[j]],1))
      ST110.append(p(xmode110_list[i-1]))
```

B.1.2.1. Predefined initial radial stresses

As the ST110 is obtained, it would be applied as the initial guess in the added predefined radial stresses. In the following part the layers being used for the application of predefined initial radial stresses are defined, and then the ST110 is applied as the first guess for the predefined initial radial stresses.

```
for i in range (1,40+1):
    mdb.models['Model-1'].rootAssembly.Set(faces=
      mdb. models['Model-1'].rootAssembly.instances['Sub+Layer-1'].faces.findAt(((
      0.766667, (1.702-i*0.005), 0.0), )), name='Layer-'+str(i))
for i in range(1,40+1):
  mdb.models['Model-1'].Stress(distributionType=UNIFORM, name=
    'Predefined Field-'+str(i), region=
    mdb.models['Model-1'].rootAssembly.sets['Layer-'+str(i)], sigma11=ST110[i-1], sigma12=
    0.0, sigma13=0.0, sigma22=0.0, sigma23=0.0, sigma33=ST110[i-1])
```

The job is run. After defining 11 paths, the radial stress profiles in these 11 paths are saved as txt file. Subsequently the averaging between the obtained trend in the mentioned paths are done.

```
o3 = session.openOdb(name='D:\Thesis_Abaqus\PHD-thesis-Al\pressure_read from ovideo\job-5'+'.odb')
session.viewports['Viewport: 1'].setValues(displayedObject=o3)
session.viewports['Viewport: 1'].makeCurrent()
session.viewports['Viewport: 1'].odbDisplay.display.setValues(plotState=(
  CONTOURS_ON_UNDEF, ))
session.viewports['Viewport: 1'].view.setValues(nearPlane=6.62149,
  farPlane=9.5912, width=0.471231, height=0.283124, viewOffsetX=-0.822098,
  viewOffsetY=0.674144)
session.viewports['Viewport: 1'].view.setValues(nearPlane=6.61823,
  farPlane=9.59446, width=0.470999, height=0.282985, viewOffsetX=-0.791323,
  viewOffsetY=0.557147)
firstpoint_list=[18449,18466,18484,18534,18574,18620,18688,18749,18819,18876,18902]
secondpoint_list=[1002,985,967,917,877,831,763,702,632,575,549]
for i in range(1,11+1):
  session.Path(name='Path-'+str(i), type=NODE_LIST, expression=(('SUB+LAYER-1', (firstpoint_list[i-1],
    secondpoint_list[i-1], )), ))
num=1
for i in range (1,11+1):
  session.viewports['Viewport: 1'].odbDisplay.setPrimaryVariable(variableLabel='S', outputPosition=INTEGRATION_POINT, refinement=(COMPONENT,'S11'))
```

```
    #### create the XYdata here
    pth = session.paths['Path-'+str(i)]
    session.XYDataFromPath(name='XYDataS11_'+str(i)+'_'+str(num), path=pth,
includeIntersections=True,
        projectOntoMesh=True, pathStyle=PATH_POINTS, numIntervals=10,
        projectionTolerance=0, shape=UNDEFORMED, labelType=TRUE_DISTANCE,
        removeDuplicateXYPairs=True, includeAllElements=True)
    x0 = session.xyDataObjects['XYDataS11_'+str(i)+'_'+str(num)]
    session.xyReportOptions.setValues(numberFormat=AUTOMATIC)
    session.writeXYReport(fileName='XYDataS11_'+str(i)+'_'+str(num)+'.txt',
xyData=(x0, ))
x11_list=[]
s11_list=[]
for i in range(1,11+1):
    import os
    path='D:\Thesis_Abaqus\PHD-thesis-Al\pressure_read from ovideo'
    os.chdir(path)
    file=open('XYDataS11_'+str(i)+'_'+str(num)+'.txt','r')
    f=file.readlines()
    lis11=[]
    for line in f:
        reading=line.split()
        lis11.append(reading)
    for i in range(len(lis11)-1,-1,-1):
        if len(lis11[i])==0:
            del lis11[i]
    lis11=lis11[2:]
    x11_lis_ex=[]
    s11_lis_ex=[]
    for j in range(0,len(lis11)):
        x11_lis_ex.append(float(lis11[j][0]))
        s11_lis_ex.append(float(lis11[j][1]))
    counter=0
    for i in range(0,len(x11_lis_ex)):
        if (0.001>x11_lis_ex[i]>-0.001):
```

```
        counter=counter+1
    SSUM=0
    SAV=0
    if (counter>1):
      s11_liss_ex=[]
      for j in range(1, counter+1):
        SSUM=SSUM+s11_lis_ex[j-1]
      SAV=SSUM/counter
      x11_liss_ex=x11_lis_ex[counter-1:]
      s11_liss_ex. append(SAV)
      for i in range(counter,len(x11_liss_ex)+1+counter-2):
        s11_liss_ex. append(s11_lis_ex[i])
    else:
      s11_liss_ex=s11_lis_ex
      x11_liss_ex=x11_lis_ex
    x11_list. append(x11_liss_ex)
    s11_list. append(s11_liss_ex)
s11_avg=[]
x11_avg=x11_list[0]
for j in range(1,41+1):
    V=0
    for i in range(1,11+1):
     V=s11_list[i-1][j-1]+V
    s11_avg.append(V/11)
```

The differences between the stress in single particle impact and the obtained averaged stress will be checked, in order to make sure it is lower than a threshold. If the threshold is surpassed, the applied predefined initial radial stresses will be modified by taking into consideration the difference between the desired stress profile obtained from the single particle impact analysis, and the averaged stress profile in radial direction.

```
K=0
for i in range (2,41+1):
  K=K+abs(ST110[i-1]-s11_avg[i-1])
s11z_list=[]
for i in range (1,41+1):
```

```
  s11z_list. append((ST110[i-1]-s11_avg[i-1]))
s11m_lis=[]
for i in range(1,41+1):
  s11m_lis.append(s11z_list[i-1]+s11m_list[i-1])
for i in range(1,40+1):
  mdb.models['Model-1'].Stress(distributionType=UNIFORM, name=
    'Predefined Field-'+str(i), region=
    mdb.models['Model-1'].rootAssembly.sets['Layer-'+str(i)], sigma11=(s11m_lis[i-
1]+s11m_lis[i])/2, sigma12=
    0.0, sigma13=0.0, sigma22=0.0, sigma23=0.0, sigma33=(s11m_lis[i-
1]+s11m_lis[i])/2)
```

B.1.2.2. Radial Pressure

In the case of definition of the radial pressures applied on the right free edge of the 2D model, the subroutine DLOAD was used successively till the error criterion was satisfied. Hereafter the subroutine will be read by dividing the applied edge to small intervals to have better control for inducing the stress trend obtained from the single particle impact model.

```
file1 = open(str(number)+'subroutine'+".for","w")
file1.write('     SUBROUTINE DLOAD(F,KSTEP,KINC,TIME,NOEL,NPT,LAYER,KSPT,\n')
file1.write('    1 COORDS,JLTYP,SNAME)\n')
file1.write('C\n')
file1.write("     INCLUDE 'ABA_PARAM.INC'\n")
file1.write('C\n')
file1.write('     DIMENSION TIME(2), COORDS (3)\n')
file1.write('     CHARACTER*80 SNAME\n')
file1.write('     x=coords(1)\n')
file1.write('     y=coords(2)\n')
for i in range(1,41):
  p=0
  file1.write('                    if ((+str(xmode110_list[i-1])+'>y) .and.
(y>'+str(xmode110_list[i])+')) then\n')
  p=poly1d(polyfit([xmode110_list[i-1],xmode110_list[i]],[ST110[i-1],ST110[i]],1))
  file1.write('     F'+'='+str(-1*p((xmode110_list[i]+xmode110_list[i-1])/2))+'\n')
```

```
  file1.write('     end if\n')
file1.write('     RETURN\n')
file1.write('     END\n')
file1.close()
```

Then through the use of ODB file, 3 paths close to the free edge has been defined. As already mentioned, the overall radial trend is ruled by predefined initial radial stresses, however in order to make more uniform stress field independent of the radial position in the substrate, the radial pressure is applied as well. The mentioned 3 paths are defined close to the edge of the model considering the local effect of the added pressure.

The same strategy represented in Axial Stress part of the Appendix, is used in the case of comparison with the radial stress profile obtained from single particle impact model. The loads are modified if the error criterion is not satisfied. Then the new subroutine is written for the next iterations.

B.1.3. Generalization phase

Generalization refers to the implementation of the obtained predefined initial radial stresses, axial pressure, radial pressure being added successively to show the evolution of addition of coatings during cold spray process.

In this part simply the loads are summed together by sequentially shifting position, considering the added layers.

```
list1=ST220m
listTotal=[]
listTotal.append(list1)
N=Number of added layers
for i in range(1,N):
  list=[]
  for k in range(0,i*2):
    list.append(listTotal[i-1][k])
  for j in range(0,len(list1)-2):
    list.append(listTotal[i-1][j+2+(i-1)*2]+list1[j])
  list.append(list1[-2])
  list.append(list1[-1])
  listTotal.append(list)
```

if the list1=[1,1,1], and the number of added layers are 2, then the resulting listTotal which is a list of lists would be [[1, 1, 1], [1, 1, 2, 1, 1], [1, 1, 2, 1, 2, 1, 1]] each list being

used in 1 job for application of the loads responsible for induction of the stress field obtained from single particle impact.

B.2. Thermal Stress

As already mentioned for obtaining the thermal stress field during cold spray process, an uncoupled thermal- mechanical analysis is used. Initially the thermal field with the presence of convection and radiation, and conduction through the added layer and substrate was obtained. Then the obtained thermal temporal field was used in an implicit model to obtain the stresses due quenching and post cooling.

For obtaining the thermal field, initially the part is sectioned in the exact manner as the part has been used in the model for obtaining peening stress. The part regarding the added layers have been sectioned, and the bottom edges of the sectioned parts has been used for application of heat flux with specific amplitude. The amplitude is used to deactivate the heat transfer whenever, the following layer is about to be deposited.

In this model, as already mentioned the top edges are used to have radiation and convective heat transfer between the assembly of added layer- substrate assembly with the environment. In addition, on the right side of the model- the free side of the 2D model, the radiative and convective heat transfer was applied. In the case of the added heat transfer on the horizontal edges, deactivation of the interactions is necessary to show the addition of new layer, however, in the case of vertical edges, no amplitude would be needed, as they are exposed to the environment the whole time.

```
##Definition of the horizontal surfaces
for num in range(1,41):
  mdb.models['Model-1'].rootAssembly.Surface(name='Surf-horizontal-'+str(num),
side2Edges=
    mdb.models['Model-1'].rootAssembly.instances['Sub+Layer-1'].edges.findAt(((
    0.575, 1.7+(num*0.01), 0.0), )))
## Application of the heat flux in the appropriate step, and deactivation in the
##following steps. (the amplitudes are already defined and used.
for num in range(1,41):
  mdb.models['Model-1'].SurfaceHeatFlux(createStepName='activation_'+str(num),
    magnitude=1000.0, name='HT_'+str(num), region=
    mdb.models['Model-1'].rootAssembly.surfaces['Surf-horizontal-'+str(num)])
for i in range(1,40):
  mdb.models['Model-1'].loads['HT_'+str(i)].deactivate('activation_'+str(i+1))
##Application of Convection
```

```
for num in range(1,41):
 mdb.models['Model-1'].FilmCondition(createStepName='activation_'+str(num),
definition=
    EMBEDDED_COEFF, filmCoeff=0.0107, name='Int_convection_H_'+str(num),
    sinkAmplitude='', sinkDistributionType=UNIFORM,
    sinkFieldName='', sinkTemperature=298, surface=
    mdb.models['Model-1'].rootAssembly.surfaces['Surf-horizontal-'+str(num)])
for num in range(1,40):
   mdb.models['Model-1'].interactions['Int_convection_H_'+str(num)].deactivate(
     'activation_'+str(num+1))
###Definition of vertical edges to be used for definition of radaiative and convective
##heat transfet with the environment.
mdb.models['Model-1'].rootAssembly.Surface(name='Surface_vertical_'+str(0),
side1Edges=mdb.models['Model-1'].rootAssembly.instances['Sub+Layer-
1'].edges.findAt(((2.3+(15-2.3), 1.7-0.2-0.006+0.005-0.1, 0.0), )))
for num in range(1,121):
  mdb.models['Model-1'].rootAssembly.Surface(name='Surface_vertical_'+str(num),
side1Edges=mdb.models['Model-1'].rootAssembly.instances['Sub+Layer-
1'].edges.findAt(((2.3+(15-2.3), 1.7-0.2-0.006+0.005+(num)*0.005, 0.0), )))
for num in range(0,121):
 mdb.models['Model-1'].FilmCondition(createStepName='activation_'+str(1),
definition=
    EMBEDDED_COEFF, filmCoeff=0.0107, name='Int_convection_V_'+str(num),
    sinkAmplitude='', sinkDistributionType=UNIFORM,
    sinkFieldName='', sinkTemperature=298, surface=
    mdb.models['Model-1'].rootAssembly.surfaces['Surface_vertical_'+str(num)])
```

It should be mentioned that in order to show the addition of layers, model change interaction is used. But initially the layers are defined.

```
###Definition of the added layers
for i in range(1,40+1):
  mdb.models['Model-1'].rootAssembly.Set(faces=
    mdb.models['Model-1'].rootAssembly.instances['Sub+Layer-1'].faces.findAt(((
    0.766667, (1.702+i*0.01-0.002), 0.0), )), name='Layer-'+str(i)+'-1')
############below half of each layer
for i in range(1,40+1):
  mdb.models['Model-1'].rootAssembly.Set(faces=
```

```
    mdb.models['Model-1'].rootAssembly.instances['Sub+Layer-1'].faces.findAt(((
    0.766667, (1.702+i*0.01-0.002-0.005), 0.0), )), name='Layer-'+str(i)+'-2')
###Model change is applied
for num in range (1,41):
 mdb.models['Model-1'].ModelChange(activeInStep=False,
createStepName='deactivation', includeStrain=False,
name='int_deact_act_1_'+str(num), region=mdb.models['Model-
1'].rootAssembly.sets['Layer-'+str(num)+'-1'])
 mdb.models['Model-1'].ModelChange(activeInStep=False,
createStepName='deactivation', includeStrain=False,
name='int_deact_act_2_'+str(num), region=mdb.models['Model-
1'].rootAssembly.sets['Layer-'+str(num)+'-2'])
for num in range(1,41):
 mdb.models['Model-
1'].interactions['int_deact_act_1_'+str(num)].setValuesInStep(activeInStep=True,
stepName='activation_'+str(num))
 mdb.models['Model-
1'].interactions['int_deact_act_2_'+str(num)].setValuesInStep(activeInStep=True,
stepName='activation_'+str(num))
```

List of Figures

List if Tables

Acknowledgments

I would like to express my special thanks of gratitude to my family, especially to my dearest, my father, who has recently passed away. The great man undoubtedly unconditionally supported us during our lives. I would remember the sweet memories of my father till the moment I breathe. My father is gone, but his memories are alive. My father used to tell me in the humorous way," I am sure if you have been working on the Apollo project instead of your thesis project, it would have been done by now, every single time, I ask you what you are doing, you tell me you are working on your thesis."

I am extremely grateful to pay my special regards to Dr. Sara Bagherifard, my thesis supervisor, Amir Ardeshiri Lordejani and Professor Mario Guagliano my thesis co-supervisors, for their invaluable advice, continuous support, and encouraging spirit. I would also like to thank Giuseppe Ghilardi, and Ludovica Rovatti, for their great contribution during experimental phase of the thesis.